Structural and functional studies on microbial superantigens

Baker, Matthew Douglas

Award date:
2001

Awarding institution:
University of Bath

STRUCTURAL AND FUNCTIONAL STUDIES ON MICROBIAL SUPERANTIGENS

submitted by Matthew Douglas Baker

for the degree of PhD

of the University of Bath

2001

Copyright

ProQuest LLC
789 East Eisenhower Parkway
P.O. Box 1346
Ann Arbor, MI 48106-1346

Acknowledgements

I would like to thank Prof Ravi Acharya for giving me the opportunity to undertake this research and for being an excellent supervisor.

I would also like to thank Tassos Papageorgiou for being a great friend and mentor, Jawahar Swaminathan for all his help and discussion on everything; from the nature of hydrogen bonds to the latest cricket score and all in between, Howard Tranter for his help and guidance during my time at CAMR, my Mother, Father, Sister and Brother-in-law for their day to day support, James Pilgrim, James Randerson, and Rebecca Michael for being great friends and to Eve Ashley for always being there to help me through times of stress.

I would also like to thank the various members of the laboratory during the last three years Dan, Michelle, Shalini, Evangelia, Gayatri, Ester, Mohan, Lori, Hazel, Kate, Laurie and Natesh. I am grateful to the staff at the various synchrotron radiation sources (CLRC laboratory, Daresbury, U.K., EMBL, Hamburg, Germany., Elettra, Trieste, Italy., Max Lab, Lund, Sweden.) for help with data collection and to the Medical Research Cuncil (UK) for funding this research.

Foreword

Unconsciously to myself, I looked at a film of sand I had picked up on my hand, when I suddenly saw the exquisite beauty of every little grain of it; instead of being dull, I saw that each particle was made up on a perfect geometrical pattern, with sharp angles, from each of which a brilliant shaft of light was reflected, while each tint crystal shone like a rainbow.

Then suddenly, my consciousness was lighted up from within and I saw in a vivid way how the whole universe was made up of particles of material which, no matter how dull and lifeless they might seem, were nevertheless filled with this intense and vital beauty. For a second or two the whole world appeared as a blaze of glory. When it died down, it left me with something I have never forgotten and which constantly reminds me of the beauty locked up in every minute speck of material around us.

Aldous Huxley

1956, Heaven and Hell

Abstract

Bacterial superantigens are potent T cell stimulatory protein molecules produced by *Staphylococcus aureus* and *Streptococcus pyogenes.* Their superantigenic activity can be attributed to their ability to cross-link MHC class II molecules with T cell receptors to form a tri-molecular complex. Unlike conventional antigen, they are not processed internally by antigen presenting cells (APC), and are thus not displayed as peptide antigen in the peptide-binding groove of the MHC class II molecule. Superantigens bind to APCs on the outside of MHC class II molecule and to T cells via the external face of the T cell receptor (TCR) V β element. Each superantigen interacts with a specific Vβ region of the TCR, and with a specific subset of the total TCR Vβ elements available Therefore, superantigens stimulate populations of T cells in a V β specific, non-MHC restricted manner. This enables them to stimulate a far greater proportion of resting T cells compared to conventional antigen. Using X-ray crystallography, the structures of several superantigens both in native and mutant forms have been elucidated. This has enabled us to characterise the regions of these proteins that interact with the immune system and govern their specificity and potency; namely the MHC class II binding regions and the T cell receptor binding regions. Firstly, this study has investigated the role of zinc ions as high affinity MHC class II binding sites for superantigens by determining the crystal structure of SpeA1 in complex with zinc. Secondly, the crystal structure of SEB variant Thr 112 Ser has served to further characterise the TCR binding site of the superantigen family. Thirdly, by solving the crystal structures of three TSST-1 mutants – Tyr 13-Ala, His 141-Ala, and Tyr 174-Ala this study has addressed the structural and functional significance of these three residues on TCR recognition for the toxin. Finally, by producing SEC2 mutants with substitutions within its zinc binding site (His 118-Ala and His118:122-Ala) an attempt has been made to structurally assess

the functional contribution of these residues to the topology of the SEC2 zinc binding site and the involvement of these residues in interacting with MHC class II molecules. Ultimately, this has also allowed the identification of several mechanisms by which this family of proteins could elicit an immune response. Although these mechanisms share common features throughout the family, each superantigen has adopted a unique combination of subtle structural differences to optimise its interactions with both MHC class II molecules and T cell receptors.

Abbreviations

Å – Angstrom 10^{-1}nm.

APC – Antigen presenting cell.

B-factor – Thermal parameter.

MHC – Major Histocompatibility complex.

PEG – Polyethylene glycol.

PBMC – Peripheral blood mononuclear cell.

r.m.s – Root mean square.

SAg – Superantigen.

TSS – Toxic shock syndrome

TSST-1 Toxic shock syndrome toxin - 1

SEA – Staphylococcal enterotoxin type A.

SEB – Staphylococcal enterotoxin type B.

SEC – Staphylococcal enterotoxin type C.

SED – Staphylococcal enterotoxin type D.

SEE – Staphylococcal enterotoxin type E.

SEH – Staphylococcal enterotoxin type H.

SpeA – Streptococcal pyrogenic exotoxin type A.

SpeC – Streptococcal pyrogenic exotoxin type C.

TCR – T Cell receptor.

TCR Vβ - T cell receptor variable β chain.

Contents

-1-

Chapter one

An Introduction to Protein Crystallography

X-ray crystallography

The knowledge of accurate molecular structures provided by X-ray crystallography can provide answers to many of the questions faced by the modern structural biologist, from global folds of a protein to atomic detail of inter- and intra-molecular bonding that may help identify protein interactions and enzymatic mechanisms (Rhodes, 1993). Indeed, it can be said that underlying principle of biological function is biological structure. Structural biology is an ever-evolving state-of-the-art technique; over the years the advent of increasingly faster computers, improved X-ray technology- both in terms of machinery and our understanding of the behaviour of X-rays has lead to many improvements in the speed and accuracy of structure solution (Helliwell, 1992). In turn, the information from the many completed molecular structures has allowed us to further improve our interpretation of X-ray diffraction data.

In this section the various stages of determining the structure of a given protein will be discussed. These stages are:

- Availability of pure protein
- Crystallisation of the pure sample
- Selection of the appropriate data collection conditions
- Determination of the unit cell parameters
- X-ray data collection to a given resolution
- Solution of the crystallographic phase problem
- Interpretation of the electron density map
- Refinement of the molecular model against the observed data
- Structure analysis and validation
- Structure deposition (atomic co-ordinates and structure factors) with PDB.

Further to this, the basic principles of X-ray diffraction will be discussed along with an outline of the kinds of x-ray, computer hardware, software and detectors used to carry out data collection.

Protein purification

The aim of protein purification for crystallisation trials is to produce a pure (> 99%), correctly folded, monodispersed, structurally homogenous protein sample. A complete review of methods for protein purification is beyond the scope of this work, however certain aspects should be considered when purifying proteins for crystallography. These include:

- Protein source – wild type or recombinant
- Expression system
- Fusion proteins and cleavage of tag
- Purification method
- Assessment of purity.

The choice of protein source, expression system and to some degree, purification method can have a profound effect on the amount of protein produced/recovered. As protein crystallisation requires a relatively large amount of pure material, these processes must be optimised. The purification method and assessment of purity are important as lack of purity in a sample may lead to (*i*) complete failure to crystallise (*ii*) the production of only small crystals or (*iii*) large crystals that do not diffract X-rays well. Contaminating species, which are able to satisfy only a portion of the bonding interaction necessary to propagate the lattice, will reduce crystal formation. Heterogeneity in the protein solution will at best reduce the pool of available material in the crystallisation medium which can be incorporated into the lattice. Micro-heterogeneity in the protein of interest may be as much of a problem to crystallisation as

contamination with an unrelated protein molecule as the accumulated defects at the crystal surface which result are believed to play a role in limiting crystal size. Incorporation of protein molecules other than that of interest into the crystal will result in increased disorder within the crystal producing poor diffraction.

Crystallisation of proteins

A crystal is an orderly three-dimensional array of molecules held together by non-covalent interactions. The aim of a crystallisation experiment is to produce crystals of diffraction quality. Ideally, a crystal should be homogenous and well ordered, of reasonable size and free from flaws such as cracks. The apparently simple task of crystallising any given protein is considered to be the limiting step to protein structure determination. The process involves the 'controlled' precipitation of the protein from solution to form ordered crystals. This process begins with the association of protein aggregates whose intermolecular contacts resemble those found in the final crystal (Salemme *et al.*, 1988). Eventually these aggregates reach the critical nuclear size and growth proceeds by the addition of molecules to the crystalline lattice. The processes of nucleation and crystal growth both occur in supersaturated solutions where the concentration of protein exceeds its equilibrium solubility value (see Figure 1.1). Supersaturation is a function of the protein and factors which affect its solubility. It can be achieved at high protein concentrations and by altering factors that affect protein solubility. These factors include: additives such as alcohols; hydrophilic polymers such as polyethylene glycol and addition of detergent. These agents are commonly known as precipitants. Salt concentration, pH and temperature also have an affect on protein solubility. Proteins are usually less soluble at both high and low salt concentrations, so crystallisation strategies that either include or exclude salt could induce crystallisation. The supersaturation requirements for nucleation and crystal growth differ. The phase

diagram in Figure 1.1 shows the supersaturation zone as being further divided into regions of higher supersaturation (the labile zone) where both growth and nucleation occur, and lower supersaturation (the metastable phase) where only growth is supported.

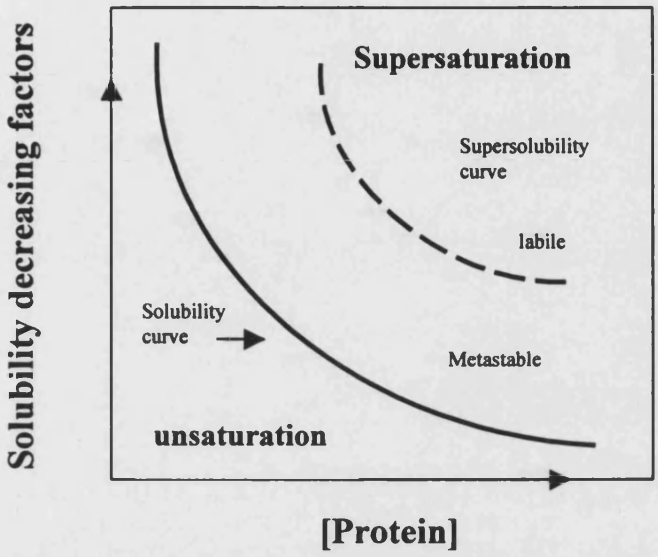

Figure 1.1: Phase diagram of crystal growth. Nucleation and crystal growth occur in supersaturated solutions where the concentration of protein exceeds its equilibrium solubility value.

There are several variants of the vapour diffusion technique, all of which are based on the principle of diffusion through the air from a high concentration of soluble protein to a reservoir of precipitant. Nucleation occurs through the increase in protein concentration through dehydration-driven reduction of solution volume caused by equilibration of water vapour from the protein-containing drop to a more hygroscopic reservoir solution. Figure 1.2 shows the experimental set-up for a hanging drop, whereby the protein solution is suspended in a drop on a coverslip above a reservoir of precipitant (also known as mother-liquor) in a sealed system. Once nucleation occurs, the solution remains highly supersaturated, so that nucleation and rapid crystal growth can occur simultaneously. The hanging drop vapour diffusion technique is perhaps the most widely used method for protein crystallisation. The fact that a majority of the

drops set up in a typical crystallisation trial do not produce crystals suggests that although a high degree of nucleation supporting supersaturation may be achieved, it is not sustained during the course of the experiment. Many factors, including the decrease in macromolecule concentration due to formation of nuclei or precipitates, macromolecular incorporation into growing crystals, or macromolecular denaturation at the solution-air interface could decrease protein concentration to lesser values more suited to growth.

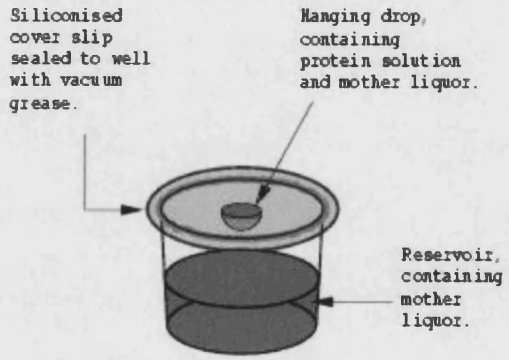

Figure 1.2: Experimental set-up for the hanging drop vapour diffusion technique

Because the specific supersaturation requirements for nucleation and growth differ from protein to protein, a convenient starting point for crystallisation is to use a screen of the most commonly used precipitants, salts and pHs. Such screens (e.g. Magic 50, Hampton research crystal screen, PEG/ion screen and others) contain approximately 50 separate crystallisation conditions. The temperature of crystallisation can also be varied so as best to control the precipitation and produce better crystals. Once a suitable condition has been found, optimisation of the condition should be carried out in order to further

improve the quality of the crystals produced. If optimisation fails to yield diffraction quality crystals, a number of techniques such as seeding can be employed. A seed (a small crystal of the protein to be crystallised from a previous trial) provides a template on which further molecules can assemble in order to produce a crystal of a more favourable size. The seed is transferred into a new drop under conditions suitable for growth but ideally, not further nucleation.

Principles of X-ray crystallography

X-rays are electromagnetic radiation, which are diffracted by even the smallest molecules. Even though individual atoms diffract X-rays, it is still not possible to produce a focussed image of a molecule.

Figure 1.3 illustrates the collection of X-ray diffraction data. A crystal is mounted on the goniostat between the X-ray source and the X-ray detector in the direct path of the X-ray beam. The crystal diffracts the source beam into many discrete beams each of which produces a distinct spot in an orderly array. These spots are called reflections because they emerge from the crystal as if reflected from planes of atoms. These reflections are measured using a detector. Several types of detectors are used such as CCD (charge coupled device), Image plate and the area detector.

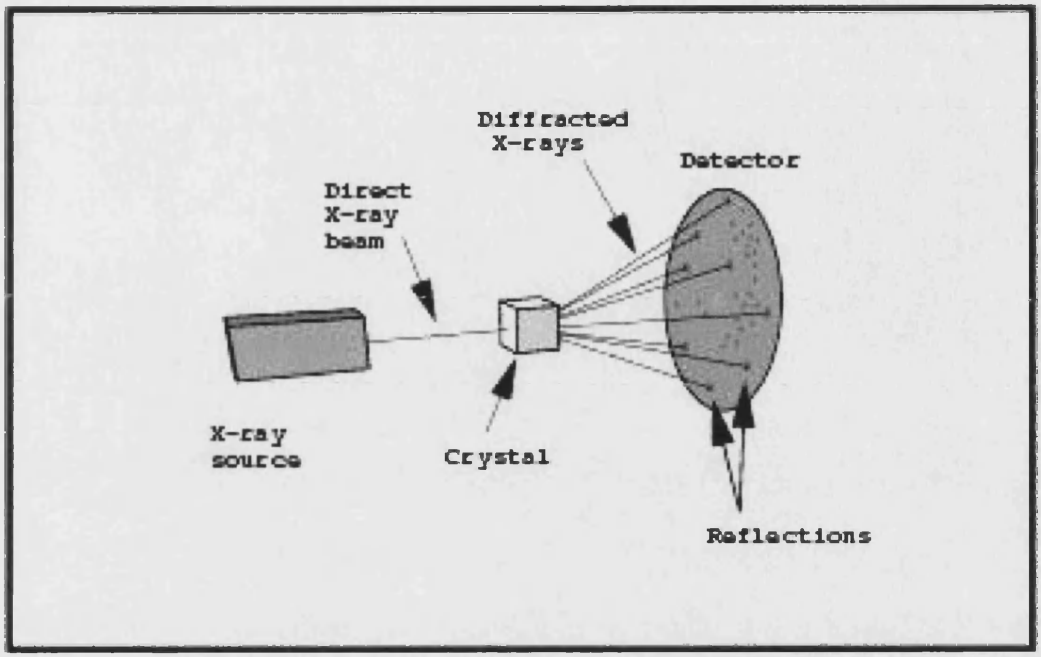

Figure 1. 3: Schematic representation of the data collection set up.

The greater the intensity of the X-ray beam that reaches the detector at a particular position the darker the reflection. The position and intensity of each reflection is precisely measured by the detector and is transmitted in digital form to the computer for analysis. The position of the reflection can be used to obtain the direction in which that particular beam was diffracted by the crystal. The intensity of the reflection is calculated by measuring the optical absorbance of the spot. This gives a measure of the strength of the diffracted beam that produces a particular spot. The position of each reflection can be assigned three co-ordinates or indices in reciprocal space of the diffraction pattern designated *h*, *k*, and *l*. The central beam position is taken as the origin and assigned the co-ordinates (*h, k, l*) = (0, 0, 0) or *hkl* = 000. This reflection is not measured as it is obscured by the direct beam. The other reflections are assigned whole-number co-ordinates counted from this origin. Thus, the parameters we can measure and analyse are the position *hkl* and the intensity I_{hkl} of each reflection. The position of each

reflection is related to the angle by which the diffracted beam diverges from the source beam. For a unit cell of known dimensions, the angle of divergence uniquely specifies the indices of a reflection.

Bragg's law

Bragg's law predicts the angle of reflection of any diffracted beam from specific atomic planes whereby:

$$n\lambda = 2d \sin\theta$$

Where d is the interplanar spacing of that set of planes, λ is the wavelength of the X-rays and n is an integer. For a fixed λ, the closer the separation of the planes the larger the value of θ, the diffraction angle (see Figure 1.4a). The geometrical construction by Ewald can be used to illustrate the nature of space and diffraction geometry. There are two conditions for a diffracted beam, the first on the frequency (wavelength) and the second on the wavevector. Where k denotes the wavevector ($k = 1/\lambda$) and ω the frequency of the incident beam; k' and ω' refer to the scattered beam. Then

a) The scattering is elastic, so that the energy of the X-ray quantum is conserved:

$$\hbar\omega' = \hbar\omega$$

where $\hbar = h/2\pi$ and h is Planck's constant.

By the dispersion relation for electromagnetic waves in free space we have $2\pi\omega' = ck'$ and $2\pi\omega = ck$, so;

$$k' = k$$

b) The scattering condition on the wavevector is that $\delta k = G$

(where $G = ha^* + kb^* + lc^*$), or

$$k' = k + G$$

This leads to the geometric construction shown in Figure 1.4b. The points in the diagram are reciprocal lattice points of the crystal. The vector k is drawn in the direction of the incident X-ray beam and it terminates at the origin of reciprocal space (point A) A sphere of radius $k = 1/\lambda$ is drawn about the crystal position (which is where k starts). A diffracted beam will be formed if this sphere intersects any other point on the reciprocal lattice. As drawn, the sphere intercepts a point (B) connected with the end of k by a reciprocal lattice vector G. The diffracted X-ray beam is in the direction k'. This is a graphical way of saying that:

$$n\lambda = 2d \sin \theta$$

In other words, the process of diffraction from a crystal can be considered to be the rotation of a 3-D grid of points around an origin so that they diffract where they intersect the surface of a sphere centred on the crystal. The origin of this rotation is a point $1/\lambda$ away from the crystal in a direction along the vector of the incident X-rays.

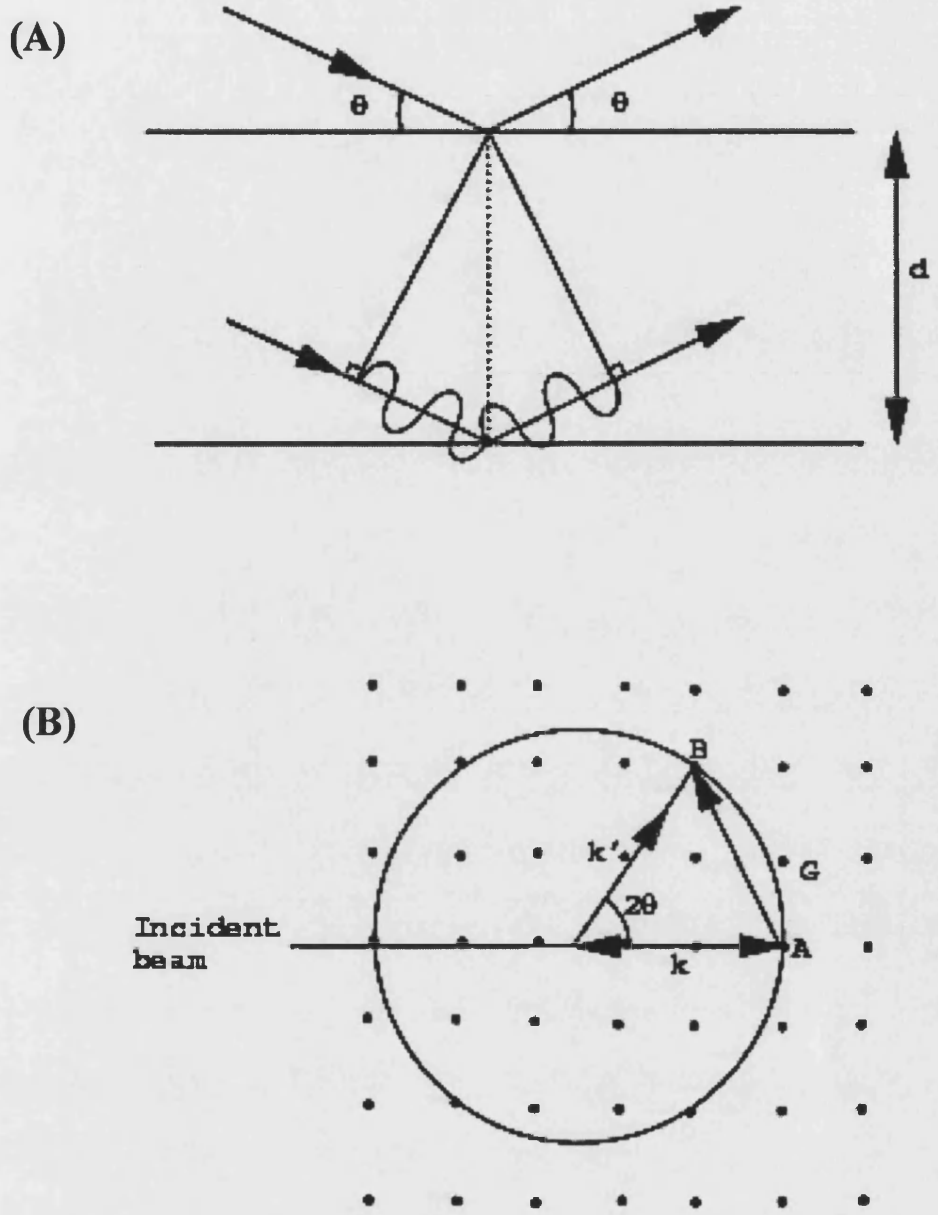

Figure 1.4a: Schematic representation of Bragg's law.
1.4b: The Ewald's Geometric construction.

Unit cell

The unit cell is the smallest and simplest volume element that is completely representative of the whole crystal. We can imagine the crystal as being composed of a repeating array of the unit cell stacked beside and on top of each other like boxes. The image obtained in a crystallography experiment is representative of the average unit cell in the crystal. The location of an atom within the cell is given by a set of three-dimensional cartesian co-ordinates, x, y and z. One of the vertices (a lattice point, or any other convenient point) is used as the origin of the unit cells co-ordinate system and is assigned the co-ordinates $x = 0$, $y = 0$, $z = 0$ (0,0,0) (see Figure 1.5a).

The dimensions of the unit cell are designated by six numbers: the lengths of the three unique edges a, b and c; and three unique angles α, β and γ (Figure 1.5b). A cell in which $a \neq b \neq c$ and $\alpha \neq \beta \neq \gamma$ is called *triclinic*, if $a \neq b \neq c$ and $\alpha = \gamma = 90°$, and $\beta > 90°$, the cell is *monoclinic*. If $a = b$, $\alpha = \beta = 90°$, and $\gamma = 120°$, the cell is *hexagonal*. For cells in which all three cell angles are 90°, if $a = b = c$, the cell is *cubic*, if $a = b \neq c$ the cell is *tetragonal*, if $a \neq b \neq c$, the cell is *orthorhombic*. In the orthogonal co-ordinate system, the **a** edge of the cell is parallel to the *x* axis, **b** parallel to *y*, and **c** parallel to *z*. Thus the atom co-ordinates in real space *x*, *y* and *z* describing real special positions of the atoms in the unit cell, can be related to the position of a reflection in reciprocal space described by its indices *(hkl)* (Blundell and Johnson, 1976).

(A)

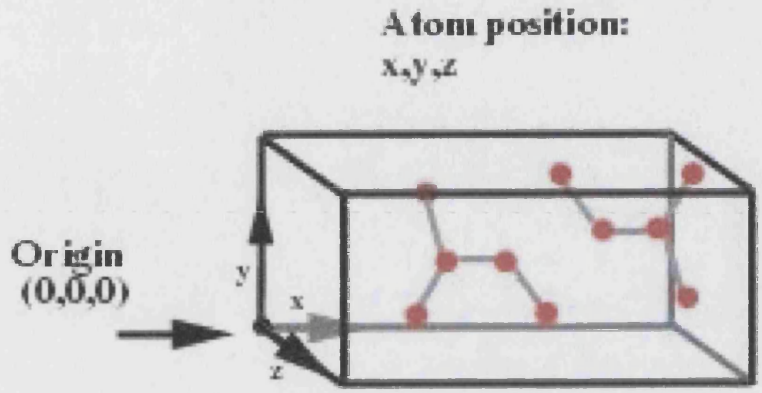

(B)

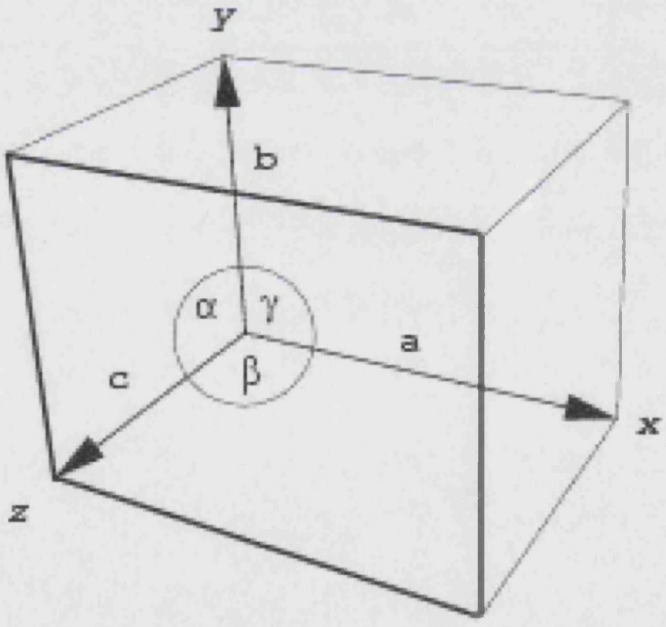

Figure 1.5a: The atomic position within the unit cell.
1.5b: The unit cell dimensions and angles.

X-ray sources

Laboratory sources of X-rays such as sealed tubes and rotating anode tubes accelerate electrons to a voltage of 40-50 kV at a metal target such as copper which has a characteristic wavelength copper Kα radiation (λ = 1.5418 Å). The X-rays produced are then filtered by a monochromator and focused by curved mirrors. Monochromators are made from either nickel or a single crystal. They effectively remove absorbed radiation and have no contribution to the diffraction pattern. The mirror then deflects the focused X-rays through a low angle which increases the brilliance of the beam. Brilliance is defined as the fraction of flux (number of photons emitted) over the angle through which radiation is emitted multiplied by the cross sectional area of the source (Rhodes, 1993).

However, the nature of protein crystallography is better suited to synchrotron radiation (SR). Particle accelerators were originally developed for high-energy physics research into the subatomic structure of matter. The synchrotron radiation, which was produced in circular electron accelerators ('synchrotrons') was little more than an annoying by-product of this process; a loss of energy from the system. Through the increase in use of SR the process of its production and properties has been fine-tuned. As a result modern SR is of high flux (large number of photons), high brightness (well collimated), high brilliance (small source size and well collimated), tuneable, polarized, defined time structure (fine time resolution) with an exactly calculable spectra. SR allows the user to measure the highest possible resolution data, to study crystals with large unit cells and to collect data from crystals too small to be of any use with conventional sources (Daresbury user information, 2001). Synchrotron light is produced when an electron beam travelling at close to the speed of light is accelerated in a magnetic field .The light covers a broad spectrum of the electromagnetic spectrum, from infrared through to hard

X-rays. X-rays produced at synchrotron sources are much more intense than those produced from a conventional laboratory source. This allows experiments to be carried out in a much shorter time. The particles are accelerated by a series of devices to as close to the speed of light as is possible (99.999997% the speed of light) and stored in a storage ring. The first step in producing SR at the Synchrotron Radiation Source (SRS) Daresbury (U.K) is the linear accelerator (Linac), which accelerates particles from 0.511 MeV to 12 MeV and injects them into the booster ring. Here they are accelerated further to 600 MeV before being transferred to the storage ring where they are further accelerated to 2000 MeV. The sixteen-dipole magnets keeping the electron beam on its circular path all produce a broad spectrum of wavelengths, with the most intense output in the soft X-ray region (~$4x10^{-10}$ m). Insertion devices between the dipole magnets further tune and enhance the beam. The first such device is an 'undulator' magnet. The undulator is formed from a periodic array of permanent magnets that are arranged to gently wave the electron beam in a sine-like path through the magnets length. Synchrotron light results from each undulation, and constructive interference between these consecutive emissions gives a very bright and narrow beam of light (high brilliance). The second type of insertion device, a 'wiggler' magnet also known as a 'wavelength shifter', so called because it shifts the most intense output further into the hard X-ray region. These are superconducting magnets which force the beam to take a 'hairpin' turn, causing an enormous amount of acceleration and generating very short wavelengths of light. The beam is then carried from the storage ring to the experimental area through a high vacuum beamline. Within these beams are focussing mirrors to concentrate the synchrotron light at the sample (Helliwell, 1992).

Data collection

Crystals can be mounted in one of two ways, depending on the conditions of data collection. Room temperature data are collected from crystals mounted in thin walled glass capillaries. The crystal is sealed in the capillary in a small amount of the mother liquor from the crystallisation process. Glass has minimal absorption of the scattered X-rays and gives low background which can be corrected for. A second method of crystal mounting is used for collecting data at cryogenic temperatures. Crystals are usually picked directly from the hanging drop with a loop of fine nylon or glass fibre. The crystal is then transferred to a second solution identical to that of crystallisation except that a volume of the water in the solution is replaced with a suitable cryoprotectant such as glycerol or polyethylene glycol. The crystal is then removed by from the solution using the loop which holds it in place by surface tension and frozen immediately in a stream of nitrogen gas. The temperatures used typically in the range of 80 to 100°K. The choice of cryoprotectant is of great importance and varies depending on the crystal. The ideal cryoprotectant should surround the crystal with a thin 'amorphous glass' which prevents the formation of ice crystals which interfere with the diffraction pattern of the crystal. The practice of cryo-crystallography is a relatively new method in modern crystallography. The benefits of collecting data at such low temperatures are numerous: (*i*) Primary and secondary radiation damage is reduced, increasing the lifetime of the crystal, in turn this often allows the collection of a data set from one single crystal which generally has improved quality compared to a data set collected from several crystals. (*ii*) Manipulation of smaller, more fragile crystals is permitted due to a reduction of mechanical stress on the crystal. (*iii*) The low temperature reduces the thermal parameters and allows measurement at higher resolution. New experimental techniques have been established due to the use of cryogenic temperatures; for example

catalytic mechanisms can be deduced by solving the structure of enzymes in complex with reaction intermediates. The low temperature of data collection slows down the reaction mechanism significantly to allow a 'movie of catalysis' to be seen. (Garman and Schneider, 1997; Rodgers, 1994).

Unfortunately, cryogenic data collection is not ideal. Unfavourable changes in the nature of the crystal may be observed. The most common problem is increase in mosaicity. The freezing of the crystal alters the alignment of each unit cell with its neighbours resulting in an amount of disorder. This causes the individual reflections to be more diffuse rather than sharp spots. However, this can be corrected for while processing the data. Unit cell volume changes as the temperature is lowered causing non-isomorphism between crystals. This becomes a problem when collecting native and derivative data sets. The cryoprotectant may interact with the protein causing conformational changes and may also interfere with ligand binding studies. If the cryoprotectant is not optimal, ice may form within the loop and a diffraction pattern for ice is produced which can obscure the data from the protein crystal.

Mounting and alignment of crystals

Once the data collection method has been decided upon the crystal must be mounted and aligned with the X-ray beam. First the crystal is mounted on the goniometer. This is a device that allows the orientation of the mounted crystal to be set precisely. Alignment is carried out by rotating the crystal in one direction; usually perpendicular to the beam and checking to make sure the crystal is in the beam path at 0, 90, 180, 270° of rotation. The initial orientations are determined by physical examination. Well-formed crystals show distinct faces that are parallel to unit cell edges, and the initial diffraction pattern should be obtained by placing a crystal face perpendicular to the

beam. Preliminary examination of the diffraction pattern allows determination of unit cell dimensions and internal symmetry. The diffraction limit of the crystal can be deduced by observing the resolution where a minimum of one third of the possible reflections are distinguishable from background. It is important to collect data to the highest resolution the quality of the crystal will allow. The more reflections that can be used in the integration, reduction and refinement the higher the quality and validity of the structure produced. The spot size and shape (mosaicity) in the direction of rotation should be taken into account when setting the rotation angle as well as the quality of the crystal and the desired resolution. Programs such as Strategy in MOSFLM (Leslie, 1992) and predict can provide a data collection strategy based on an initial diffraction pattern. It is important to note that data cannot be collected in the area of reciprocal space near to the rotation axis (Dauter, 1997). This 'blind region' results from the fact that some reciprocal lattice points do not cross Ewald's sphere surface throughout a 360° rotation. It should also be noted that there are further areas where data cannot be collected due to the Lorentz correction being too high. Lorentz correction is dependent on the geometry of the detector and is used in order to account for the amount of time a reflection spends under diffracting conditions while being rotated through the Ewalds sphere. Less intensity will be seen for those reflections that would spend less time in the Ewald's sphere (i.e. under diffraction conditions) than for the slower moving reflections that spend longer under diffraction conditions. The amount of data required for a complete data set depends on the crystal system. The higher the symmetry, the fewer degrees of rotation and therefore less number of images need to be collected in order to have complete data.

Data integration and reduction

After data collection, the raw intensities must be processed to improve their consistency and to maximise the number of measurements that are sufficiently accurate to be used. The processing of data involves the indexing of each reflection from each diffraction image. There are several computer programmes that automate this process, the most commonly used being the HKL package (Otwinowski and Minor, 1997) and MOSFLM (Leslie, 1992, CCP4, 1994). The HKL program suite consists of: *(i)* DENZO – which carries out autoindexing, refinement and integration. *(ii)* XdisplayF – for image display and measurement. *(iii)* Scalepack– for data scaling. With the increased speed of modern computing and improvements in detector readout time, data collection and processing is often a synchronous task. As such the suite can initially be used to index the first few diffraction images and assess the data being collected in near real time. This allows the user to assess the quality of the data that can be collected and indicates whether it is worthwhile proceeding with data collection with that particular crystal.
Autoindexing using DENZO involves the determination of a standard lattice. A complete search of all possible indices of all reflections is performed. When the program finds values (integers) of one index (e.g. **h**) for all reflections, this is equivalent to having found one real-space direction of the crystal axis (e.g. **a**). The search for real space vectors is performed by Fast Fourier Transform (FFT) and takes advantage of the fact that finding all values for one index for all reflections is independent of finding all values of another index. After the search for real space vectors is completed, the program finds the three linearly independent vectors with minimal determinant (unit cell volume) that would index all of the observed peaks and reduces the cell by conversion into a standard cell according to the International Tables for Crystallography, which contain an index for standard space group and symmetry

classification. The highest symmetry lattice with minimal distortion is selected and processing of the remainder of the data proceeds using the initial estimates as a reference.

A complete set of measured intensities often includes distinct blocks of data obtained from several crystals or different areas of the same crystal. Because of variability in the diffraction quality between crystals and changes in intensity of the X-ray beam over the time-course of data collection one cannot assume that the absolute intensities are consistent from one data block to the next. For this reason, the indexed reflections must be scaled. Scaling is the comparison of reflections of the same index that were measured from more than one crystal or at a different beam intensity. The intensities of identical reflections from these data blocks are then scaled to give an average intensity relative to background levels. The program SCALEPACK (Otwinowski and Minor, 1997) from the HKL suite allows the user to analyse the quality of the diffraction data statistically. There are several ways to assess data quality. Firstly, data completeness (the number of unique reflections measured divided by the number of complete reflections possible) indicates how inclusive the data is in each resolution bin. Secondly, the R_{merge} value, which is the agreement between symmetry related reflections given by:

$$R_{merge}(I) = \frac{\sum_h \sum_i |(I_h - I_{hi})|}{\sum_h \sum_i I_{hi}} \times 100$$

Where I_h is the weighted mean measured intensity of the observations I_{hi} in which the intensities of the symmetry related reflections are compared, thus R_{merge} is the measurement of the disagreement (I_h, I_{hi}). Finally, the ratio of intensity over the error of intensity (I/σI) is in effect the signal to noise of the data. As such it defines a resolution limit because data at high resolution with a I/σI of less than two is not reliably distinguishable from background and cannot be used. σI of a reflection intensity is an

estimate of the accuracy of an individual measurement taking into account height, variance and the number of times the reflection was measured.

In practice, it is a good idea to collect as much data as possible in order to reduce the errors in the observed data.

MOSFLM (Leslie, 1992) consists of a graphical user interface through which the process of data processing can be carried out. Unlike DENZO it does not use key word input so is relatively straightforward to use. The end result of data processing with MOSFLM is an MTZ file of reflection indices with their intensities and standard deviations. The MTZ file is then passed onto the program Scala for scaling and merging. Both the HKL suite and MOSFLM/Scala perform the same tasks and use the same statistical assessment of scaled data.

Structure factor and the Phase problem

The vector (amplitude and phase) representing the overall scattering from a particular set of Bragg planes is termed the structure factor (**F**). The structure factors for the various points on the crystal lattice correspond to the Fourier transform of the electron density within the unit cell and vice-versa. (Blundell and Johnson, 1976)

Whole unit cell

$$\mathbf{F}(h,k,l) = V\int_{x=0}\int_{y=0}\int_{z=0}\rho(x,y,z).\exp[2\pi i(hx + ky + lz)].dx\,dy\,dz$$

A reflection — Electron density

All reflections — Phase

$$\rho(x,y,z) = 1/V \sum_h\sum_k\sum_l |F(h,k,l)| \exp[2\pi i(hx + ky + lz) + i\alpha(h,k,l)$$

Electron density At a point — Amplitude

Unfortunately, the diffraction pattern produced by the crystal contains no information about the phase of the diffracted beam that produces each reflection. The reasons for this become clearer when we look more closely at the nature of X-ray diffraction. When waves are diffracted from a crystal, they give rise to reflections. Each reflection corresponds to a point in the reciprocal lattice and represents a wave with an amplitude and a relative phase. In reality photons are reflected from the crystal in different directions with a probability proportional to the square of the amplitude of this wave. We count the photons, and we lose any information about the relative phases of the diffraction. This is known as the 'phase problem'. This problem can be solved using

several different methods: (*i*) Molecular replacement (MR). By determining the correct orientation and position of a molecule in the unit cell using a previously solved structure as a 'search model'. This model can then be used to calculate phases (Rossman, 1972). (*ii*) Isomorphous replacement (IR) provides indirect estimates of the protein phase angles by observing the interference effects of the intensities on scattered beams by a heavy atom marker (Ke, 1997) (Blundell and Johnson, 1976). (*iii*) Anomalous scattering in which the scattering information of an atom whose absorption frequency is close to the wavelength of the source beam produces phase information. Multi-wavelength anomalous dispersion, requires intensity measurements at several wavelengths, while resolved anomalous scattering requires intensity measurements at one wavelength (Hendrickson, 1991). Both (*ii*) and (*iii*) can be used when solving a novel structure for which there are no homologous structures or when molecular replacement methods fail to produce a satisfactory solution.

Molecular replacement

The basic principle of molecular replacement is to determine a rotation matrix, [C], and a translation vector, $\underline{d}$, to apply to the co-ordinates of the search model $\underline{x}$ to solve the target structure $\underline{x}'$. Hence,

$$\underline{x}' = [C]\underline{x} + d$$

The problem is six dimensional because it involves three rotational and three translational parameters. This is simplified by separating the search into two stages, namely the rotation and translation searches.

The search model is placed in tentative positions in the unit cell and agreement between the calculated and observed structure factors for each placement is assessed. Several factors can affect the success of this procedure. Firstly, The homology between the search model and the actual molecule should be high. Secondly, the quality and completeness of the data should be as high as possible. Other factors include the relative size of the search model compared to the unit cell and the how the agreement between the model and experimental data are assessed.

Several programs are available for solving structures by molecular replacement. AMoRe (Automated Molecular Replacement) , by far the most commonly used, is part of the CCP4 program suite (CCP4, 1994; Navaza, 1994; Navaza and Saludjian, 1997). AMoRe consists of a set of programs to calculate and assess the rotation function (ROTING) and translation function (TRIANG). Peak height and correlation coefficient are used to assess the rotation and translation, a map is calculated (FFT) and the model is then submitted for rigid body refinement (FITING).

Isomorphous replacement and anomalous scattering

In isomorphous replacement, the idea is to make a change to the crystal that will perturb the structure factors and, by the way that they are perturbed, to make some deductions about possible phase values. Heavy atoms are introduced to the crystal through soaking, changing the scattered intensity significantly by disproportionately contributing to the overall intensity. All the electrons in the heavy atom will scatter essentially in the same phase. This means that different heavy atoms contribute to the scattered intensity in proportion to the square of the number of electrons they contain. For example, a uranium atom contains 15 times as many electrons as a carbon atom, so its contribution to the intensity will be equivalent to that of 225 carbon atoms. As a

result, the change in intensity from the addition of just one uranium atom to each molecule of protein in the crystal is easily measured. In practice, diffraction data is collected for both native and heavy atom soaked crystals. The differences in scattered intensities will largely reflect the scattering contribution of the heavy atoms, and these differences can be used to plot a Patterson map. Because there are only a few heavy atoms present, such a map should be relatively easy to deconvolute. Once the positions of the heavy atoms in the crystal are known, we can calculate their contribution to the structure factors. If the heavy atom doesn't change the rest of the structure, then the structure factor for the derivative crystal (F_{PH}) is equal to the sum of the protein structure factor (F_P) and the heavy atom structure factor (F_H), or

$$F_{PH} = F_P + F_H$$

By producing a Harker construction we are able to calculate the two possible values for F_P that agree with both the measured amplitudes and with the heavy atom model. By preparing a second derivative crystal with heavy atoms that bind to other sites it is possible to resolve this twofold phase ambiguity as only one phase choice will be consistent with all the observations from both derivatives and the native crystal.

If the X-ray photon energy is close to the transition energy of electrons from certain atoms (e.g heavy atoms) in the structure there will be a small shift in phase and amplitude. This is known as anomalous scattering. The effect of anomalous scattering is to make the amplitude of the Friedel mates different. If we have a model for the anomalous scatterers in the crystal, we can draw vectors for their contribution to the structure factors for the Friedel mates and construct a Harker diagram. By collecting data at several wavelengths near the absorption edge of an element in the crystal, we can obtain phase information analogous to that obtained from MIR. This technique is called MAD (multiple-wavelength anomalous dispersion). The most common use of MAD is

to introduce selenomethionine into the protein structure in place of a methionine. The selenium atoms have a strong anomalous signal at wavelengths that can be obtained from synchrotron sources.

Refinement

The correctly positioned molecule(s) from molecular replacement, MIR or MAD must now be refined in order to produce a valid representation of the crystal structure. The model will differ from the actual molecule in the crystal in terms of amino-acid sequence and main chain and side chain conformation. The objective of crystallographic refinement is to optimise the agreement between the atomic model with the observed data within the bounds of accepted chemical geometries. Because of the poor observation : parameter ratio typical of macromolecular crystallography, it is possible to overfit the data. So, validation is of paramount importance. There are different aspects to validation. Some types of validation look at the fit to the diffraction data. The agreement of observed and calculated structure factors is often measured with the traditional R-factor, which is the average fractional disagreement:

$$R = \Sigma(|F_o - F_c|)/\Sigma|F_o|$$

The problem of overfitting the data can be avoided by excluding 5-10% of the data from refinement (test set). The test data are used to calculate R-free, which is computed in the same way as the conventional R-factor but using only that subset of data. There is no pressure to overfit R-free, which leads to a more valid model. This idea, introduced by Axel Brunger is known as cross validation (Brünger *et al.*, 1992).

Crystallographic refinement can be formulated as a search for the global minimum of the target function (Brünger *et a.l*, 1997)

$$E = E_{chem} + w_{xray} E_{xray}$$

Where E_{chem} is the empirical potential energy function of all atomic positions, describing covalent (bond length, bond angle, torsion angle, chiral centres, and planarity of aromatic rings) and non-covalent (van der Waals, hydrogen bonding, and electrostatic) interactions. w_{xray} is a weight chosen to balance the forces arising from each term. The choice of w_{xray} can be critical : too large, and the refined structure will show deviations from ideal geometry; too small and the refined structure will not satisfy the diffraction data.

$$E_{chem} = \sum_{bonds} k_b (r - r_0)^2 + \sum_{angles} k_\theta (\theta - \theta_0)^2$$

$$+ \sum_{dihedrals} k_\phi \cos(n\phi - d) + \sum_{chiral,\ planar} k_\omega (\omega - \omega_0)^2$$

$$+ \sum_{atom\ pairs} (ar^{-12} + br^{-6} + cr^{-1})$$

The parameters of the empirical potential energy E_{chem} are inferred from experimental and theoretical investigations. Additional restraints and constraints such as fixing atom positions, bond lengths, angles and dihedrals improve the ratio of observations to the refined parameters. If multiple copies of the molecule are present in the asymmetric unit, non-crystallographic symmetry can be used to average equivalent molecules, increasing the signal to noise ratio.

E_{xray} describes the difference between observed and calculated diffraction data:

$$E_{xray} = \sum_{h} [\,|\mathbf{F}_{obs}(\mathbf{h})| - k\,|\mathbf{F}_{calc}(\mathbf{h})|\,]^2$$

This equation only incorporates information about the amplitudes of the observed reflections. Phase restraints can be added based on the difference between experimental phases and those calculated from the model:

$$E_{xray} = \sum_{h} [|F_{obs}(\mathbf{h})| - k|F_{calc}(\mathbf{h})|]^2 + w_p \sum_{h} f[\phi_{obs}(\mathbf{h}) - \phi_{calc}(\mathbf{h})]$$

Where w_p is the weight given to the phase restraint and f is a square-well function with a width equal to the arccosine of the Figure of merit [m(**h**)] for each reflection.

Methods of refinement

There are two basic types of approach to optimisation; stochastic methods and deterministic methods. Deterministic methods such as Conjugate Gradient (CG) which identifies the nearest minimum in the target function by increasing the radius of convergence; and least squares (LSQ) – the weighted sum of squares of the deviations between the observed and calculated quantities. Optimisation problems in protein crystallography generally suffer from there being multiple minima, which arise largely from the high dimensionality of the parameter space (at least three times the number of atoms in the molecule). Both LSQ and CG tend to have problems with the many local minima of the target function. LSQ assumes that the current phase is correct, that the atoms should move towards or away from a certain plane rather than an unknown plane. These methods are simply not capable of shifting the atomic co-ordinates enough to correct errors in the initial model. Maximum likelihood target functions avoid these assumptions (Brünger *et al.*, 1997). Simulated annealing is an optimisation technique particularly suited to overcoming local minima thus exploring a larger area of parameter space. Annealing is a physical process whereby a solid is heated to sufficient temperature such that it becomes a viscous liquid of randomly arranged particles. Slow cooling of the liquid phase causes the particles to arrange themselves in the lowest energy state. By formally defining the target E as the potential energy of the system the annealing process can be simulated. Simulated annealing as a molecular dynamics

refinement method, in combination with the optimisation techniques is the most commonly used protocol. The temperature of the system initially at 300°K is heated to 5000°K before cooling. The simulated annealing temperature has no physical meaning and simply defines the likelihood of overcoming the barriers of the target function. The most commonly used programs for crystallographic refinement are CNS (Brünger, 1998), X-PLOR (Brünger *et al.*, 1992) and REFMAC as part of the CCP4 program suite (CCP4, 1994). All three of these programs use minimisation and simulated annealing in combination. Uniquely, CNS uses a combined simulated annealing/maximum likelihood protocol for model refinement (Brünger *et al.*, 1998, Adams *et al*, 1997). The use of a maximum likelihood protocol necessitates the computation of cross-validated σ A values. The cross-validated σ A error estimates and the weight between X-ray diffraction target function and the geometric energy function are recalculated during the refinement procedure. Since the maximum likelihood function depends on σ A error estimates recalculation is extremely important, so this step is performed after the initial energy minimisation and after molecular dynamics. The position (*x,y,z*) and thermal parameters (B – factor) of each atom are then refined against the X-ray observations. It is here that the R-factor becomes important. The value of R indicates the agreement between calculated and observed intensities. Successive cycles of refinement followed by rebuilding of the model are necessary in order to produce a well refined structure with an R-factor of approximately 0.20, and an R-free in the region of 0.25 –0.28. Other ways of assessing the model as refinement progresses include the RMS deviation of bond lengths and angles from ideal. Large errors within the structure are not usually corrected for by the previously mentioned refinement procedures. These errors are normally corrected by manual rebuilding of the model assisted by different types of electron density maps. Calculation of omit maps is performed to remove model

bias from ambiguous areas of the model. Techniques such as bulk solvent correction are used to improve the signal to noise ratio of electron density maps for missing parts of the model.

The program 'O' is by far the most widely used model-building tool in crystallography (Jones *et al*, 1991). It provides a set of tools for manipulating the model and viewing electron density maps. The model can be rebuilt using a set of macros to rotate/move small parts of the model manually, insert, mutate or delete residues and assign side chain rotamers from a database. Local real space refinement can also be carried out during rebuilding in order to improve the model. The process of model building and refinement is an iterative process that continues until compliance is reached.

Structure analysis

Once the structure has been refined to a satisfactory $R_{conventional}$ and R_{free} value, the overall architecture of the molecule is assessed. The Ramachandran plot (φ and ψ angles of the polypeptide backbone) allows the evaluation of the geometry of the structure. Programs such as PROCHECK (Laskowski *et al.*, 1993) provide this and various other assessments on geometry, bond length and temperature factors based on an analysis of 118 structures of resolution at least 2.0Å and an $R_{conventional}$ less than 20%. Close examination of the intra- and intermolecular contacts in the crystal and polar and non-polar interactions should also be performed. By superposition of the structure with known homologous structures, other crystal forms of the same structure, or native/mutant comparisons, functional regions can be assessed.

Structure deposition

Once a structure has been completed the atomic co-ordinates, experimental details, sequence data, points of interest about the structure, references, contact information and the names of the authors are submitted to a central database. The Protein Data Bank (PDB) is the global repository for structural information for X-ray crystallographic, NMR and theoretical models (Bernstein *et al*, 1977). Deposition is usually carried out via a web interface such as Auto Dep. The PDB is an open access searchable database that provides unique research resources for the biomedical community.

-2-

Chapter two

Superantigens: Structure, function and diversity

Overview of Superantigens

The focus of this research is the structural and functional features of superantigens (SAgs). SAgs fall into two broad categories; bacterial and viral. Bacterial superantigens are potent T cell stimulatory protein molecules produced by *Staphylococcus aureus* and *Streptococcus pyogenes* (Marrack and Kappler, 1990). Their function in the microbe appears primarily to debilitate the host sufficiently through their effects on cells of the immune system to permit the causation of disease (Kotzin *et al.*, 1993). Their superantigenic activity can be attributed to their ability to bind to both MHC class II molecules and T cell receptors by forming a trimolecular complex (Marrack and Kappler, 1990). Unlike conventional antigens they are not processed internally by antigen presenting cells (APC), and are thus not displayed as peptide antigen in the peptide-binding groove of the MHC class II molecule. Superantigens bind to APCs on the outside of MHC class II molecule and to T cells *via* the external face of the T cell receptor (TCR) V_β element (Figure 2.1). Each superantigen interacts with a specific V_β region of the TCR, stimulating a large fraction of T cells (for example, up to 10% of resting T cells) (White *et al.*, 1989).

Staphylococcal enterotoxins (SEs) A, B, C1-3, D, E, H; toxic shock syndrome toxin-1 (TSST-1); the streptococcal pyrogenic exotoxins (Spes) A, C, H; streptococcal mitogenic exotoxin SME-Z_2 and streptococcal superantigen (SSA) are the most well studied superantigens to date :for a recent review see Papageorgiou and Acharya (2000). Other pathogens, such as *Mycoplasma arthritidis* and *Yersinia enterocolitica* have also been shown to secrete superantigenic proteins, though they are yet to be fully characterised (Cole *et al.*, 1996). Viral superantigens are implicated with infections caused by rabies virus, Epstein-Barr virus, human herpesvirus including HIV (Huber *et*

al., 1996, Huber, 1995). Throughout this work discussion will be focussed on bacterial superantigens.

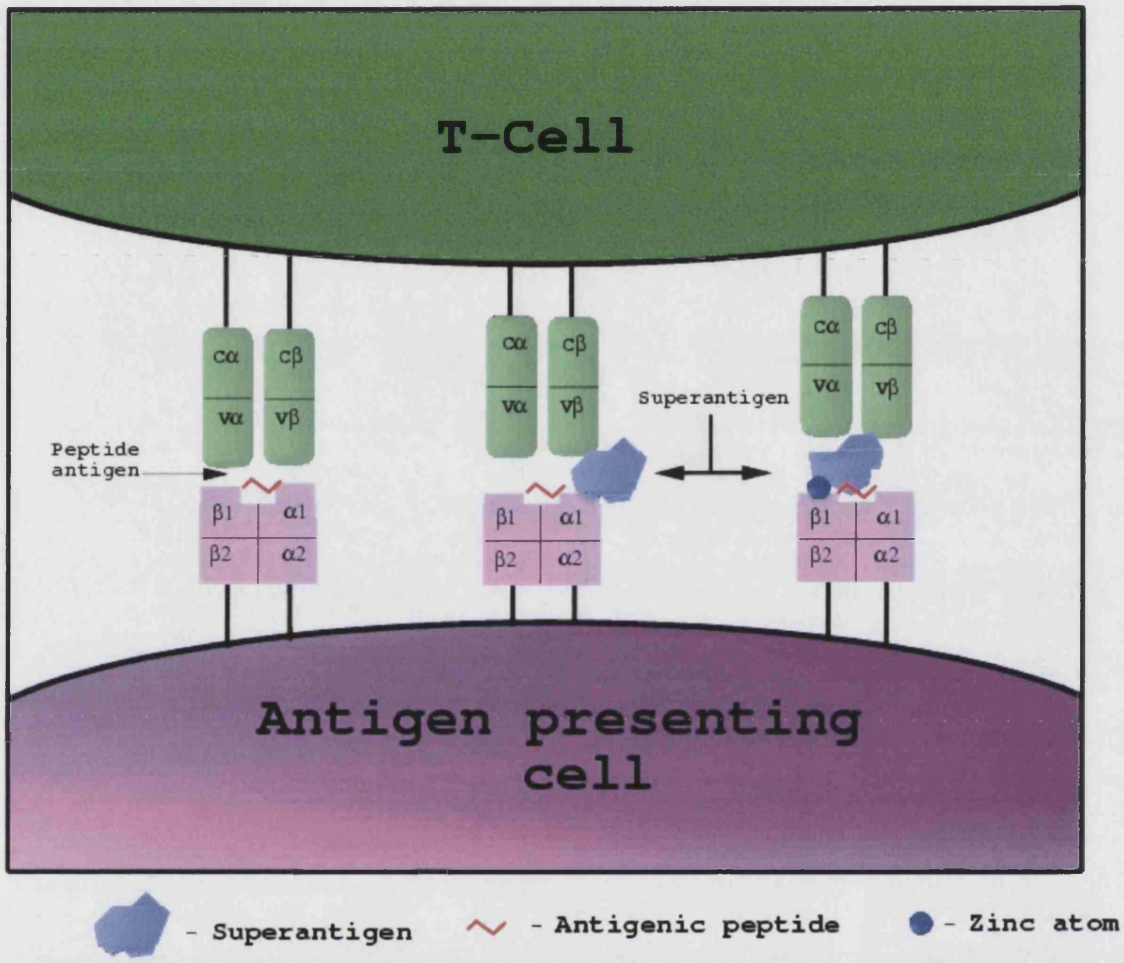

Figure 2.1: Schematic representation illustrating the differences between conventional peptide antigen presentation and superantigen presentation to MHC class II and TCRs: *Left to Right*- conventional antigen is processed by the antigen presenting cell and displayed as discrete peptide fragments within the peptide binding groove of MHC class II molecules. Interaction occurs between TCR and MHC class II molecule through two possible modes: a) superantigens bind to the solvent exposed face of the MHC class II molecule (α1) *via* its generic site, forming a bridge between TCR (V_β) and MHC class II molecule; b) Interaction also occurs between TCR V_α and MHC class II molecule involving the β-chain (β1) where the superantigen binds to MHC class II molecule via a bridging zinc atom. In both cases the MHC class II associated antigenic peptide has been shown to influence T cell recognition of superantigen/MHC class II molecule complex.

Common Architecture

The superantigen family comprises proteins of 22-29 kDa in size that are highly resistant to proteases and heat denaturation (Marrack and Kappler, 1990).

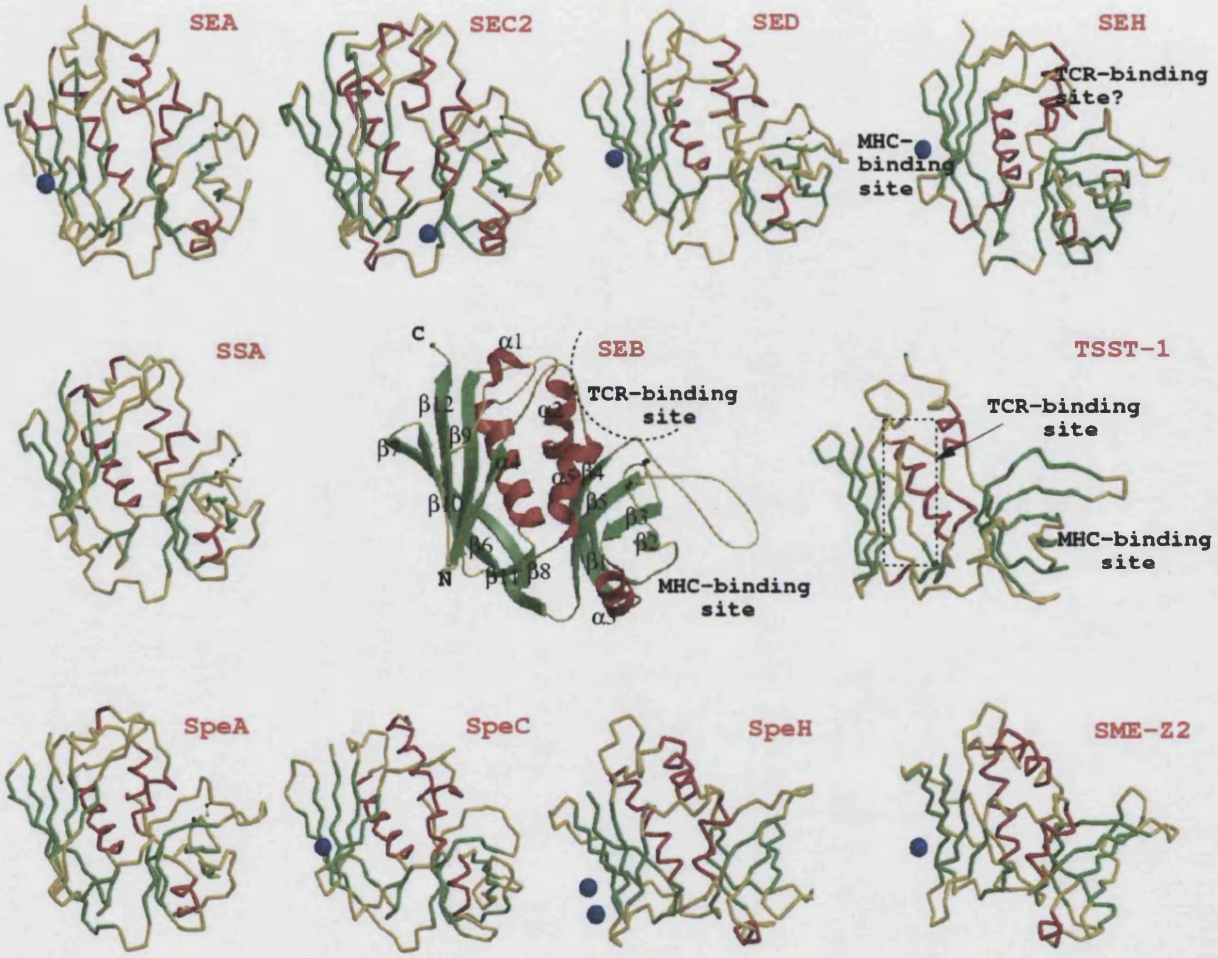

Figure 2.2: Ribbon diagrams of the known superantigen structures illustrates the 2 domain architecture of the family. SEB (centre), TSST-1, and SEH are shown with annotations. The blue spheres represent zinc atoms.

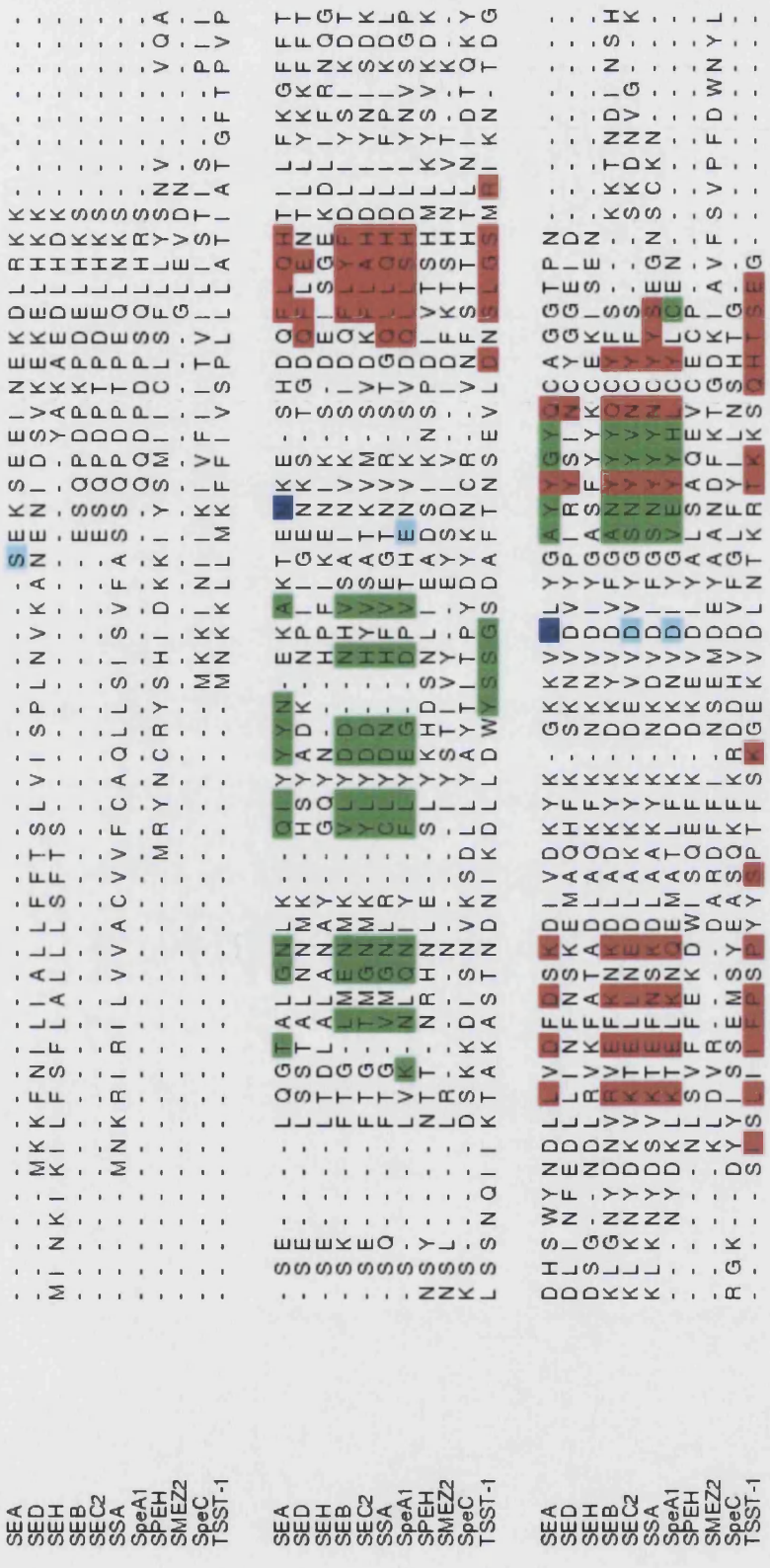
SEA
SED
SEH
SEB
SEC2
SSA
SpeA1
SPEH
SMEZ2
SpeC
TSST-1

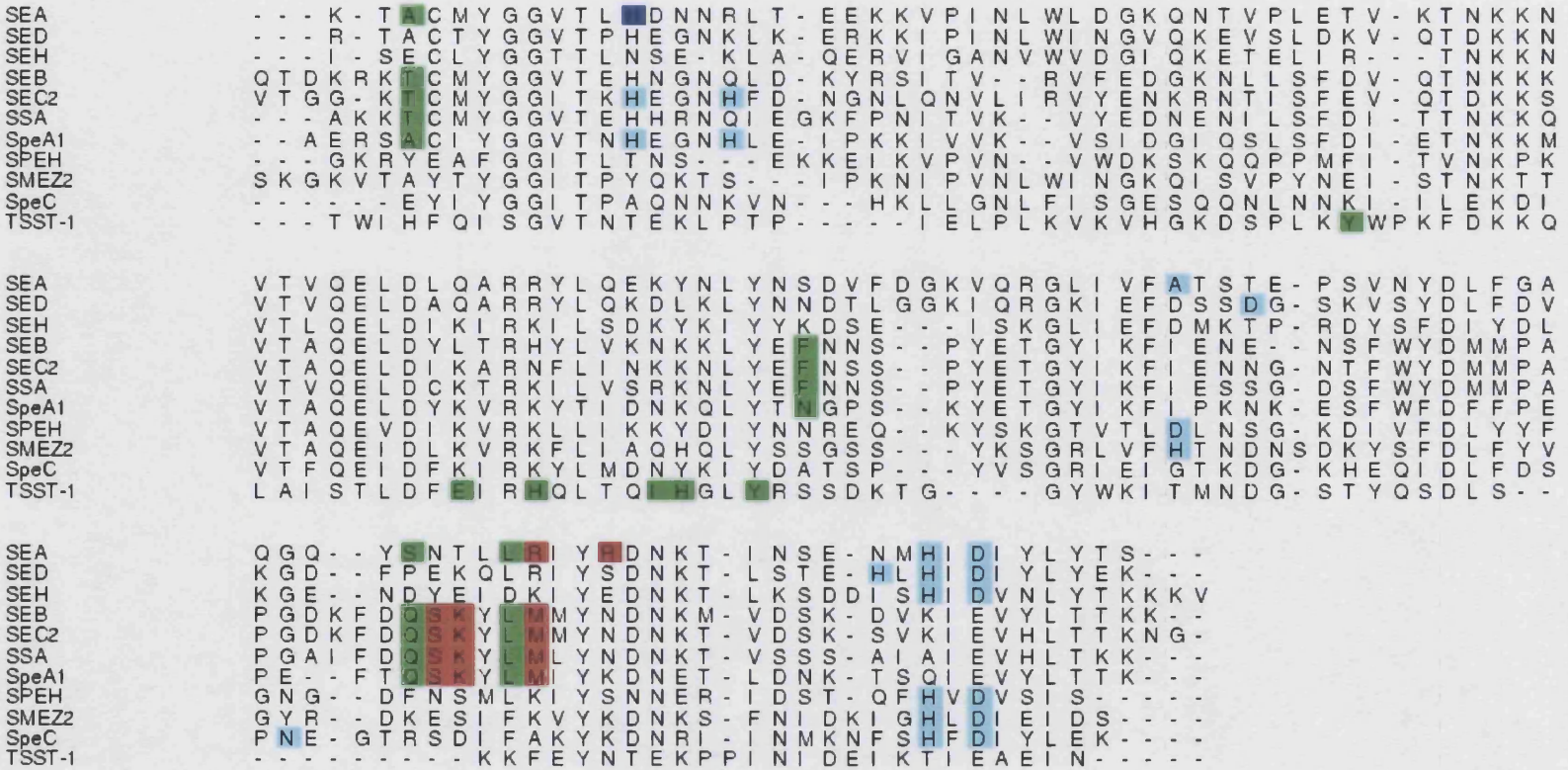

Figure 2.3: Multiple sequence alignment of superantigens with known structure. Residues implicated in TCR recognition are shown in green, residues involved in MHC II binding are shown in red, and those residues that act as zinc ligands are shown in light blue. The secondary zinc site in SEA is shown in dark blue. This figure was prepared using the program Alscript (Barton, 1993).

Based on amino acid sequence alignment of streptococcal and staphylococcal superantigens (Figure 2.3) it is possible to divide them into three subfamilies- (a) SEA, SED, SEE, SEH and SEI; (b) SEB, SEC1-3, SpeA1-3, SSA and SEG and (c) SpeC, SpeJ, SpeG. TSST-1 has ~28% homology with other SEs and cannot be grouped with any of these subfamilies.

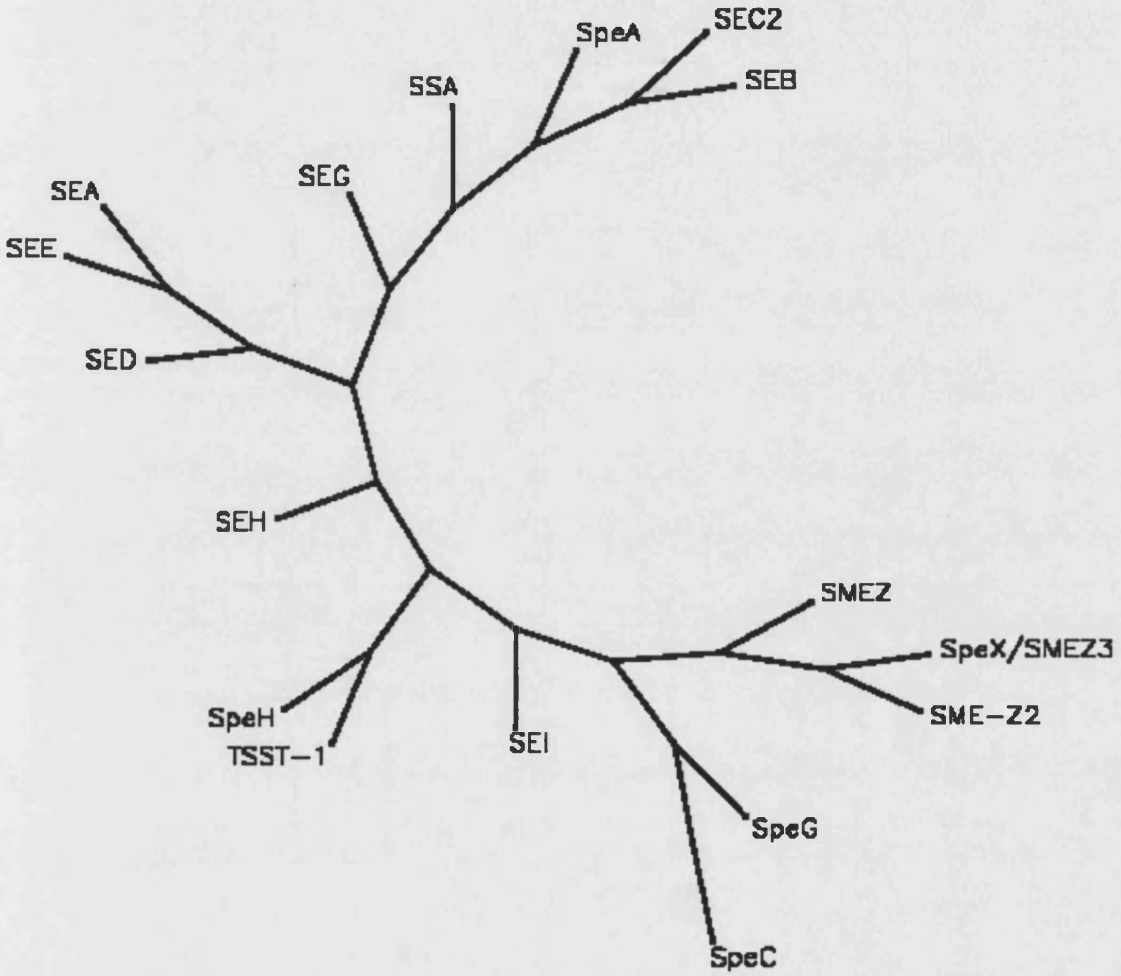

Figure 2.4: Dendrogram (un-rooted) of the members of the superantigen family. Allignments created using the program ClustalX (Thompson *et al.*, 1994).

Calculation of an un-rooted tree including SpeH, SpeX, SMEZ, and SMEZ2 as shown in Figure 2.4 gives a slightly different grouping. SEG, SSA, SpeA, SEC2 and SEB form one family, SEA, SED, SEE, and SEH form a second family, SMEZ1, SMEZ2, SpeX, SpeG, and Spec a third family, and TSST-1 is grouped SpeH and SEI.

Comparison of the three-dimensional structures of superantigens [see Papageorgiou and Acharya (2000) and references therein] reveals a conserved two-domain architecture (N- and C- terminal domains) and the presence of a long, solvent-accessible α-helix spanning the centre of the molecule (Figures 2.2 and 2.5). The N-terminal domain has considerable structural similarity to the oligosaccharide/ oligonucleotide-binding fold (OB-fold) found in other proteins of unrelated sequence such as staphylococcal nuclease and the AB_5 toxins, and is characterised by the presence of hydrophobic residues in its solvent exposed regions. As its name implies, in other proteins the OB-fold is involved in DNA binding or carbohydrate recognition though no such activity has been attributed to superantigens so far. The C-terminal domain is composed of a four-stranded β-sheet capped by the central α-helix. Structurally, it is reminiscent of the β-grasp motif found in other proteins such as ubiquitin and 2Fe–2S ferredoxin. Other common features include a highly flexible disulphide loop (see Figure 2.5), present in the N-terminal domain of SEs and SpeA, but not in TSST-1 and SpeC. This flexible loop is implicated in the emetic properties of the SEs and indeed mutation of the residues that form this disulphide loop to alanine abolishes the emetic activity in SEC1 (Hovde *et al.*, 1994). Moreover mutation of either one of the cysteine residues in SpeA also reduces its ability to stimulate certain populations of T cells significantly (Kline and Collins, 1997).

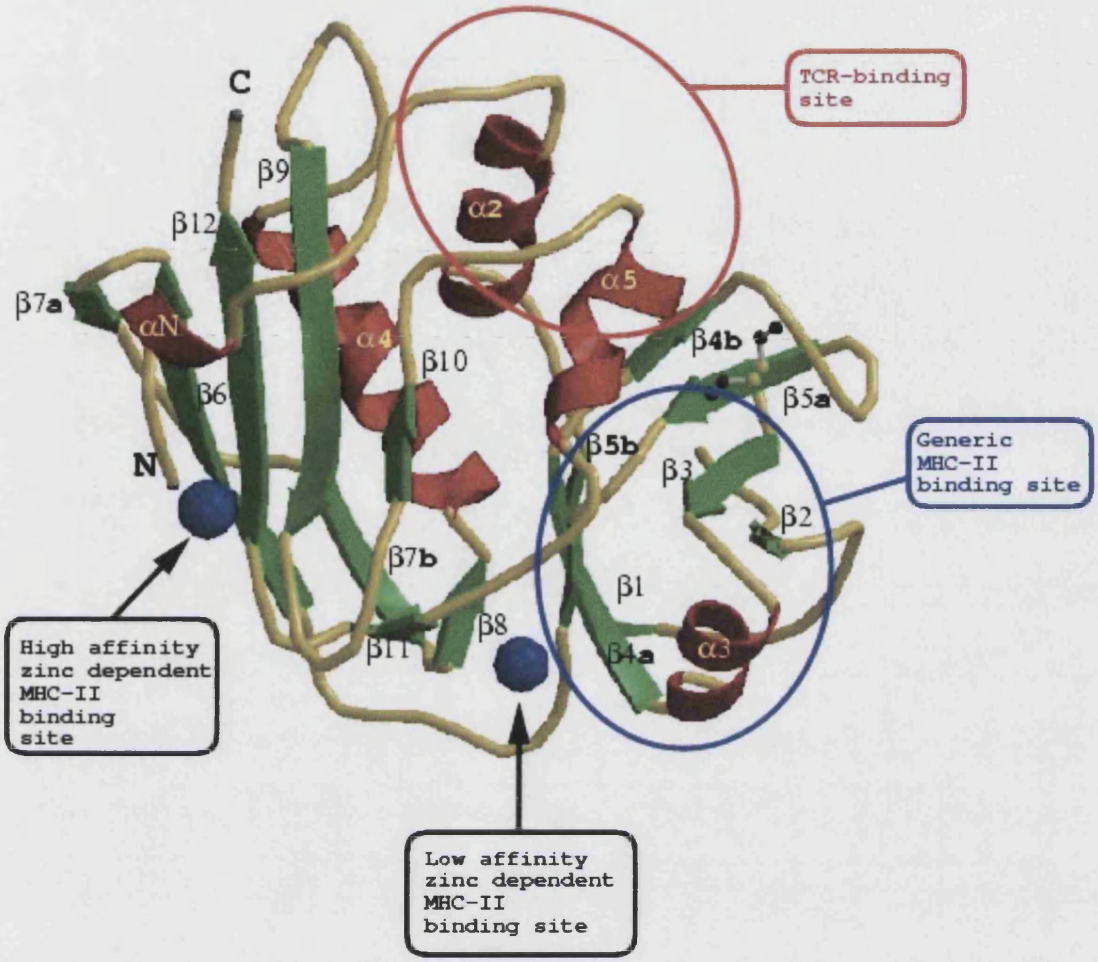

Figure 2.5: Ribbon diagram of SEA as a representative superantigen highlighting the common structural features of the family.

Purification Procedures

Several procedures have been adopted to purify superantigens in their native forms (Avena and Bergdoll, 1967, Chu *et al.*, 1966, Ende *et al.*, 1983, Reynolds *et al.*, 1988, Robern *et al.*, 1975). Most of them are multi-step procedures and are not always suitable for large scale toxin production. Brehm *et al* (1990) developed a single-step dye ligand chromatography assay for the purification of SEA, SEB, SEC2, and TSST-1 using Red A gel. The procedure caters for both small- and large-scale preparations of toxins from

S. aureus with good yields. Many studies have favoured the use of recombinant toxins. These proteins can be produced as fusion proteins such as GST tagged (Proft *et al.*, 1999; Sundberg and Jardetzky, 1999) or His-tagged toxins (Munson *et al.*, 1998) allowing a simple two-step cleavage and purification method. In all cases, whether native or recombinant, further purification by isoelectric focussing may be required to produce a single isoform. The exclusion of bioactive contaminants during toxin purification is esstential. For example, native SpeA, commercially available SpeA and recombinant SpeA preparations were all shown to be contaminated with DNase and an unknown protease. This contamination interferes with many immunological assays as DNase has been shown to independently induce cytokines (Fagin *et al.*, 1997). A balance must be achieved therefore, between ease of purification and the purity of the final sample.

Detection Methods

There are several reliable assays for the detection of bacterial superantigens; namely the micro-slide, double diffusion and ELISA based methods. Qualitative assays for bacterial superantigens are performed using the following technique (Schlievert, 1988). Briefly, an agar plate cultured with the test organism has hyperimmune antisera and purified superantigen added to separate wells punched 4 mm to each other from the growing organism. After 12 hours incubation at 37°C the plate was examined for the formation of a precipitation arc that forms between antibodies present in the anti-sera and the superantigen, both in its purified form and from the cultured organism, if present. Quantitative assays such as the double immunodiffusion allow an estimate of the amount of toxin present in an isolate by comparison to an assay performed on a control toxin of known concentration. The detection range of this method, approximately 4 μg/ml, can be extended 2- to 4- fold by drying and staining the slides

(Schlievert, 1988). Several ELISA based methods for the detection of superantigens have been developed (Parsonnet *et al.*, 1985, Sriskandan *et al.*, 1996a, Sriskandan *et al.*, 1996b) allowing multiple samples to be tested accurately and relatively quickly. Commercially available kits based on several of the above methods are available such as Ridascreen (R-Biopharm GmbH, Germany) and TECRA (International Bioproducts, Redmond, WA, USA) which are ELISA kits for the detection of SEs A to E. A reversed passive latex agglutination assay kit, SET-RPLA (Oxoid, Ontario, Canada) can also be used for the detection of SEA, B, C, D and E.

Binding to MHC class II Molecules

Structural analyses using X-ray crystallography have shown that MHC class II molecules possess two distinct superantigen binding sites [for details see Papageorgiou and Acharya (2000)]. The first, a low affinity binding site (referred to as the generic site) is located on the α-chain of the MHC class II molecule and the second, a high affinity (~100 times higher affinity than the generic site) zinc-dependent site is located on the β-chain (Figure 2.1). The structures of SEB and TSST-1 in complex with HLA-DR1 *via* the low affinity site (Jardetzky *et al.*, 1994), SpeC in complex with HLA-DR2 (Li *et al.*, 2001) and SEH in complex with HLA-DR1 (Petersson *et al.*, 2001) *via* the high affinity site have yielded a great deal of information about the binding of SAgs to MHC class II molecules (Figure 2.6 A – D). Each superantigen binds to different haplotypes of class II molecules to varying degrees. Whilst the majority of the superantigens including TSST-1 and SEB bind preferentially to HLA-DR alleles, superantigens such as SEC, SpeA and SSA bind predominantly to HLA-DQ alleles (Sundberg and Jardetzky, 1999).

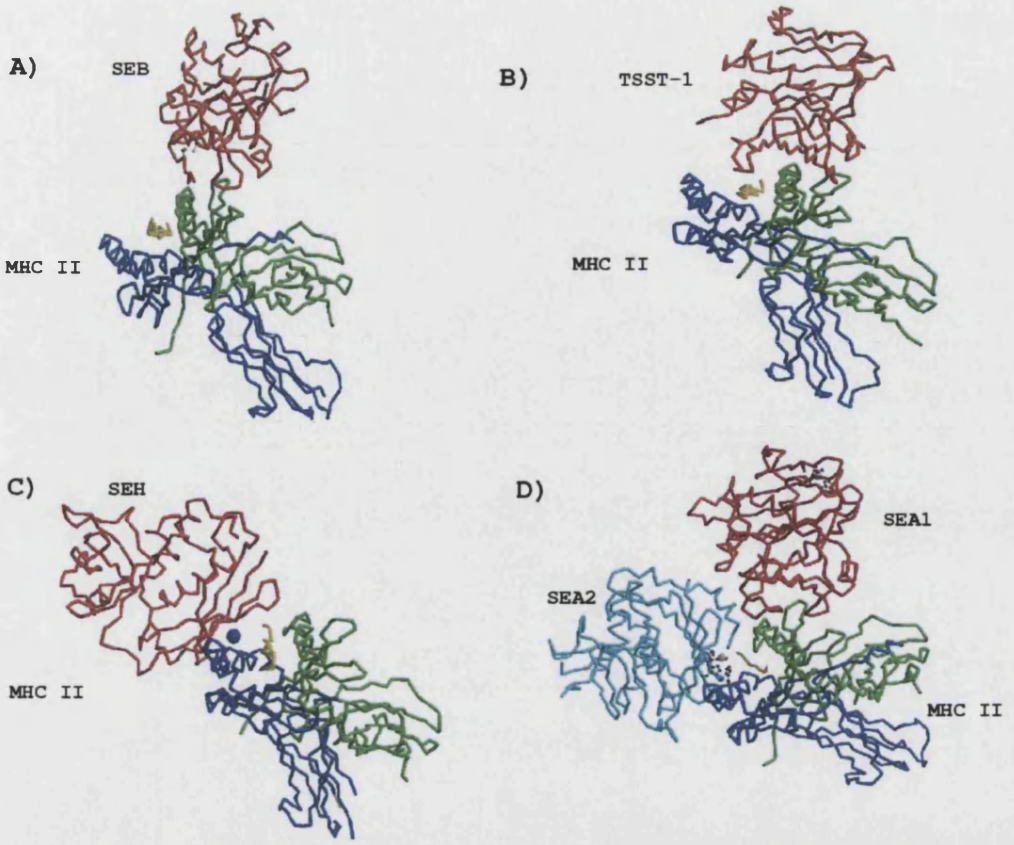

Figure 2.6: Ribbon diagrams of the structures of SAgs complexed with MHC class II molecules. **(A)** SEB – DR1 complex (Li *et al.*, 1998). **(B)** TSST-1- DR1 complex (Kim *et al., 1994).***(C)*** SEH in complex with DR1 via its high affinity zinc binding site (Petersson *et al.*, 2001). **(D)** A model of the bivalent SEA binding to DR1 (Tiedemann *et al.*,1995). Superantigens in red, MHC II βchain blue α chain green, zinc ions are shown as blue spheres and the antigenic peptide is coloured yellow.

For both SEB and TSST-1 in complex with HLA-DR1, similar binding modes with the α-chain of DR1 involving the solvent exposed, hydrophobic core at the N-terminal domain of the toxin molecule were evident (Figures 2.6A, 2.6B, 2.7). Similar hydrophobic ridge regions (except SpeC, SpeH and SME-Z_2) form the generic site and are implicated in class II binding. However, in the case of TSST-1 additional contacts with the peptide antigen were also present (Kim *et al.*, 1994). Indeed, truncating the C-terminal end of the peptide dramatically effects TSST-1 binding to murine I-Ab (Wen *et al.*, 1997).

In addition, several members of the superantigen family (except SEB, TSST-1 and SSA) possess either one or two zinc binding sites (Papageorgiou and Acharya, 2000) (for

details see Table 2.1, Figures 2.2, 2.5, 2.6). The presence of the zinc ion is important for the recognition of class II molecules. Mutational and structural analyses have identified a high affinity zinc binding site in SEA at the C-terminal domain with a K_d of 100 nM for DR1 recognition (Fraser *et al.*, 1992). However, the zinc-independent generic site at the N-terminal domain has considerably lower affinity (K_d of 10 μM) for class II binding. If the two binding sites co-exist, SEA shows a K_d of 13 nM. Mutations of residues in either of these sites results in a toxin unable to induce cytokine expression in peripheral blood mononuclear cells (PBMC) (Abrahmsen *et al.*, 1995). Thus in the case of SEA molecule, it possesses two distinct MHC class II binding sites which might enable the formation of the trimeric SEA-MHC-SEA complex as observed in solution experiments (Tiedemann *et al.*, 1995) (Figures 2.6 D and 2.7). Similar arguments can be put forward for SEE as both SEA and SEE possess identical zinc ligands.

In the case of SEC and SpeA, the high affinity zinc-binding site observed in SEA is not present. However, a new zinc binding site with somewhat lower affinity compared with the high affinity zinc binding described above (the estimated dissociation constant for the zinc ion in SEC2 is <1 μM) was identified at the N-terminal domain which also appears to be important for MHC class II binding (Figure 2.5) (Papageorgiou *et al.*, 1999). We shall refer to this site as the secondary zinc-binding site. In SED (Sundstrom *et al.*, 1996) and SpeC (Roussel *et al.*, 1997), the situation is slightly different since this toxin can form zinc-dependent homodimers (in SED) and zinc-independent homodimers (in SpeC) and binds solely to the β-chain of MHC class II molecule by a zinc-mediated mechanism similar to that of SEA and could form either trimers or tetramers. A similar binding mechanism has been proposed for SEH which also lacks a generic MHC class II binding site (Hakansson *et al.*, 2000) (Figures 2.6 and 2.7).

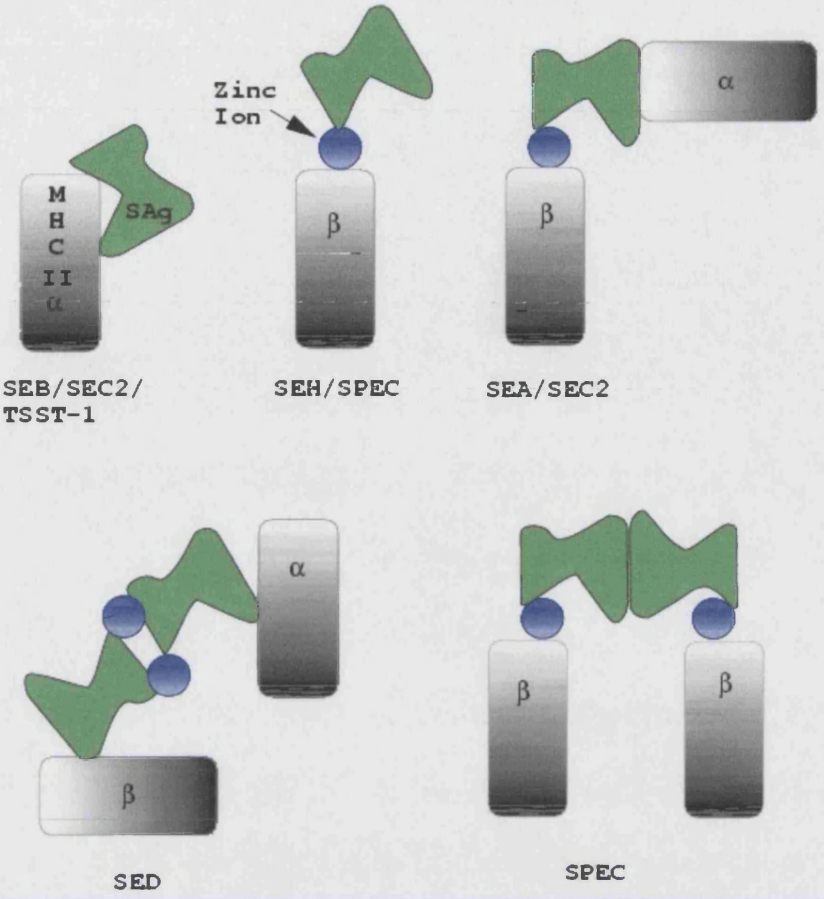

Figure 2.7: Schematic diagram illustrating the multiple modes by which superantigens can interact with MHC class II molecules.

The recent structures of SpeC in complex with HLA-DR2 (Li *et al.*, 2001) and SEH in complex with HLA-DR1 (Petersson *et al.*, 2001) *via* the high-affinity zinc-dependent site have shed more light on the interactions of superantigens with MHC class II molecules (Figures 2.6C, and 2.7). The interaction between both superantigens and their MHC class II molecules is mediated by a bridging zinc ion, which tetrahedrally co-ordinates three ligands from the SpeC (His 167, His 201 and Asp 203) and two from SEH (His 206, Asp 208 and a water molecule) with one from the MHC class II β1 helix (His 81).

There is also extensive contact between SpeC and the class II associated antigenic peptide (approximately one third of the contact surface area) and stabilisation of the SEH–MHC class II complex also occurs through interaction with the antigenic peptide. Both the SpeC and SEH complexes have similar interactions with the antigenic peptide despite the fact that the peptides in each structure are different. This indicates that although the peptide plays an important role in the complex interaction, superantigen/MHC binding is not entirely peptide specific as a majority of the interactions with the peptide is with its backbone atoms.

Zinc is also shown to play a role in the binding of SME-Z_2, SpeG, and SpeH to MHC class II molecules, as the binding of all three of these superantigens to LG-2 cells is significantly reduced by the addition of EDTA (Proft *et al.*, 1999). The proposed zinc-binding site in each of these superantigens is shown to be closest to that of SEA and SpeC, both of which have geometrically and spatially equivalent site (Roussel *et al.*, 1997). As the presence of the zinc binding ligands suggest, all three of these superantigens bind to MHC class II molecules in a zinc dependent fashion.

There appears to be a great deal of diversity in the mechanism by which superantigens can mediate with MHC class II molecules, either through zinc-mediated interaction or *via* the generic site or involving both site/s giving each superantigen a unique array of possible interactions through which it can exploit the immune system.

Table 2.1: Comparison of the high affinity (zinc-dependent), and low affinity (generic) MHC class II binding sites in Staphylococcal and Streptococcal superantigens

Superantigen	MHC-II binding generic site	Zinc ligands	Reference
Staphylococcal			
SEA	yes	**High affinity site** S1, H187, H225, D227. **SEC2-like site** D86, H114, $E39_{(mol2)}$, H_2O	(Fraser *et al.*, 1992) (Sundstrom *et al.*, 1996)
SEB	yes	No	(Papageorgiou *et al.*, 1998)
SEC2	yes	H118, H122, D83, $D9_{(Symmetry\ related\ molecule)}$	(Papageorgiou *et al.*, 1995)
SED	yes	$H218_{(mol1)}$ $D182_{(mol2)}$, $H220_{(mol2)}$, $D222_{(mol2)}$*. **SEC-like site** H8, E12, $H109_{(mol2)}$, $K113_{(mol2)}$.	(Sundstrom *et al.*, 1996)
SEE	yes	H187, H225, D227	(Fraser *et al.*, 1992)
SEG		No	(Munson *et al.*, 1998)
SEH	No generic site	H206, D208	(Hakansson *et al.*, 2000)
SEI		No	(Munson *et al.*, 1998)
TSST-1	yes	No	(Papageorgiou *et al.*, 1996)
Streptococcal			
SpeA	yes	G33, D77, H106, H110.	(Papageorgiou *et al.*, 1999) (Earhart *et al.*, 2000)

			(Baker, 2001)
SpeC	No generic site	H167, H201, D203.	(Roussel *et al.*, 1997) (Li *et al.*, 2001)
SpeG	No generic site	#H167, H202, D204.	(Proft *et al.*, 1999)
SpeH	No generic site	#H198, D200, D160	(Proft *et al.*, 1999)
SME-Z	No generic site	#H202, D204, H162	(Proft *et al.*, 1999) (Proft *et al.*, 2000)
SME-Z2	No generic site	#H202, D204, H162	(Proft *et al.*, 1999) (Proft *et al.*, 2000)
SMEZ3/SPEX	No generic site	#H202, D204, H162	(Gerlach *et al.*, 2000)
SSA	yes	No	(Sundberg andJardetzky, 1999)

* And vice-versa (mol1 –mol2) for second zinc atom
# Proposed residues based on sequence alignment

Binding to TCR-V_β Regions

The characterisation of superantigen-TCR binding region reveals many similarities and differences. This is reflected by the fact that they bind to TCR through a somewhat similar mechanism, yet have different V_β specificities. The binding is mediated by interactions between the side-chains of the superantigen and the V_β backbone atoms in a manner similar to that of MHC-peptide and antigen-antibody complexes (Figure 2.8) (Li *et al.*, 1998). The TCR binding site has been shown to involve a shallow cavity between the two domains of the molecule. For SEB this cavity is formed by residues 22-33 (mostly α2 helix), 55-61 (β2-β3 loop), 87-92 (β4 strand and β4-β5 loop), 112 (β5 strand) and 210-214 (α5 helix) (Swaminathan *et al.*, 1992) (Figures 2.2, 2.5 and 2.7).

Analogous sites for SEC and SEA have also been proposed. The crystal structures of SEC2 and SEC3 in complex with TCR V_β chain by Fields *et al* (1996) and the complex between a T cell receptor beta chain and SEB have further elucidated the detailed interactions of superantigens with a TCR molecule (Figure 2.7). The main interactions are shown to be between the side-chain atoms of the superantigen and complementarity determining regions one and two (CDRs 1 and 2), and hypervariable region 4 (HV4) of the V_β chain. Comparison of this TCR binding site (from SEC2/3) with the corresponding regions of SEA and SEB identifies an invariant asparagine residue (Asn 23 in SEB/SECs; Asn 25 in SEA), as being crucial for direct interactions with the TCR. Mutation of this residue in SEB results in the loss of T cell stimulation (Kappler *et al.*, 1992). This residue is solvent exposed in SEA, SEB and SEC, and is thought to be involved in similar interactions with the TCR in all the SEs. Leder *et al* (1998) evaluated the functional contribution of individual SEC3 residues to the stabilisation of the SEC3/V_β complex by alanine scanning mutagenesis of all the residues of SEC3 shown to be in contact with the β-chain in the crystal structure (Fields *et al.*, 1996). It was found that the mutations that had the most effect on binding to the TCR β-chain were Asn 23, Tyr 90 and Gln 210. Tyr 90 and Gln 210 are conserved among SEC1-3, SEB, SpeA, and SSA has analogous residues Asn 49, Tyr 116 and Gln 223 (Swaminathan *et al.*, 1992).

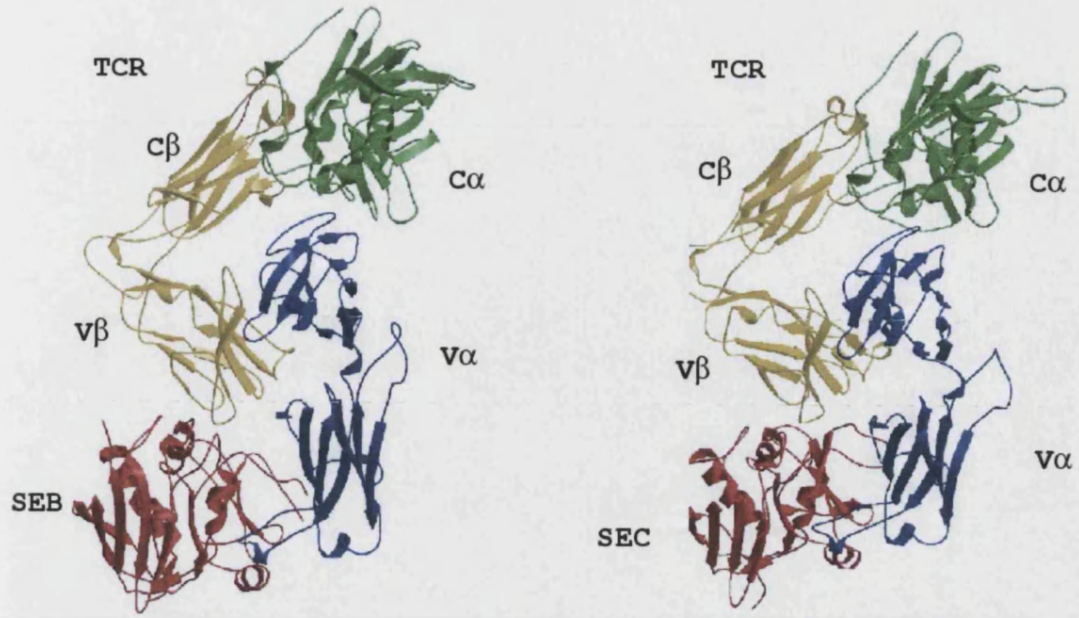

Figure 2.8: (Left to right)The structures of SEB (Li *et al.*, 1998) and SEC2/3 (Fields *et al.*, 1996) in complex with T cell receptors.

Modelling experiments with the TCR-SEB complex and a peptide/MHC class II complex indicate that V_α of the TCR interacts with the MHC beta chain in the TCR-SAG-MHC complex (Li *et al.*, 1998). The extent of the interaction is shown to be variable and is largely determined by the geometry of V_α/V_β domain association. This variability could account for the preferential expression of certain V_α regions among T cells reactive with SEB.

As mentioned earlier, the variance between superantigens with regard to TCR affinity and specificity can be accounted for by several residues unique to each particular superantigen as well as the any topological influence that each of these might have. For example, the residue Tyr 26 of SEC2 confers specificity between SEC1 and SEC2 via its interaction with Gly 53 from the V_β chain (Deringer *et al.*, 1996). This residue is not conserved in SEA or SEB. Val 91 of SEC2 is also implicated in TCR binding. This residue is not conserved in SEA (Tyr 94) or SEB (Tyr 91) either (Tiedemann *et al.*, 1995) and it is thought that the replacement of Val 91 by a tyrosine residue in SEB may

be responsible for its reduced affinity for the Vβ8.2 chain (Fields *et al.*, 1996). Ser 206, Asn 207 and Thr 21 have been identified as the probable specificity defining residues in SEA (Swaminathan *et al.*, 1992). This is highlighted by the exchange of residues 206 and 207 in SEA for the homologous residues in SEE causing the profile of V_β elements on the responding T cells to change to that of SEE (Hudson *et al.*, 1993). Ser 206 and Asn 207 in SEA correspond to Gln 210 and Ser 211 respectively in both SEB and SEC2. The greatest energetic contribution to the stability of the V_β–superantigen complex is made by those residues that define its specificity for particular V_β elements (Li *et al.*, 1998).

The TCR binding site of TSST-1 is located in the C-terminal domain on the long α2 helix and between the β7-β8 and α2-β9 loops as part of the α1 helix (Figure 2.2). In this regard, it is unique from the SEs (Acharya *et al.*, 1994). Mitogenicity is lost either partially or completely, by mutation of residues in the region 115-144. Specifically, residues Tyr 115, Glu 132, His 135, Ile 140, His 141, and Tyr 144 were shown to be of major importance for TSST-1 binding to TCR (Acharya *et al.*, 1994, Deresiewicz *et al.*, 1994). Mutation of these residues produce substantially less mitogenic toxins, yet they can still be recognised by a specific antibody (Deresiewicz *et al.*, 1994). The TCR binding site of SpeC is as yet not fully characterised. As it is structurally very similar to TSST-1 it is possible that SpeC shares similar TCR binding characteristics.

In summary, the interactions between superantigens and TCR share a common core of residues with specificity for particular V_β elements being supplied by further residues unique to each toxin, giving rise to a characteristic V_β repertoire.

Signal Transduction Pathways of Superantigens

The primary targets of superantigens are the $CD4^+$ T cells (Bavari and Ulrich, 1995), activation of which results in T helper type 1 (Th1) cytokine release with no apparent Th2 response (Krakauer, 1995). The consequences of a dominant Th1 response include suppression of antibody expression and reduced clearance of the invading microbe. A model of superantigen signal transduction can be constructed based on the TCR-oligomerisation model of T cell activation. This model proposes that binding of a ligand to TCR induces clustering of the TCRs on the cell surface, facilitating the recruitment of the intracellular components required for signal transduction (Germain, 1997). It would seem that superantigens have evolved to mimic peptide antigens with respect to receptor clustering (Woodland *et al.*, 1997), either through direct clustering events, or by the binding of superantigen homodimers to multiple MHC class II molecules which would in turn promote T cell clustering (Tiedemann *et al.*, 1995). Superantigens that act as monomers and that possess only a single MHC class II binding site appear to rely on the interactions of the TCR V_α and MHC class II-β1 which increases the stability of the ternary complex to within the range seen for conventional antigen. A stable MHC/superantigen/TCR complex with an extended half-life would therefore facilitate receptor clustering.

The consequences of superantigen exposure

Figure 2.9 shows a model for superantigen induced shock. The massive T cell proliferation induced by superantigens results in the release of high levels of a variety of cytokines both from macrophages and from T cells. These include IL-1 and TNF-α from macrophages and TNF-β, IL-2 and IFN-γ from T cells (Herman *et al.*, 1991). All these cytokines have deleterious effects on the host when present in high concentrations, including the production of hypotension through capillary leak (Figure 2.9) and are involved in the aetiology of toxic shock, food poisoning and scarlet fever in man and animals.

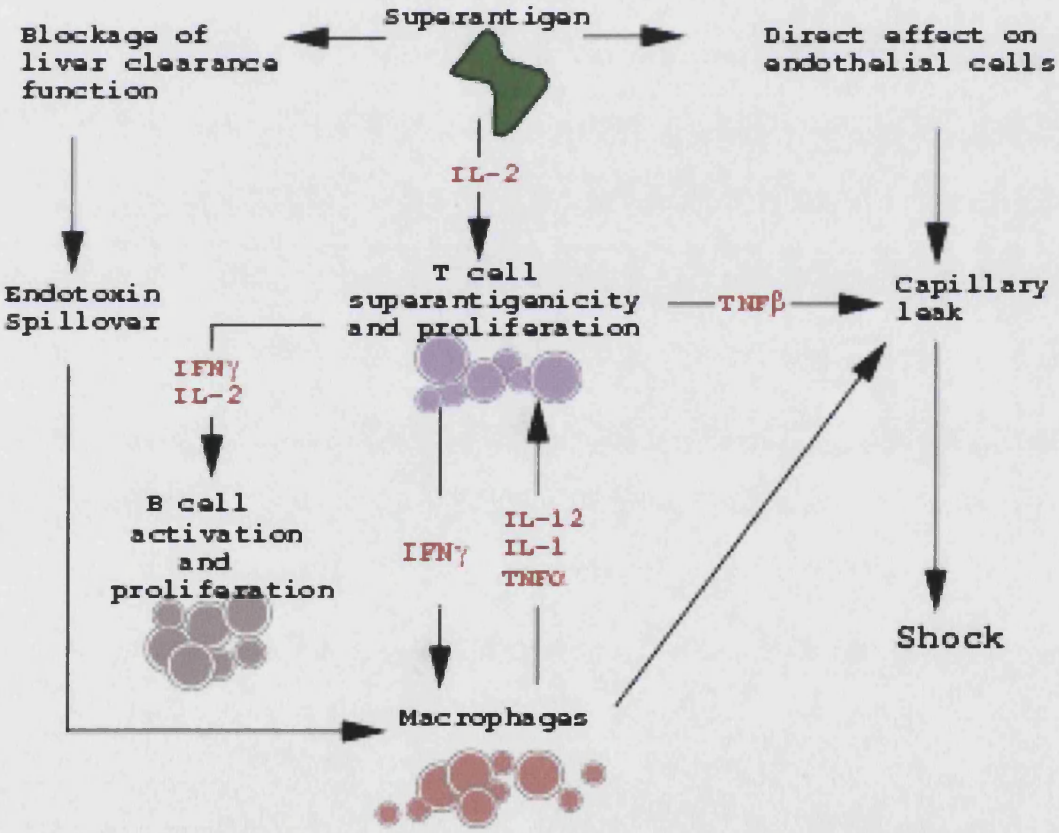

Figure 2.9: The consequences of superantigen exposure. The culminative effects of superantigen on the immune system leads to hypertension and systemic shock as a result of capillary leak. Prolonged exposure to superantigen can lead to immunosuppression and tolerance.

In vivo experiments with SEB show that most cytokine expression is transient and occurs within the first twelve hours whereas signals involved in proliferation such as DNA synthesis and IL-2 receptor expression are not apparent until over twenty four hours from SEB exposure (Picker *et al.*, 1995). Once cells have undergone DNA synthesis they are then capable of re-expressing cytokines prior to a second round of proliferation (Mehta and Maino, 1997).

Roles of Superantigens in Disease

Toxic Shock Syndrome

Toxic shock syndrome (TSS) is a serious, life threatening disease resulting from an infection of a susceptible host by Staphylococci or Streptococci expressing superantigens *in vivo*. TSST-1 is the key virulence factor responsible for TSS, inducing most TSS symptoms in animals. TSST-1 is responsible for nearly all menstrual TSS cases and approximately 60% of non-menstrual Staphylococcal TSS. The remainder of the cases can be attributed primarily to SEB production, and to a lesser extent SEC and SEA (Bernal *et al.*, 1999). Streptococcal TSS can be attributed mainly to SpeA (Hauser, 1991).

The pathogenesis of the disease is yet to be fully elucidated, although it is clear that toxic shock is in part a result of the superantigenic nature of the toxins. The high levels of cytokines released due to massive T cell proliferation affect the cardiovascular system by causing extensive epithelial damage, capillary leak and decrease in peripheral vascular resistance resulting in shock as well as reducing kidney and liver function. TSST-1 is unique among the superantigens as it is capable of crossing the epithelial barriers and subsequently inducing toxicity (Schlievert *et al.*, 2000). This activity is

thought to be due to the unique structural features of TSST-1 that are not present in other members of the superantigen family. The mechanism by which TSST-1 crosses the epithelial barrier could include either passive diffusion, or more likely, the use of cellular receptors (Schlievert *et al.*, 2000). The most pronounced structural differences between TSST-1 and the other superantigens are the lack of an α-helix in the C-terminal domain, the long N-terminal extension and the disulphide loop. TSST-1 also has unique patches of hydrophobic and neutral residues on the front and rear of the β-barrel at the N-terminal domain. Many of these features could combine to produce a receptor specific binding site in order for TSST-1 to traverse epithelial cells and allow systemic shock.

Superantigens and Food Poisoning

Staphylococcal food poisoning (SFP) is the leading cause of microbial food-borne illness worldwide. Food sources that are contaminated most often include foods that are high in protein, salt and sugar. Abdominal pain, nausea, vomiting, and diarrhoea are commonly seen within two to six hours of ingestion of contaminated food, the absence of fever suggests that toxemia is at most, minimal. Little is known about how superantigen structure relates with emetic and diarrhoea activity. It has been suggested that the symptoms of food poisoning are a result of the high levels of cytokines released following superantigen induced T cell proliferation. Indeed, cancer patients receiving IL-2 therapy often experience side effects that mimic SFP. More recent work indicates that the emetic properties of these toxins are not completely correlated with their superantigenicity (Harris and Betley, 1995). Work by Hoffman *et al* (1996) indicated that the carboxy-terminal histidine at position 225 of SEA was important for both the superantigenic and emetic activity, yet histidine 61 appears to be important only for emetic activity. Harris and Betley. (1995) have identified further areas in the N-terminal

region of SEA that are important for both emetic and superantigenic function. A different study on the carboxymethylation of His residues in SEB abrogates emetic activity but still induces peripheral blood cell proliferation in monkeys (Alber *et al.*, 1990) consistent with the hypothesis that the two activities are separable in staphylococcal enterotoxins. This is supported by investigations using peptides encompassing distinct regions of SEC1. Intravenous administration of one such peptide, a 22kDa C-terminal fragment, was found to induce diarrhoea but not emesis in primates (Spero *et al.*, 1978). One of the main regions of these toxins thought to be responsible for emesis is the disulphide bond and loop (Hovde *et al.*, 1994). They reported that the disulphide bond itself is not an absolute requirement for emetic activity. However, conformation within or adjacent to the loop is important for emesis. Thus, it is evident that further work is required in order to assess the contribution of certain amino acids to the various biological activities shown by superantigens in the context of the diseases they cause.

Superantigens and Autoimmunity

Due to their mode of action superantigens have been identified as a possible candidate for one of the causative agents of autoimmune disease (Kotzin *et al.*, 1993, Friedman *et al.*, 1993). Since autoreactive T and B cells can easily be isolated from the peripheral blood of healthy individuals (Hohlfeld *et al.*, 1984, Wucherpfennig *et al.*, 1991), superantigens could stimulate auto-reactive T cells both locally and systemically, since they do not discriminate between autoimmune and normal lymphocytes (Brocke *et al.*, 1998). Thus the delicate balance of tolerance could be broken. Although superantigens are yet to be directly implicated in human autoimmune disease, there is growing evidence to suggest their involvement. For example, SED and SED-reactive T cell lines have been shown to stimulate auto-antibody production by B cells *in vitro* (Renno and

Acha-Orbea, 1996). It has been shown that *Staphylococcus aureus* strain AB-1 is responsible for the spontaneous outbreak of staphylococcal arthritis in a colony of rats (Bremell *et al.*, 1994). When this strain was isolated from a swollen joint and injected intravenously into healthy rats, erosive, persistent arthritis developed in a majority of the rats. The arthritic lesions were characterised by the infiltration of T cells into the synovium. These T cells were later shown to be activated by a superantigen present in the infectious pathogen (Bremell and Tarkowski, 1995).

In the absence of infection, injection of low doses of SEA or SEB induces relapsing paralysis in Experimental Autoimmune Encephalomyelitis (EAE), the animal model of multiple schlerosis (Brocke *et al.*, 1993). Further studies have shown that SEB can induce MBP-specific T cells expressing different V_β to respond to myelin-antigens and mediate this relapsing paralysis (Gaur *et al.*, 1993). Autoimmune conditions such as arthritis, diabetes and multiple schlerosis are characterised by heterogeneous T cell infiltrates during active bouts of the disease. This implies that a broad spectrum of superantigens could cause this exacerbation (Soos *et al.*, 1997). Type I diabetes is associated with a retroviral superantigen which is thought to activate and expand T cells carrying the TCR $V_\beta 7$ element which in turn has been implicated in the pathogenesis of insulin dependent diabetes mellitus (Conrad *et al.*, 1997). Recently, the first case of type I diabetes associated with a bacterial superantigen mediated disease was reported (Couper *et al.*, 2000). However, it still remains unclear whether superantigens are the initial trigger of autoimmune disease; as environmental factors that can change a controllable illness into one that becomes relentless for susceptible individuals.

In vivo Models

The mouse model for toxic shock firstly requires the administration of D-galactosamine to sensitise the mice two hours prior to injection of superantigen (Miethke *et al.*, 1993a; Miethke *et al.*, 1993b). D-galactosamine destroys liver function and without its prior administration milligram quantities of toxin can be given to mice without inducing hypotension or shock. The model therefore, is not ideal, though it provides a starting point for experiments which can be expanded with other animal models. A rabbit model with most of the symptoms characteristic of human toxic shock syndrome (TSS) excluding rash and desquamation can be induced by injection of TSST-1 and endotoxin (Schlievert, 1982). Rabbits are first given a sublethal dose of TSST-1 as it is important to pre-condition the animals because TSST-1 is lethal to unconditioned animals. Four hours after the initial dose endotoxin is administered and the disease monitored by following the onset of TSST-1 induced fever by rectal thermometers and checking for signs of diarrhoea, hypothermia and awkward breathing. High doses of exotoxin can cause death within 3 hours. It is important to note that the symptoms observed in this model are not typical of endotoxin shock, but rather, are greatly accelerated in timescale (Bohach and Schlievert, 1988). A variation on this rabbit model was devised using a subcutaneous infusion pump to deliver a constant toxin dose at 150 μg over seven day period (Parsonnet *et al.*, 1987). The highly reproducible nature of this model makes it ideal for studying the pathogenesis of TSS.

The monkey feeding test for Staphylococcal enterotoxins allows the potency of a particular sample to induce emesis and other symptoms of superantigen induced food poisoning to be assessed (Bergdoll, 1988). This model has been used both to test drugs designed to inhibit emesis and to determine the efficacy of vaccines designed to prevent illness in humans (Bergdoll, 1966).

In vitro Models

TSST-1 pre-treated rat renal tubular epithelial cells (RTC) are sensitive to endotoxin induced necrosis at concentrations of less than 1ng/ml (Keane *et al.*, 1986). Briefly, RTC are incubated with non-toxic levels of TSST-1 for 20 minutes, washed, and then exposed to endotoxin. Cytotoxicity is assessed by either trypan blue staining or by using chemiluminescence to detect reactive oxygen species generated by those cells destroyed by endotoxin.

Direct assessment of complex formation, T cell stimulation and cytokine production can be assessed by using a T cell stimulation assay. Superantigen is incubated with antigen presenting cells and T cells (Leder *et al.*, 1998) and stimulation can be assessed by either incorporation of [^{3}H] thymidine into DNA and counting on a scintillation counter, which measures secreted cytokine levels, or by fluorescence-activated cell sorting (FACS).

PBMC (peripheral blood mononuclear cells) assays measure the superantigen induced proliferation directly without the need for antigen presenting cells to be present (Braun *et al.*, 1993) and stimulation can be assessed as with T cell assays.

TCR V_β analysis can be performed using the reverse dot-blot procedure (Hudson *et al.*, 1993). Total TCR V_β mRNA enrichment in human peripheral blood T cell cultures can be determined by a novel single-tube amplification technique using a redundant V_β-specific primer. Peripheral blood lymphocytes (PBL) are incubated with toxin for three days. TCR V_β-chain mRNA is then reverse transcribed using a set of primers specific for the conserved region in all V_β-chain genes. A radio-labelled V_β probe is then reverse blotted onto filters containing the individual V_β-chain genes. Relative changes in V_β-chain mRNA levels from superantigen stimulated PBL are then compared to mRNA levels in unactivated PBL.

Superantigens- Vaccines and Therapeutic Potential

Historical evidence suggested that treatment with superantigens might be of potential therapeutic value for cancer patients. Over one hundred years ago William B. Coley administered heat killed bacterial cultures to cancer patients (Crossley, 1997). Many of the patients who had been injected with bacteria experienced a dramatic regression in their tumours and several experienced apparent cure. It is likely that these effects can be attributed to the immunostimulatory properties of superantigens in the injected bacterial preparation. Further evidence for the involvement of supeantigens in these early experiments was provided by the attempted immunoadsorption of tumour-blocking antibodies by passing the patients' plasma over a protein A column. It was observed at the time, that treatment with this preparation was accompanied by all the symptoms of superantigen induced shock in the patient. It was later discovered that the columns were heavily contaminated with SEA and/or SEB. Protein A effectively binds several subclasses of immunoglobulins, but in contrast to SEs it has no immunoactivating properties compatible with the side effects observed in the patients. When protein A was produced recombinantly in *E.coli.*, no toxic or therapeutic effects were observed. This suggestion of a therapeutic window where tolerable systemic immune activation can result in tumour regression has lead to recent attempts to specifically target superantigens towards tumours. The production of fusion proteins from tumour specific mAbs linked to superantigens represent the modern equivalent of these historic examples.

A majority of the recent work in this field has focused on the use of SEA fused to a tumour-reactive monoclonal antibody (Hansson *et al.*, 1997). The therapy works by targeting the superantigen directly towards the tumour; inducing infiltrating lymphocytes, the local release of tumour suppressive cytokines and the induction of apoptosis in tumour cells (Litton *et al.*, 1996, Dohlsten *et al.*, 1995a; Dohlsten *et al.*,

1995b). A limitation to this approach is the accumulation of Fab-SEA fusion proteins in normal healthy tissues expressing MHC class II molecule. This causes immune activation and dose limiting toxicity (Hansson *et al.*, 1997, Dohlsten *et al.*, 1998). Mutation of residues in the high affinity MHC class II binding site reduces the systemic toxicity of the fusion protein whilst retaining potent anti-tumour activity (Hansson *et al.*, 1997). Similarly, several cell-based vaccines for the stimulation of immunity to metastasic cancers also employ superantigens in order to boost the immune response towards the tumour (Ostrand-Rosenberg *et al.*, 1999). Third generation vaccines consisting of tumour cells transfected with MHC class II, CD80, and SEB genes are very effective agents for the treatment of mice with established metastasic disease.

The available data for the superantigens highlights their involvement in many diseases through one common mechanism. The production of a vaccine against bacterial superantigens could therefore lead to the abolition of such diseases. At present especially with the number of reported cases of Multi-resistant *Staphylococcus aureus* (MRSA) on the rise, the need for a broad-spectrum vaccine or prophylactic effective against all structurally related bacterial superantigens is of paramount importance. Studies with SEA show that the MHC class II binding regions of superantigens represent the best target for site directed mutagenesis in order to produce a vaccine (Bavari *et al.*, 1996). In contrast, the TCR binding mechanisms of superantigens are not conserved (Ulrich *et al.*, 1998) and mutating a key amino acid residue in these sites may cause the acquisition of a new TCR Vβ profile (Kappler *et al.*, 1992). As MHC class II binding residues are conserved reasonably well amongst the superantigens this seems like a more sensible area to start in order to produce an effective vaccine (Bavari *et al.*, 1996, Ulrich *et al.*, 1998). Ulrich *et al* (1998) developed several vaccines based on conserved regions of SEA and SEB. These regions included residues in the hydrophobic pocket (Tyr 89-Ala,

Thr 115-Ala, Glu 67-Gln) and residues in the hydrophobic binding loop (Gln 43-Pro, Phe 44-Pro, Leu 45-Arg). Immunisation with these vaccines was found to protect mice and rhesus monkeys from lethal toxic shock. The antibodies produced against these vaccines also recognised and neutralised distantly related superantigens (Ulrich *et al.*, 1998). Other strategies for attenuating superantigen action include low molecular weight peptides that can interfere with the binding of superantigen *via* the peptide binding groove.

Recently, Arad *et al* (2000) reported the identification of a dodecapeptide that prevents superantigen induced TSS in a mouse model. The peptide consisted of a highly conserved 12 residue stretch spanning residues 150 to 161 of SEB (β7 - strand - β8 - strand - α-4-helix). The peptide represents a region of no known function and is located outside of the known binding domains for both MHC class II molecules and TCR. Protected mice that survive subsequent lethal challenge with both staphylococcal and streptococcal superantigens rapidly develop protective antibodies against serologically distinct superantigens. The peptide was also shown to be effective at rescuing mice undergoing toxic shock. Similar work by Visvanathan *et al* (2001) using a peptide encompassing the same conserved region of superantigen structure plus a further thirteen residues (residues 150-174) gave further insight into how these peptide work. This peptide was able to protect against lethal shock in a rabbit model and block up to 90% of superantigen induced proliferation. Binding experiments indicated that the peptide binds tightly to MHC class II molecule preventing the association of superantigen. Antibodies raised against this peptide were also able to block the proliferative effects of superantigens. The broad specificity of these peptides makes them an ideal vaccine/therapy for superantigen-mediated diseases. However a clear mechanism on how these peptide/s function is yet to be elucidated.

Another approach towards the inhibition of T cell response by superantigens is the use of bispecific receptor mimics. The strategy for the design of such molecules is to incorporate structural elements of the receptors required for binding of the toxin and not as a host of the natural ligand. As a result, only toxin binding is inhibited whilst the presentation of peptide antigen allowing a normal immune response is free to occur. Lehnert *et al* (2001) recently reported such a molecule from regions of DRα and TCR V_β joined together by a linker peptide that allows the two halves of the molecule to be held in correct orientations for binding of SEB. The receptor mimic inhibited SEB binding, blocked IL-2 release and stopped T cell proliferation. The dissociation constants for SEB binding to MHC class II-TCR complex and SEB-receptor mimic were very similar (Redpath *et al.*, 1999) indicating that the amount required for competitive inhibition would also be in the nano-molar range. By extending this strategy, production of bispecific receptor mimics against other superantigens should be relatively straight forward and appears to have considerable promise.

Aims

The aim of this work is to further characterise the functional regions of bacterial superantigens that govern their specificity and potency.

By using a combination of mutagenesis and X-ray crystallography, the structural and functional contributions of individual amino acids will be assessed and their contribution to the activity of the toxin examined. In particular, the use of a zinc ion as a high affinity MHC class II binding site and the contribution that individual amino acids make to the TCR binding mechanisms of superantigens will be examined.

Ultimately, it is hoped that this work will support the previous studies suggesting that

superantigens can interact with MHC class II and TCR in a subtle variety of ways, characteristic for each toxin. Further to this, toxins may be capable of employing multiple modes of interaction in order to elicit the required immune response.

-3-

Chapter three

Structural Features of a Zinc Binding Site in Streptococcal Pyrogenic Exotoxin A (SpeA1): Implications for MHC class II Recognition.

Introduction

In recent years there has been a resurgence of severe invasive streptococcal diseases. These include streptococcal toxic shock syndrome (STSS) associated with the production of streptococcal pyrogenic exotoxins (Spes), notably SpeA (Musser *et al.*, 1991), which can be isolated from a majority of patients suffering from the condition. SpeA1 (M_r 25,787) is a member of the staphylococcal and streptococcal superantigen family. All of the toxins in the family induce fever, enhance susceptibility to lethal endotoxin shock, and stimulate T cells as superantigens. The correlation between STSS and SpeA producing strains of *S.pyogenes* is not surprising as the symptoms of toxic shock are characteristic of a superantigen mediated disease. In addition, Spes are cardiotoxic and have been postulated to be involved in diseases such as scarlet fever and erysipelas, as well as STSS and the early events leading to rheumatic fever and guttate psoriasis (Hauser *et al.*, 1995). Mutagenesis studies have begun to characterise the relationship between the different pyrogenic toxins and functional activity. A better understanding of such mechanisms will further our understanding of how microbes have evolved to interact with, and alter the human immune system and provide suggestions for novel therapeutics.

The crystal structure of SpeA1 at 2.6 Å resolution (Papageorgiou *et al.*, 1999) revealed that the toxin is considerably similar to that of other prototype superantigens (Figure 3.1). Functional regions were characterised by structure based sequence alignment in combination with previous details of superantigen functional regions (Papageorgiou and Acharya, 2000). SpeA1 was proposed to have a generic MHC class II binding site similar, but not identical to SEB.

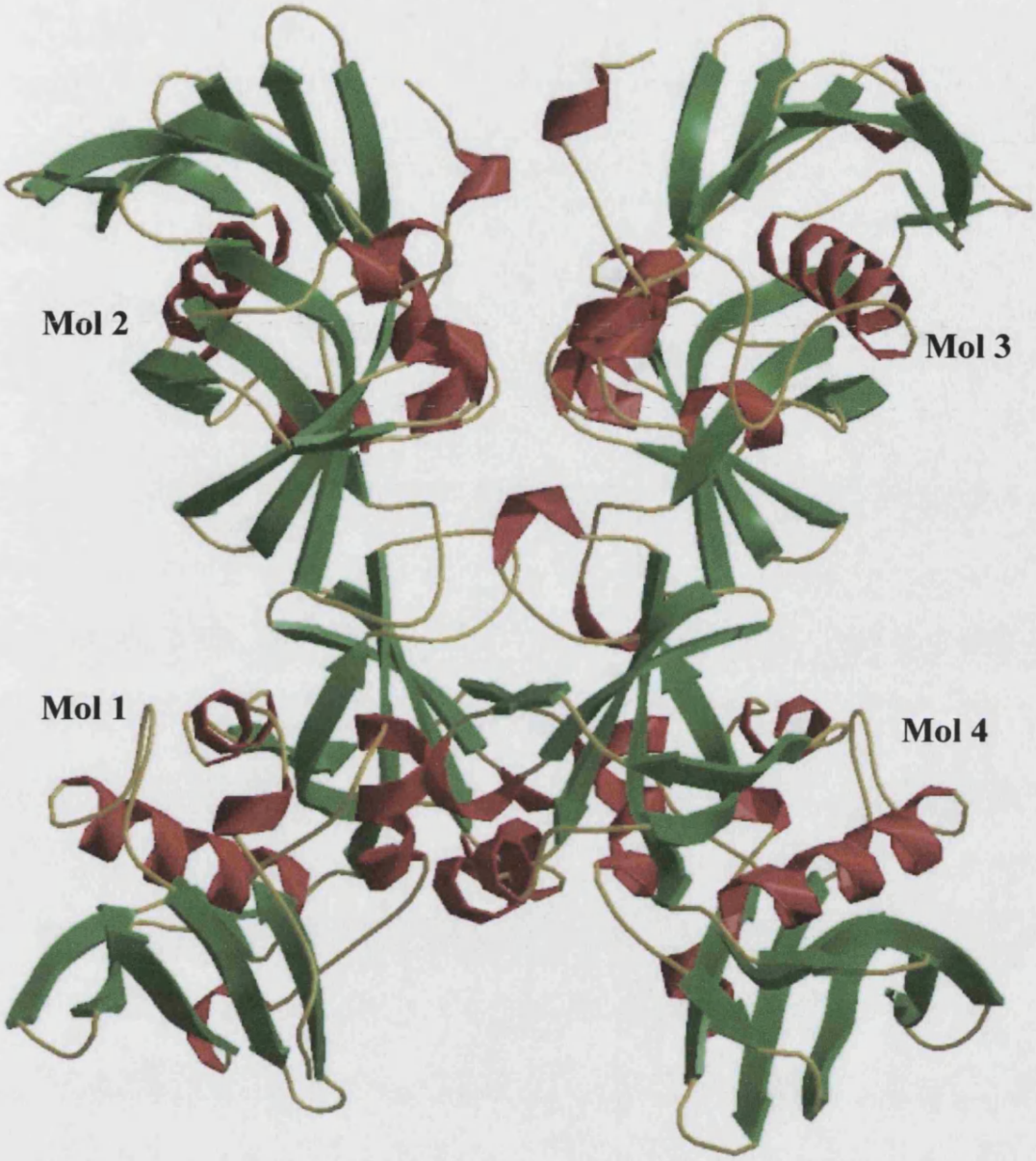

Figure 3.1: The crystal structure of native SpeA1; the arrangement of the four molecules in the crystallographic asymmetric unit. Each molecule is labelled.

Its TCR binding site was shown to have a common core like that of SEC2, with variation in several other residues that produce its unique TCR V_β specificity. The structure also revealed a putative zinc binding site similar to that of SEC2 (Papageorgiou and Acharya, 2000), although no zinc ion was found to be present in this region. As a result, this subsequent study was performed in order to identify if SpeA1

did indeed possess a zinc binding site.The presence of a zinc site is SpeA1 would indicate a second, high affinity MHC class II binding site in the toxin which combined with a generic MHC class II binding site could permit SpeA1 multiple modes of action. To further support this a model of SpeA1 in complex with HLA-DR1 was constructed and a series of mutants of the proposed zinc ligands were examined to determine the effect of zinc on the structure and function of the toxin.

Materials and methods

Purified SpeA1 was supplied by Professor Carleen Collins, University of Miami Medical School, Miami, FL, USA. Recombinant SpeA1 with an N-terminal His tag was expressed in *E. coli* BL21 (DE3) (Novagen), and purified by immobilised metal ion affinity chromatography as described previously by Papageorgiou *et al* (1999). Purification was carried out at pH 5.7 in order to inhibit dimer formation of the toxin. The eluted fusion protein was then cleaved with thrombin and tag and toxin were separated by dialysis against Phosphate buffered saline (PBS). Thrombin was removed from the preparation by chromatography over *p*-amino benziamidine agarose (Sigma Chemicals, St Louis, MO) and dialysed against PBS, 0.14M NaCl, 2.7mM KCl, 5.4mM Na_2HPO_4 and 1.8mM KH_2PO_4 before being concentrated with Centricon-10 filter units (Amicon).

Crystals were grown at 16°C using the hanging drop vapour diffusion method. Small, irregular crystals were produced in 16-19% PEG 3350, 0.1 M sodium cacodylate buffer (pH 6.5) and 16% isopropanol. These crystals were then used for microseeding of hanging drops equilibrated against a reservoir solution containing 17% PEG 8000,

0.2 M ammonium sulphate and 0.1 M sodium cacodylate buffer (pH 6.5). Crystals grown under these conditions were soaked in 2.5 mM zinc chloride (final concentration) 12 hours prior to data collection.

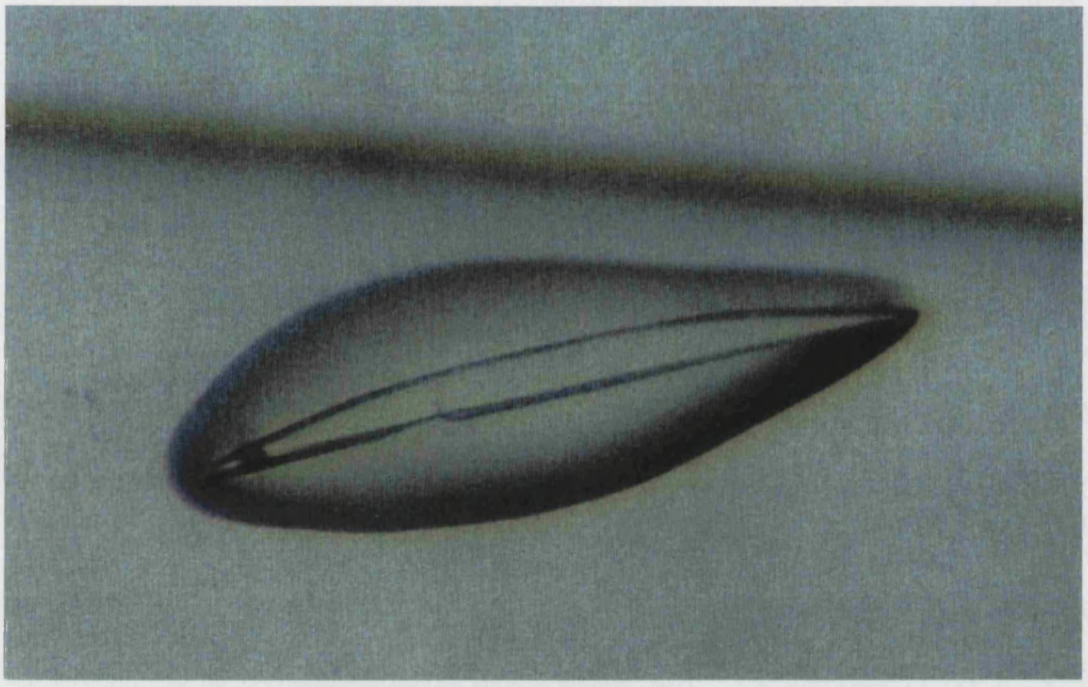

Figure 3.2: A crystal of SpeA

Data collection and refinement

X-ray diffraction data to 2.8Å were collected at 100°K using the crystallisation buffer containing 15% glycerol as a cryoprotectant at EMBL (c/o DESY), on beamline X11 equipped with a MAR345 image plate. Forty-four images were collected in dose mode (480-560 sec/image), with an oscillation range of 2° per image. A second data set was collected at MAX II, Max Lab to 2.9Å resolution using a MAR345 image plate. The exposure time was 480 sec/image and the oscillation range was 1.0°. Data processing, scaling and merging was performed using the HKL program suite. (Otwinowski and Minor, 1997). Problems with differences in unit cell volumes between the two datasets due to cryogenic temperatures became apparent during data processing. This problem

was overcome by the following scaling and merging protocol; Initially the two data-sets were scaled to produce .x files and merged to produce a .sca file. This .sca file was then merged back against the first dataset .x files in order to increase the bias towards the unit cell dimensions seen in the first set and to reduce the R_{merge}. The final R_{merge} was 10.8 % with an overall completeness of 95.8% (Table 3.1). Phases were determined using the structure of native SpeA1 (Papageorgiou *et al.*, 1999) as a starting model. The initial model was subject to rigid body refinement. Calculation of a ($|F_o| - |F_c|$) electron density map revealed extra density at the predicted zinc binding site of the toxin for all four molecules in the asymmetric unit. The structure was refined by simulated annealing using tight non-crystallographic symmetry (NCS) restraints and the maximum likelihood target as implemented in the program CNS (Brünger *et al.*, 1998). R_{free} and R_{cryst} were used to follow the progress of refinement (Brünger *et al.*, 1992). At the final stages of refinement grouped B-factor refinement and release of the NCS restraints was performed. SigmaA-weighted electron density maps ($|F_o| - |F_c|$) and ($2|F_o| - |F_c|$) were calculated after each cycle of refinement and visualised using the program 'O' (Jones *et al.*, 1991). Water molecules were added to the model towards the end of refinement with the aid of difference maps and the program water_pick in CNS (Brünger *et al* ., 1998). The final model has a crystallographic R_{factor} (R_{cryst}) of 22.5% for all data from 40 to 2.8Å resolution, and an R_{free} of 27.7% for 5% of the data omitted (Table 3.1).

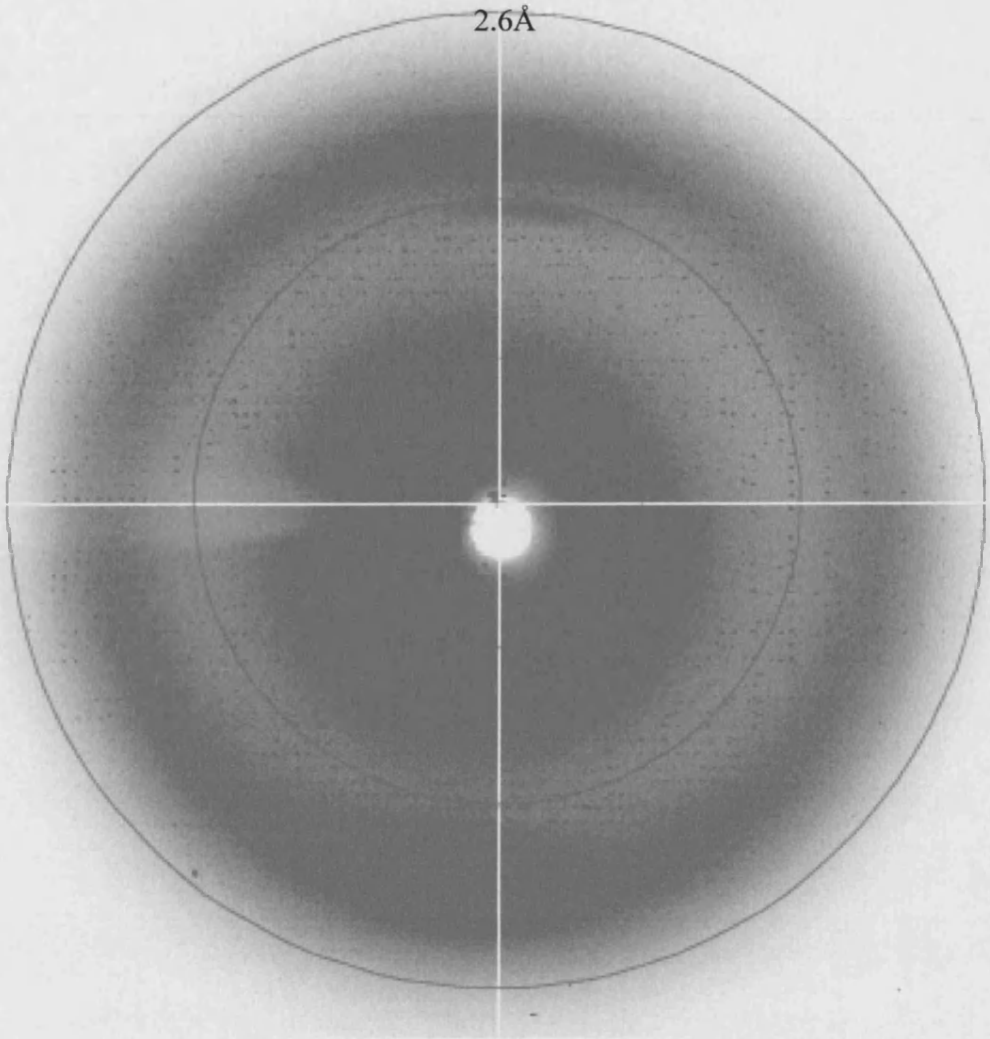

Figure 3.3: A sample diffraction image from a SpeA1 with zinc data set.

Molecular modelling of SpeA1 in complex with MHC class II via its zinc site.

Molecule one of SpeA1 was docked onto MHC class II in close proximity to His 81 of HLA-DR1 via its zinc site. Following energy minimisation using the program CNS (Brünger *et al.*, 1998) the complex was examined visually for further interactions and clashes between the two structures.

Results and discussion

Quality of the structure

The crystallographic data processing and refinement statistics are shown in Table 3.1. The final model consists of four molecules in the asymmetric unit containing 7,031 non-hydrogen protein atoms, four zinc ions, and 143 water molecules. The root mean squares (r.m.s) deviation between the zinc-bound structure and the native structure is 0.33 Å (mol1), 0.35 Å (mol2), 0.30 Å (mol3), and 0.38 Å (mol 4). The regions that deviate most between the two structures include the flexible disulphide loop and the first six residues at the N-terminus. Exclusion of these areas from the calculation improves the r.m.s deviation to 0.26 Å (mol1), 0.25 Å (mol2), 0.24 Å (mol3), and 0.33 Å (mol4). The Ramachandran plot for all four molecules shows 85% of the residues in allowed regions and none in disallowed regions. Residues 1 and 2 were not modelled due to poor density. Residues 5, 88, 112, 115, 179 and 180 in all four molecules and residues 91 and 92 in molecules 2, 3 and 4 were modelled as alanine due to insufficient density. Molecule 1 will be used throughout for discussion.

Table 3.1 Crystallographic data collection and refinement statistics

Cell Dimensions (Å)	a = 126.9, b = 101.3, c = 82.0
Space group	$P2_12_12$ 4 mol/a.u.
Resolution (Å)	40.0-2.8
No. of measurements	144123
No. of unique reflections	26185
Completeness	95.8 (61.3)[a]
I/σ	6.5 (5.3)
R_{merge} (%)[b]	10.8 (28.5)
Refinement	
R_{cryst} (%)[c]	21.4
R_{free}(%)[d]	28
No. of protein atoms	7031
No. of water molecules	143
Temperature factors (Å^2)	
Main chain[e]	28.4, 30.1, 24.9, 43.5
Side chain	30.4, 33.2, 28.5, 45.1
Zinc ligands	29.3, 34.2, 23.2, 52.0
Zinc ions (average)	48.0
RMSD in bond lengths (Å)	0.007
RMSD in bond angles (Å)	1.32

[a] Outermost shell 2.9-2.8 Å.
[b] $R_{merge} = \Sigma(|Ij - \langle I\rangle|)/\Sigma\langle I\rangle$, where Ij is the observed intensity of reflection j and $\langle I\rangle$ is the average intensity of multiple observations.
[c] $R_{cryst} = \Sigma||F_o| - |F_c||/\Sigma|F_o|$, where F_o and F_c are the observed and calculated structure factor amplitudes, respectively.
[d] 5% of the data that were used for the calculation of R_{free} were randomly excluded from the refinement.
[e] Temperature factors for individual molecules quoted.

Overall structure

The structure of the SpeA1-zinc molecule is characteristic of the superantigen family (Figure 3.4). It contains a long central α-helix, an N-terminal domain and a C-terminal domain. Part of the N-terminal domain has a β-barrel topology formed by strands β1, β2, β3, β4 and β5, similar to the 'oligosaccharide/oligonucleotide fold' (Murzin, 1995) present in other superantigens. Strands β2 and β3 are anti-parallel, and strand β1 is parallel to β5 and anti-parallel to β4. Several hydrophobic residues from the β-barrel are solvent-exposed. Other structural features of the N-terminal domain include helices α2, α3 and α5 and a disulphide bridge in the β4-β5 loop. The C-terminal domain has features of the 'β-grasp motif' as seen in the structures of other superantigens (Papageorgiou and Acharya, 1997, 2000). With a β-sheet topology packed against the central α4 helix. Strands β6, β9, β10 and β12 form a relatively flat surface with strand β7 rotated by ~ 30° with respect to β6. The N-terminal tail (residues 3-16) is packed against the β-grasp motif, and as such is considered part of the C-terminal domain. Structure-based sequence alignment identifies SEC2 as the most similar superantigen to SpeA1. The main differences occur due to deletions in the loop regions of the structure. SpeA1 (221 amino acids) and SEC2 (239 amino acids) also show variability in their respective disulphide loop regions.

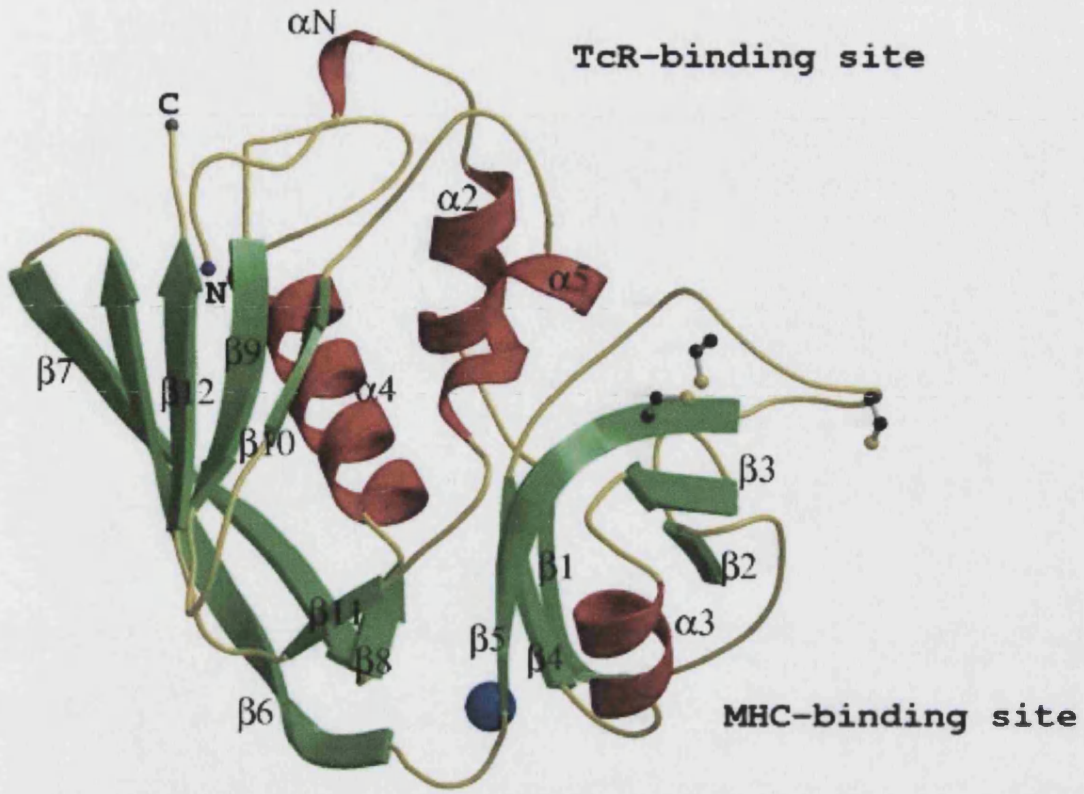

Figure 3.4: The structure of SpeA1-zinc complex. The bound zinc ion is shown as a blue sphere. The disulphide bridge is shown in ball-and-stick representation, the free cysteine, which is part of the disulphide loop is also shown.

The disulphide bridge

The SpeA1-zinc structure contains three cysteine residues; two of them (Cys 87 and Cys 98) form a disulphide bridge at the top of the N-terminal β-barrel, between strands β4 and β5 (Figure 3.4). The third cysteine (Cys 90) is solvent exposed and forms part of the disulphide loop. The disulphide loop is common to all superantigens except SpeC which does not contain any cysteine residues in the corresponding region, and TSST-1 which does not contain any cysteine residues at all (Papageorgiou *et al.*, 1999). The disulphide loop of SpeA1 is comprised of ten residues, compared to 19 for SEB, 16 for SEC, and 9 for SEA. The residues of the disulphide loop in SpeA1-zinc possess high temperature

factors, due to the highly flexible nature of this region. The loop is located at the interface between the four molecules and is involved in crystal packing interactions. However, it still retains some degree of flexibility and superposition of the residues within the loop (87-98) shows an r.m.s deviation of 0.52 Å (mol 1-mol2), 0.28 Å (mol 1-mol 3) and 0.64Å (moll-mol4).

The zinc binding site

The crystal structure of the SpeA1-zinc complex revealed the presence of a zinc binding site at the interface between the N- and C-terminal domains of SpeA1 (see Figure 3.4) the zinc ligands are Glu 33, Asp 77, His 106, and His 110. (Figures 3.5 and 3.6). In the presence of the zinc ion, slight movement of the surrounding residues can be observed compared to the previously determined native structure of SpeA1 in the absence of zinc (Papageorgiou *et al.*, 1999). The distances between the ligands and the zinc ion are Glu 33 OE1- 1.98 Å, Asp 77 OD1 – 2.47 Å, His 106 ND1- 2.06 Å, and His 110 NE2- 2.17 Å. These values are comparable to those from other zinc binding superantigens, and fall within the range of distances documented by Alberts *et al.* (1998) for tetrahedrally co-ordinated zinc ions in proteins. A similar study was recently conducted by Earhart *et al.* (2000). They reported an identical site in the structure of SpeA1 (3.0 Å; 65% complete data) to the one presented here. In addition, a cadmium binding site involving residues 87-98 from the disulphide loop was also identified. However, no attempt was made to address the biological significance of these sites. The work presented here aims to further characterise the zinc site of SpeA1 and assess its implications for MHC class II recognition by SpeA1.

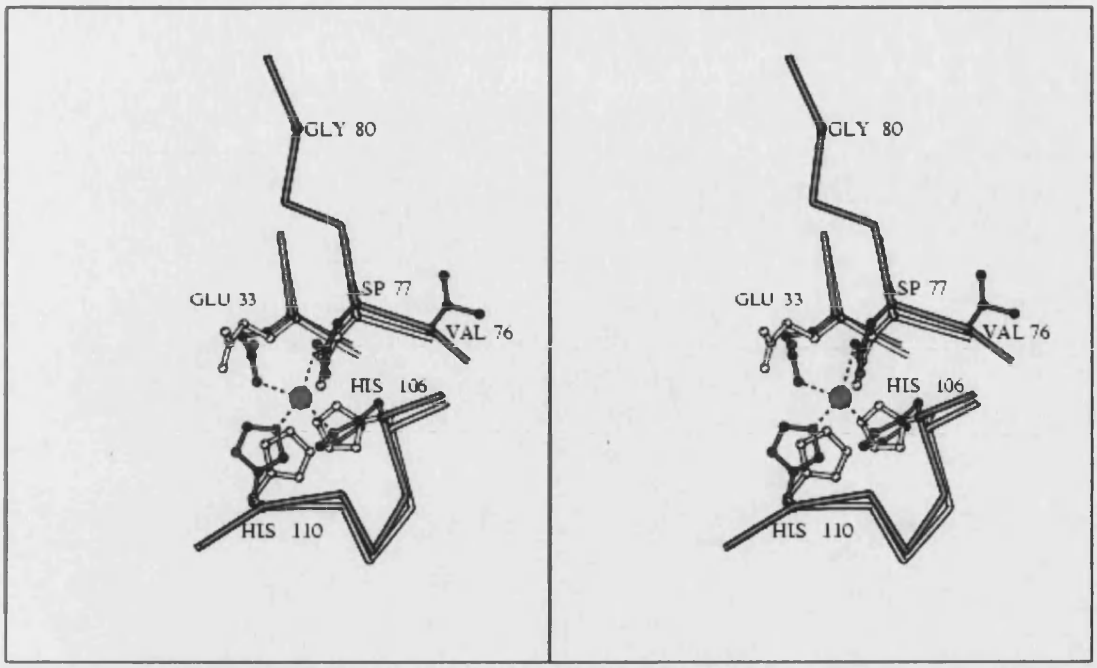

Figure 3.5: Comparison of the zinc binding site of native SpeA1 (white) and zinc complexed SpeA1 (grey).

The presence of a zinc site in SpeA1 was originally proposed by by Papageorgiou *et al* (1999) on the basis of sequence comparison and the crystal structure of SEC2. The residues Asp 77, His 106, and His 110 of the SpeA1-zinc binding site are structurally equivalent to the residues Asp 83, His 110, and His 122 in SEC2 with the fourth zinc ligand being formed by Asp 9 of a symmetry related molecule in the crystal lattice. The SEA structure contains two zinc binding sites – one on the N-terminal domain and one on the C-terminal domain (Schad *et al.*, 1997; Sundstrom *et al.*, 1996). The SEC2-like zinc binding site of SEA (N-terminal domain) also has three ligands of structural equivalence to SpeA1: Glu 39 (Glu 33 in SpeA1), Asp 83 (Asp 77), and His 118 (His 106), with a water molecule in SEA replacing the second histidine residue (His 110) found in SpeA1 (Schad *et al.*, 1997). Different and structurally non-equivalent zinc binding sites have been identified in SEA (Schad *et al.*, 1997; Sundstrom *et al.*, 1996), SED (Sundstrom *et al.*, 1996), SEH (Hakansson *et al.*, 2000), and SpeC (Roussel *et al.*, 1997). As a result, several putative roles for zinc in the structure of the superantigen

family have been proposed.: the zinc ion has been shown to have a role in in the formation of (a) stable homodimers (for SED and SEH); (b) a second high affinity MHC class II binding site (for SEA, SEC, SED, and SEH); and (c) in the thermostability of the superantigens.

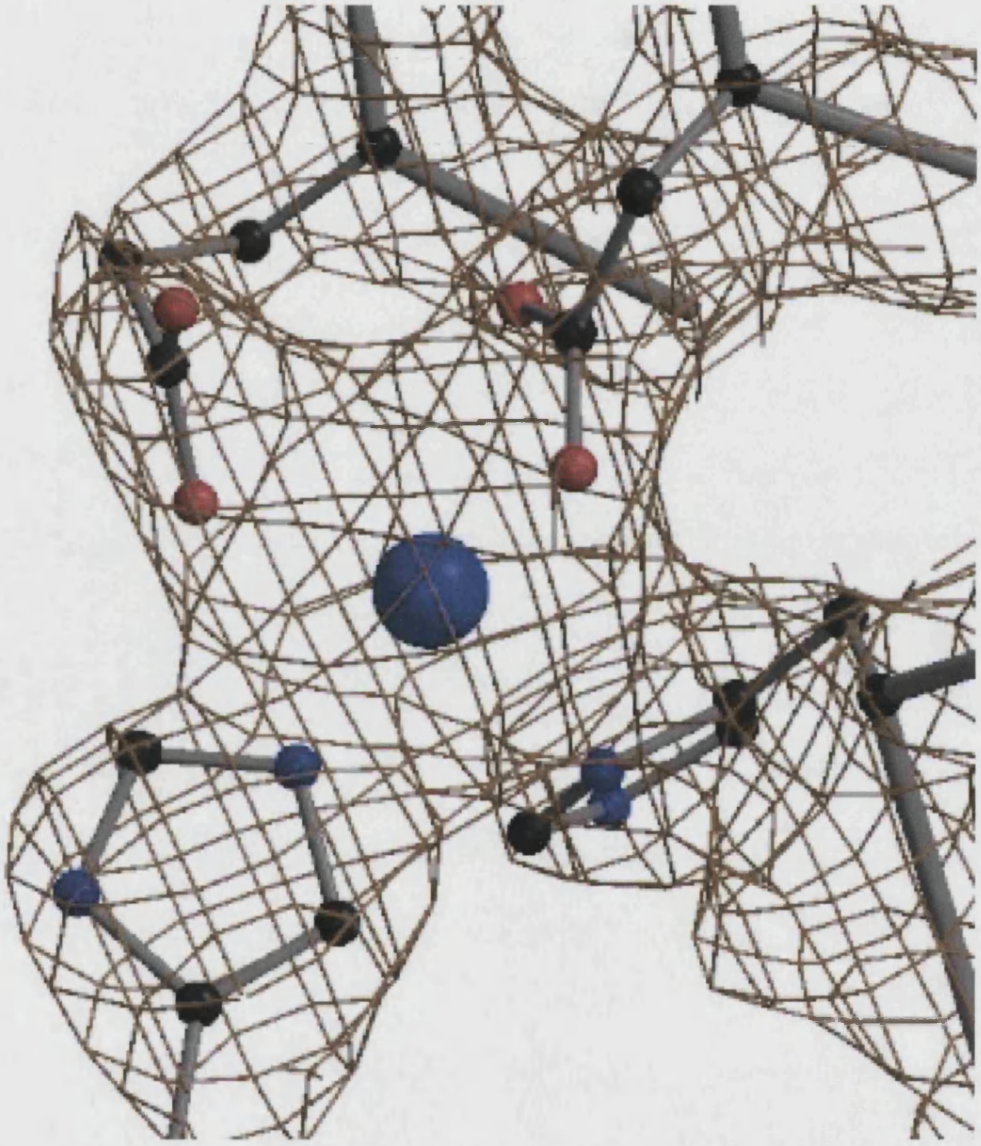

Figure 3.6 The electron density of the SpeA1 zinc binding site. $2|F_o| - |F_c|$ map contoured at 1 σ. The orientation is the same as in Figure 3.5.

To confirm that the residues Glu 33, Asp 77, His 106, and His 110 comprise a zinc binding site , mutant forms of SpeA1 with Ala substituted at each of these positions were generated and the affinity of each of these forms for zinc was determined by equilibrium dialysis (work carried out by our collaborators, Professor Carleen Collins, University of Miami Medical School, Miami, FL, USA.) (Baker *et al.*, 2001). The K_d of SpeA1 for zinc was determined to be 2.3 μM, which is approximately 10-fold higher than the K_d of the SEA-zinc interaction (0.3 μM) (Sundstrom *et al.*, 1996). The K_d of the mutant form of SpeA1- Asp 77 Ala for zinc was 60 μM, of SpeA1-His 106 Ala for zinc was 120 μM, and of SpeA1-His 110 Ala for zinc was 80 μM, indicating that the affinity for each of these mutant toxins for zinc was significantly decreased compared to the affinity of wild type toxin for zinc. The SpeA1-Glu 33 Ala-zinc interaction had a K_d of 5.8 μM, which represent only a slight decrease in affinity. No zinc binding was observed with the double mutant SpeA1-Asp 77 Ala, His 106 Ala when 150 μM of toxin was used in the experiment, indicating that the K_d of zinc for this mutant was much greater than 150 μM. Thus, the residues Asp 77, His 106, and His 110 are clearly necessary for zinc binding, while Glu 33 has a lesser role.

A possible role for the zinc ion in MHC class II recognition?

SEA has two distinct MHC class II binding sites, one at the C-terminus and the other at the N-terminus. The C-terminal binding site contains a zinc ion, and has an approximate 100-fold higher affinity for MHC class II than the N-terminal MHC class II binding site (Abrahmsen *et al.*, 1995). The generic N-terminal MHC class II binding site does not contain zinc, and is similar to the MHC class II binding sites found in other superantigens such as SEB and SEC. There is evidence to suggest that SpeA1 also contains a generic MHC class II binding site. A previous study examining the affinity of various SpeA1 mutants for MHC class II indicated that mutations at SpeA1 residues 42 to 48 decrease binding to the MHC class II DQ molecule (Kline and Collins, 1996). SpeA1 residue Leu 42 is conserved in the SEB generic MHC class II binding site. Therefore, it is possible that SpeA1 is similar to SEA in that it has two distinct MHC class II binding sites: a generic site, and a zinc-mediated site. The positions of the two predicted binding sites on within the structure of SpeA1 is similar to the positions of the MHC class II binding sites seen in the structure of SEC2 (Papageorgiou *et al.*, 1995). Mutagenesis studies have shown His 81 of the MHC class II β-chain to be important for the zinc-mediated binding of SEA to the MHC class II molecule (Fraser *et al.*, 1992). To examine the possible interactions of SpeA1 with MHC class II molecules via its zinc site, SpeA1 was docked onto mouse HLA-DR1 (Figure 3.7). The theoretical model gives a good overall fit for the interaction of the zinc site of SpeA1 and His 81 of the DR1 β-chain. There are only minor clashes in the model involving residues Leu 111, Ala 112, and Ile 113 (from strands β5 and β6) of SpeA1 with part of the antigenic peptide bound in the peptide binding groove of HLA-DR1. However, it should be noted that peptide antigen varies greatly throughout the MHC class II population (Chicz *et al,*. 1992). And several peptides have been shown to either enhance or reduce the affinity of

superantigens for MHC class II, depending on their interactions with the superantigen (Wen *et al.*, 1996).

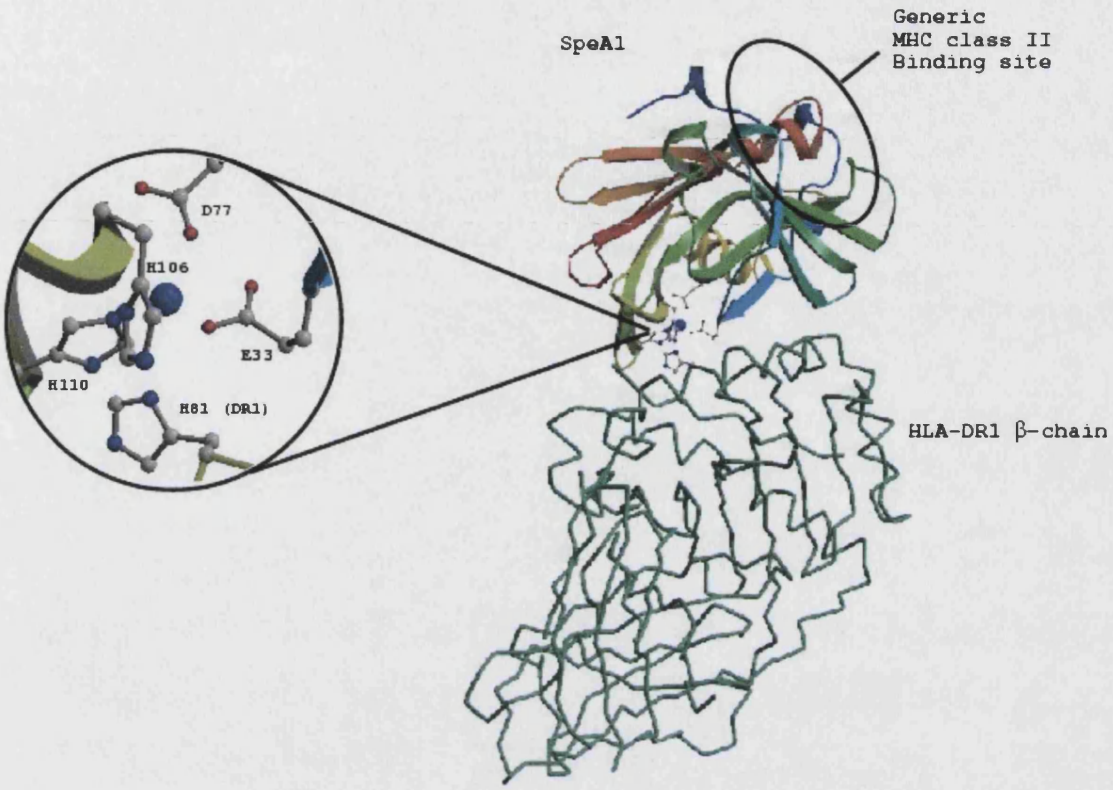

Figure 3.7: Proposed model for DR1-SpeA1-zinc mediated recognition. In this mode of binding, His 81 from the β-chain of the MHC class II molecule would replace one of the zinc binding ligands from SpeA1 (inset)

The modelled complex gives clues to the proposed zinc-mediated binding of SpeA1 to HLA-DR1 (Figure 3.7). When His 81 of the DR β-chain binds to the toxin via the zinc ion, there would be some rearrangement that would affect the overall geometry of the site, and therefore, the position of neighbouring residues allowing the optimisation of favourable contacts between the superantigen and the MHC class II molecule. It should be noted that in the present modelling exercise we used the co-ordinates of the SEB-DR1 complex (Jardetzky *et al.*, 1994), and that SpeA1 has preferential binding for

HLA-DQ. However, His 81 and its neighbouring residues are conserved in HLA DQ (Schiffenbauer *et al.*, 1987).

The recent structures of SpeC in complex with HLA-DR2 (Li *et al.*, 2001) and SEH in complex with HLA-DR1 (Petersson *et al.*, 2001) confirms this mechanism of action. Both SpeC and SEH show extensive and similar contact with the class II associated antigenic peptide have similar interactions with the antigenic peptide even though they are different. This indicates that the interactions seen in the SpeA1-DR1 model between SpeA1 and the antigenic peptide are also required for optimal superantigen/MHC binding.

There are at least four naturally occurring SpeA *alleles*, and three of these, *SpeA1*, *SpeA2*, and *SpeA3* encode for toxins that differ from each other by a single amino-acid (Musser *et al.*, 1991). SpeA3 differs from SpeA1 by a single amino Val to Ile substitution at position 76. SpeA2 differs from SpeA1 by a single Gly to Ser substitution at position 80. In the SpeA1 structure, both Val 76 and Gly 80 are buried. The allelic variants of SpeA show different binding affinities for HLA-DQ with K_is of 104, 55, and 13 μM for SpeA 1, 2, and 3 respectively. SpeA3 is the most mitogenic of these alleles, and appears to exhibit a higher affinity for HLA-DQ than SpeA1 (Kline and Collins, 1996). It is tempting to suggest that the proximity of this allele specific amino acid residue to the zinc binding site of SpeA3 (adjacent to Asp 77) may play a role in the increased affinity for HLA-DQ. Furthermore, it has been shown that a variant of SpeA1, Asp77Ala, has a much lower ability to bind HLA-DQ (Hartwig *et al.*, 1993). In addition, it is interesting to note that Ser 80 in SpeA2 is also located in close proximity to the zinc binding site of SpeA1 and to residues implicated in TCR binding. Clearly the role of these two residues needs to be investigated further. However, the presence of a zinc site does offer an alternate mode of MHC class II recognition by

SpeA1, and perhaps the possibility of additional interactions with MHC class II molecules to accommodate multiple TCR molecules. Superantigen dimerisation as a prerequisite for T cell activation has been suggested for SED (Sundstrom *et al.*, 1996) and SpeC (Roussel *et al.*, 1997).

The TCR binding site

SpeA1 binds to, and activates human T cells bearing Vβ12.2, Vβ14.1 and Vβ2.1 (Kline and Collins., 1997) (Lavoie *et al.*, 1999). It has been shown that SpeA1 utilises different residues depending on the TCR Vβ chain (Kline and Collins, 1997); a mechanism that has become evident from the known superantigen structures so far. The dissociation constant for the mouse TCR Vβ8.2 is in the same range as that of SEC2 (6.2 and 7.9 μM, respectively) (Malchiodi *et al.*, 1995). Based on the structural similarities of SpeA1 to SEC2 in combination with mutagenesis data, the TCR-binding site encompasses residues from the α2 helix, β2-β3 loop, the disulphide loop, α4-β9 loop, and the α5 helix.

As with other superantigens, high sequence variability and high flexibility is a common feature of the SpeA1 TCR binding site (Papageorgiou and Acharya, 1997). For example, Gly 19 in SEC2 is replaced with Lys 16 in SpeA1 and this may affect the number of contacts with the TCR Vβ chain. Asn 20 in SpeA1 is conserved in all superantigens and has been shown to play a critical role in the TCR binding.

The disulphide loop appears to be important for interactions with both the TCR and MHC class II. The conformation of the disulphide loop between Cys 87 and Cys 98 has been shown to be important for MHC class II binding (Kline and Collins, 1996; Roggiani *et al.*, 1997). In SEC2, four residues from the disulphide loop could make potential contacts with the complementarity determining region 1 (CDR1) chain and

Gln 72 of Vβ. The disulphide loop of SpeA1 is significantly shorter and these interactions may not be feasible. However, Cys 90 and Cys 98 from the disulphide loop of SpeA1 are required for stimulation of Vβ 12.2 expressing T cells (Kline and Collins, 1997), with Cys 90 being essential for Vβ12.2 T cell stimulation, and to a lesser extent for Vβ14.1, whilst having no observable influence on the stimulation of Vβ2.1 expressing cells (Kline and Collins, 1997).

SpeA1 recognition and binding modes

It is proposed that superantigen recognition and complex formation can occur by several different modes of action (Figure 2.7) depending on the superantigen involved. For example dimerisation of SED (Sundstrom *et al.*, 1996) and SpeC (Roussel *et al.*, 1997) has been suggested as a prerequisite for T cell ativation. Previous data for SpeA1 suggests that this toxin could also act as a dimer under certain conditions. During the purification of recombinant SpeA1 at pH 7.9 approximately 50% of the purified protein is in a biologically active, disulphide linked dimeric form (Papageorgiou *et al.*, 1999). Thus the combination of generic and zinc-dependent MHC class II binding sites with a dimeric form of the toxin would allow SpeA1 multiple modes of interaction with both MHC class II molecules and T cell receptors.

-4-

Chapter four

The Crystal Structure of Staphylococcal Enterotoxin B T-cell Variant Thr 112-Ser

Introduction

Staphylococcal enterotoxin B (SEB), a primary cause of food poisoning is also responsible for a significant percentage of non-menstrual-associated toxic shock syndrome in patients with a variety of staphylococcal infections. These include surgical and postpartum wound infections, deep abscesses, burns, abrasions, insect bites, sinusitis, and influenza-associated super-infections of the respiratory tract (MacDonald, 1996, Lowell, 1996) (Schlievert, 1993). The case fatality rate for toxic shock syndrome can be up to 50% (Freedman, 1991) and in influenza associated cases, mortality can reach 90% (Schlievert, 1993). SEB is considered to be the most potent of the staphylococcal superantigens and in an aerosolised form, is considered a potential biological warfare threat; causing incapacitation, shock and death in soldiers and civilians.

The high resolution structure of SEB (1.5Å) (Papageorgiou *et al.*, 1998) along with the crystal structure of SEB in complex with HLA-DR1 (Jardetzky *et al.*, 1994) and TCR V_β (Fields *et al.*, 1996) has allowed a detailed analysis of the functional domains of SEB. As such, it is often cited as the prototypic superantigen (Papageorgiou and Acharya, 2000). The TCR binding site lies between the two domains of the toxin in a shallow cavity formed by residues 20 – 33 (mostly α2 helix), 55 – 61 (β2 – β3 loop), 87 – 92 (β4, β4 – β5 loop), 112 (β5), 177 (α4 – β9 loop)210 – 214 (α5) (see Figure 4.1). The MHC class II binding site is located primarily in the N-terminal domain of the toxin and comprises of residues 44 – 47 (β1 – β2 loop) 65 – 69 (β3, β3 – α3 loop), 89 (β4), 92 – 96 (β4 – β5 loop), 115 (β5), 211 – 215 (α5) (Jardetzky *et al.*, 1994). It is apparent that several of the TCR binding residues and MHC class II binding residues juxtapose each other.

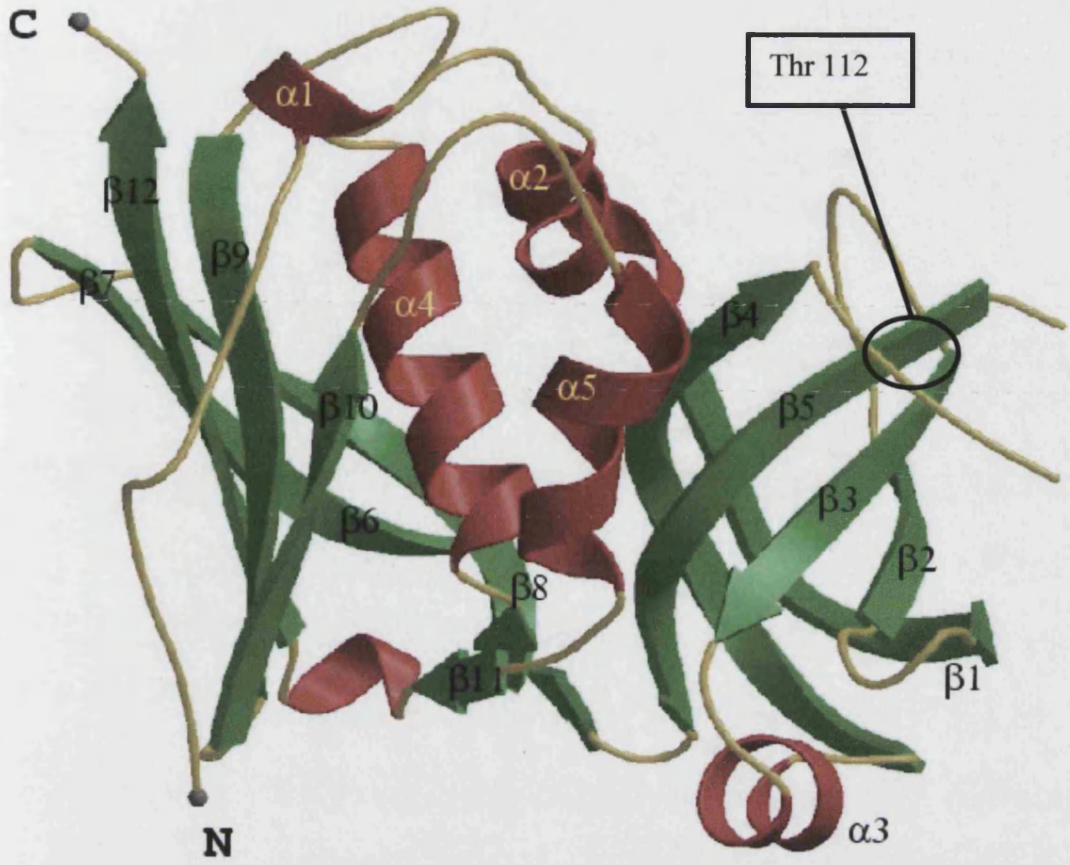

Figure 4.1: The crystal structure of native SEB. All secondary structure elements are labelled (Papageorgiou *et al.*, 1998).

Through mutagenesis of individual amino acids, it is possible to further assess each residues contribution both to the functionality of the toxin and to the overall structure of the toxin. The Thr 112 Ser variant was selected for study in order to assess the functional and structural contribution of this residue to the binding of TCR by SEB. Thr112 has been proposed to be involved in SEB – TCR interactions previously (Swaminathan *et al.*, 1992). However this residue is buried in the high resolution structure (Papageorgiou *et al.*, 1998). As such, it is presently unclear what role threonine 112 plays in TCR binding in SEB. This study undertook to elucidate the crystal structure of SEB Thr 112 Ser. In order to examine any possible effects that this

mutation might have on the toxins ability to interact with the TCR its structure was compared to that of free and TCR complexed SEB.

Materials and Methods

Expression and purification of SEB Thr 112 Ser

Purified protein was supplied by Dr Rick Titball, CBDE, Porton Down, Salisbury, UK. The procedure adopted was as follows. The recombinant plasmid pMALc2 encoding SEB Thr 112 Ser –maltose binding protein fusion protein were transformed into *E. coli* X1776. These recombinant bacteria were cultured in tryptone soya broth (Oxoid) supplemented with the following to the final concentrations indicated: 20 mM Tris – HCl pH 7.5, 5 mM magnesium chloride, 0.5 % (w/v) glucose, 0.01 % diaminopimelic acid, 0.005 % (w/v) thymidine and 50 μg/ml ampicillin. 400 ml cultures were incubated at 37 °C with shaking at 180 rpm. IPTG was added to a final concentration of 0.5 mM at an A_{600} of 0.7. Cultures were incubated for a further 3.5 hours and the cells harvested by centrifugation at 12,000 x g, 4°C for 10 minutes. The cells were resuspended in 30 ml of column buffer; 20 mM Tris – HCl pH 7.4, containing 200 mM sodium chloride, and 1 mM dithiothreitol. Lysozyme was added and the suspension incubated at 20 °C for 30 minutes. Aliquots were sonicated on ice for 3 x 20 seconds with 20 seconds rest. The crude cell extract was centrifuged at 12, 000 x g for 30 minutes at 4°C. The filtered supernatant was applied to an equilibrated 40 ml column and washed with 400 ml of column buffer. 40 ml of elution buffer (column buffer containing 10 mM maltose) was added to the drained resin and the column rolled for one hour at room temperature. The eluate was collected in 1 ml fractions and analysed at 280 nm and by SDS gel. Fusion protein containing fractions were pooled and cleaved with 1.6 ml (1600 units) of factor Xa (Amersham Pharmacia Biotech Ltd.) in column buffer containing 1mM calcium chloride and 0.05

% SDS (w/v) overnight. The cleaved product was dialysed against 25 mM Tris – HCl pH 8.0 containing 20 mM sodium chloride overnight and then filtered using a 0.22 μM filter. The filtered sample was the applied to a Mono Q anion exchange column and the run-through containing the cleaved toxin was collected. Pooled fractions were then concentrated by stirred cell ultrafiltration (Millipore U.K. Ltd) and assessed for purity and quantity by SDS gel and Coomasie blue dye binding assay (Biorad Ltd).

Crystallisation

Crystals of SEB Thr 112 Ser variant were grown at 16°C using the hanging drop vapour diffusion method. Samples (2μl) of the reservoir solution (0.8ml) containing 30 % (w/v) PEG 4000, 50mM sodium citrate buffer (pH 4.6), and 0.1 M ammonium acetate were mixed with an equal volume of protein stock solution (10 mg/ml) on siliconized cover slips. After several months crystals formed in the orthorhombic space group $P2_12_12_1$ with two molecules in the asymmetric unit. The crystallisation conditions and molecular packing in the variant structure differs from that previously reported for the native SEB toxin (Papageorgiou *et al.*, 1998). Native SEB crystallised as a monomer, whilst the Thr 112 Ser variant forms crystals as a dimer.

Data collection

Diffraction data were collected at 100K using crystallisation buffer as cryoprotectant. The first data set was collected to 2.0 Å at the synchrotron radiation source, Trieste, Italy using a Mar 345 image plate. Seventy nine images were collected with an oscillation range of 1.5° per image. A second data set (55 images) was collected at Daresbury, PX 9.5 to 1.8Å with an oscillation range of 1.5° using a MAR CCD detector. Data processing, scaling and merging of the two data sets was carried out using the HKL suite (Otwinowski and Minor., 1997). The final R_{merge} was 11% with an overall completeness of 92.7%. The data processing statistics are given in table 4.1.

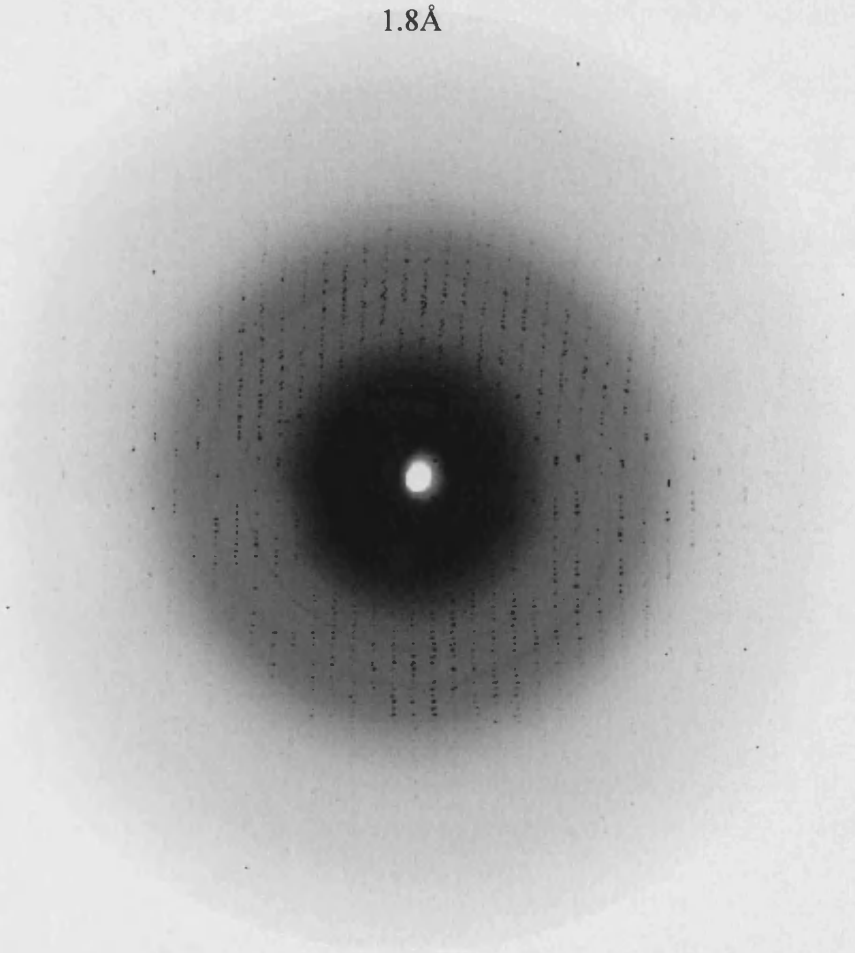

Figure 4.2: Diffraction image of SEB Thr 112-Ser variant crystal.

Structure determination and refinement

The structure of SEB Thr 112-Ser variant was solved using molecular replacement with the program AMoRe (Navaza, 1994) using the native 1.5Å native SEB monomer as the search model (Papageorgiou *et al.*, 1998). Clear solutions were found for the two models in the asymmetric unit as follows;

SolutionF	146.48	45.05	100.83	0.0091	0.3603	0.0902	65.9	38.7
SolutionF	36.43	132.01	285.80	0.4218	0.6885	0.8620	65.9	38.7

The resulting structure was subject to rigid body refinement and the calculation of an electron density map. The structure was refined by simulated annealing using the maximum likelihood target as implemented in the program CNS (Brünger *et al.*, 1998) with non-crystallographic symmetry (NCS) restraints. The progress of the refinement was followed by monitoring both R_{free} and R_{cryst} (Brünger *et al.*, 1992) values. The refinement was continued using cycles of simulated annealing and individual B-factor refinement followed by model rebuilding. Electron density maps ($|F_o| - |F_c|$ and $2(|F_o| - |F_c|)$ weighted at 2σ were calculated after each cycle of refinement and visualised using the program 'O' (Jones *et al.*, 1991). Water molecules were added to the model manually based on the density seen in the electron density maps, and also by using the water pick protocol in CNS. In the final rounds of refinement the NCS restraints were gradually released and the two molecules were checked and refined individually. The final model has a crystallographic R-factor (R_{cryst}) of 22.8% for all the data from 40 – 2.0Å resolution, and an R_{free} of 26% for 5% of the data omitted.

Table 4.1 Crystallographic data collection and refinement statistics

Cell Dimensions (Å)	a =39.5, b =98.5, c = 126.5
Space group	$P2_12_12_1$; 2 mol/a.u.
Resolution (Å)	40.0-2.0
No. of measurements	419612
No. of unique reflections	33201
Completeness	92.7 (88.3)[a]
I/σ	7.1 (2.9)
R_{merge} (%)[b]	11.0 (36.5)
Refinement	
R_{cryst} (%)[c]	22.7
R_{free}(%)[d]	24.6
No. of protein atoms	3801
No. of water molecules	170
Temperature factors (Å^2)	
Main chain[e]	22.54
Side chain	24.9
RMSD in bond lengths (Å)	0.007
RMSD in bond angles (Å)	1.169

[a] Outermost shell 2.1-2.0 Å.
[b] $R_{merge} = \Sigma(|Ij - \langle I\rangle|)/\Sigma\langle I\rangle$, where Ij is the observed intensity of reflection j and $\langle I\rangle$ is the average intensity of multiple observations.
[c] $R_{cryst} = \Sigma||F_o| - |F_c||/\Sigma|F_o|$, where F_o and F_c are the observed and calculated structure factor amplitudes, respectively.
[d] 5% of the data that were used for the calculation of R_{free} were randomly excluded from the refinement.
[e] Temperature factors for individual molecules quoted.

Results and Discussion

Quality of the structure

The three dimensional structure of Thr 112 Ser-SEB variant was determined at 2.0 Å resolution. The data collection and refinement statistics are shown in Table 4.1. The final model contains 3802 non-hydrogen protein atoms with temperature factors in the range of 5-85 $Å^2$ and 173 water molecules with temperature factors <45 $Å^2$. The root mean squares (r.m.s) deviation between monomer pairs for the variant is 0.54Å, between the variant and native SEB structures is 0.82 Å respectively. The regions that deviate most between the native and mutant structures include the disulphide loop, the first 20 residues at the N-terminus, and residues 41 to 62. Exclusion of these regions improves the r.m.s deviation to 0.43Å. The Ramachandran plot for both molecules shows 87.1% of the residues in the most favourable regions and no residues in the disallowed regions. Residues 98 to 107 have not been modelled due to poor density and residue 238 in both molecule 1 and molecule 2 was modelled as alanine due to insufficient density. Molecule 1 will be used throughout for the discussion.

General Architecture and comparison with other prototype superantigens

The architecture of SEB Thr 112-Ser variant is essentially identical to that of native SEB and similar to that of other superantigens (Figures 4.1 and 4.5). Figure 4.6 shows an overlay of the C^{α}-traces of both variant (black) and native (grey) SEB. Residues 7 to 10 are rotated by 180° with respect to the native SEB structure. Even in the 1.5 Å native structure, this region was poorly defined with B-factors in the range of 70 – 125 $Å^2$; compared to B-factors in the range of 30 – 40 $Å^2$ and good quality electron

density in the Thr 112 Ser variant. The disulphide bridge formed by Cys 93 and Cys 113 is intact in the native structure; those residues of the disulphide loop that have been modelled are in a slightly different conformation to that of the native structure, although this is to be expected as the highly flexible nature of the loop makes it hard to model. The disulphide loop of SEB encompasses 19 residues compared to nine in SEA and 16 in SEC2 and extends some 12Å from the body of SEB (Papageorgiou *et al.*, 1998) into the solvent.

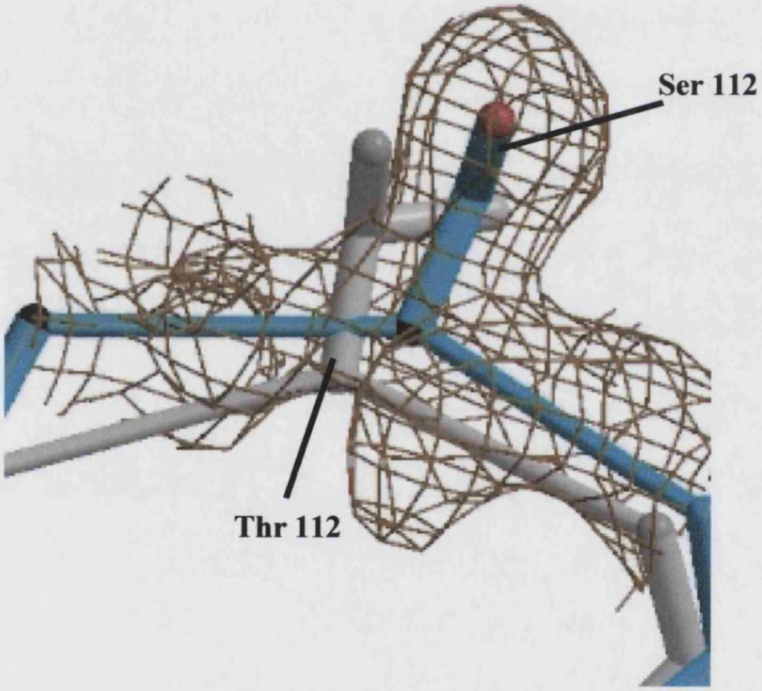

Figure 4.3: The electron density at the mutation site clearly indicates a density for a serine side-chain. 2 $|F_o| - |F_c|$ map contoured at 1 σ.

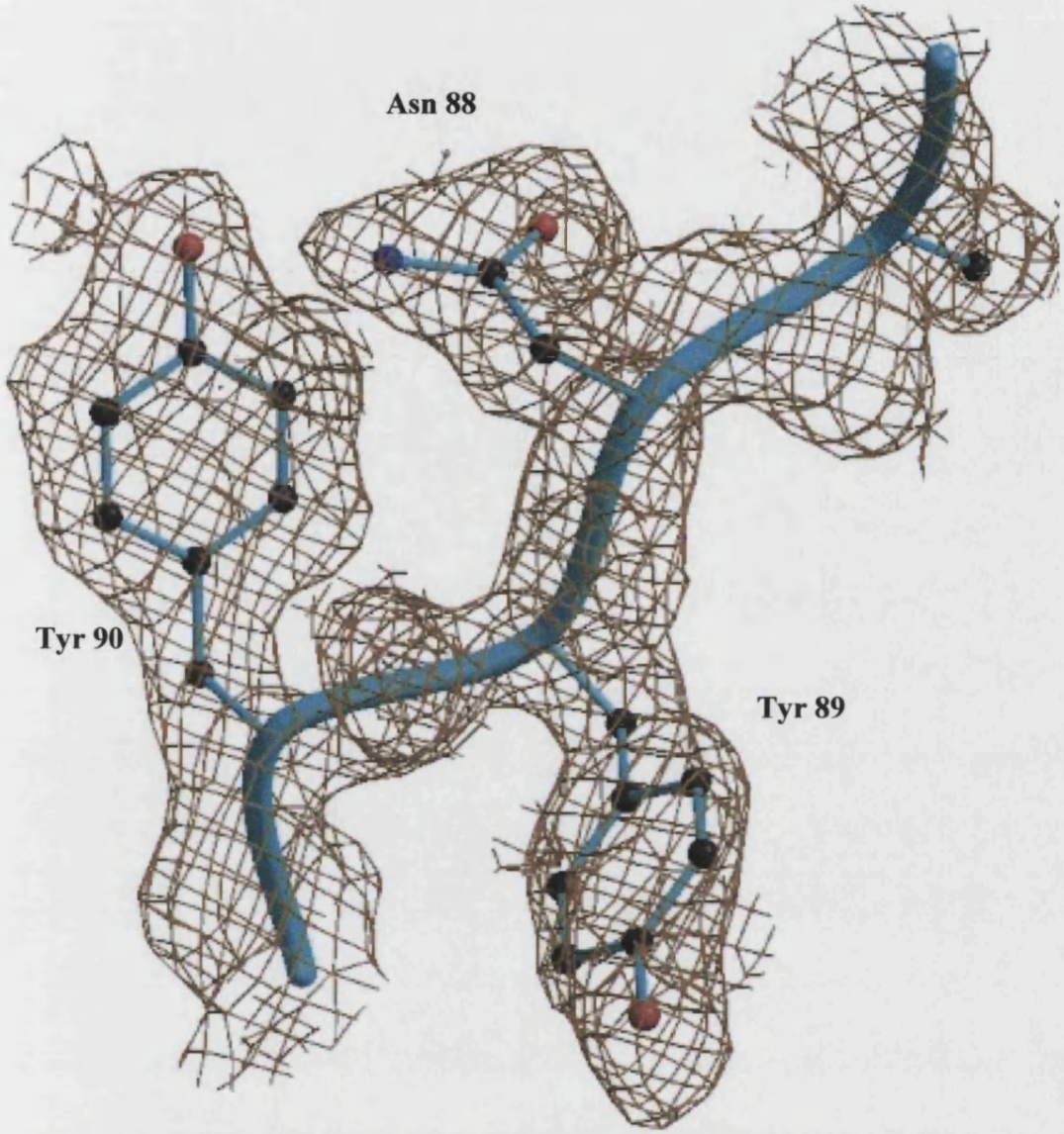

Figure 4.4: A representative portion of the electron density map at 2 Å contoured at 1 σ.

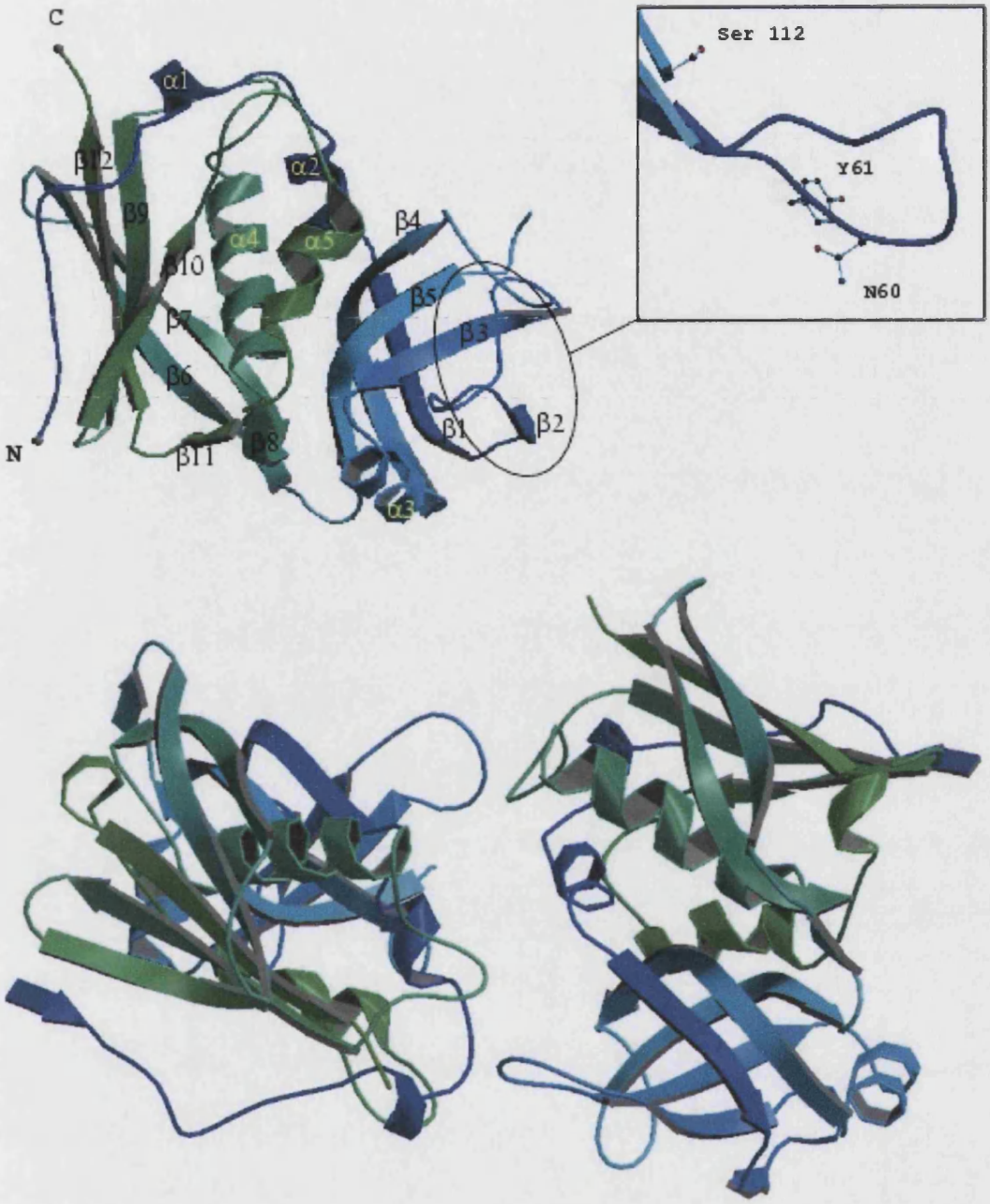

Figure 4.5: Ribbon diagram of SEB T112S monomer. All secondary structure elements are labelled (top). The 3_{10} helical turn in the C-terminal domain is labelled α-1. The mutation site is circled. Inset; the mutated threonine residue is labelled along with the TCR binding residues Asn 60 and Tyr 61.
Bottom: the arrangement of monomers to form the ncs dimer in the variant structure.

Crystal packing – Differences in the native and SEB Thr 112-Ser variant structures

Both native SEB and SEB Thr 112-Ser variant crystallise in the space group $P2_12_12_1$. Unlike native SEB which has one molecule in the asymmetric unit, Thr 112 Ser crystallises with two molecules in the asymmetric unit (Figure 4.5). The buried surface area at the interface between the two monomers is 1477Å^2. Upon dimer formation, a loss of approximately 10% of the accessible surface area is seen for each monomer, which is consistent with results from other protein-protein interfaces. Contact between the two monomers is mediated by several residues (Table 4.2). Interestingly, some of the contact between the two molecules is mediated by residues (58 and 59 in mol 1 and 54 and 58 in mol2) in the β2-β3 loop region (residues 53 to 61) which is involved in TCR binding and recognition (Table 4.3). In the Thr 112 Ser structure this loop is located at the dimer interface and residue 109 is involved in packing interactions with the N-terminal of mol 2.

Table 4.2: Contacts between molecules at the dimer interface as assessed by the program contact (CCP4, 1994)

Mol 1 Residue	Mol 2 Contact residue	No. of contacts
36	37	1
36	81	1
37	122	4
37	37	1
58	58	5
59	54	1
81	121	2
81	122	5
81	125	1
109	17	1
	18	1
122	122	1
126	193	1
238	9	3

Cut off values: C-C 4.1 Å, C-N 3.8 Å, C-O 3.7 Å, O-O 3.3 Å, O-N 3.4Å, N-N 3.4Å.

Figure 4.6: Cα trace of native SEB (black) overlayed with T112S variant (grey). View is tilted 180° forwards with respect to the standard view. The mutation site is located in the top right hand corner.

The TCR binding site

Mutagenesis and structural studies have identified regions 20 – 33 (α2 helix), 55 – 61 (β2-β3 loop), 87 – 91 (β4), 112 (β5), 177 (α4-β9 loop), 210 – 214 (α5) as being crucial for T cell receptor binding in SEB (see Figure 4.7 A, 4.7 B and Table 4.3). Contact in the SEB/TCR complex is between SEB side-chain atoms and TCR Vβ backbone atoms; mainly CD1, CDR2 and HV4 regions (Fields *et al.*, 1996). Asp 23; located in the α2- helix region is invariant among the superantigens and has been shown to be important in forming the core of TCR binding residues (Kappler *et al.*, 1992). Val 26 which is solvent exposed and situated in the middle of the α2 helix is also involved in SEB TCR binding. It has been shown that the corresponding residue in SEC1 and SEC2 confers differing TCR Vβ specificities on the two toxins. Also in this region of SEB are Asn 31 (solvent accessible) and Val 33 (buried) both of which are implicated in TCR binding specificity.

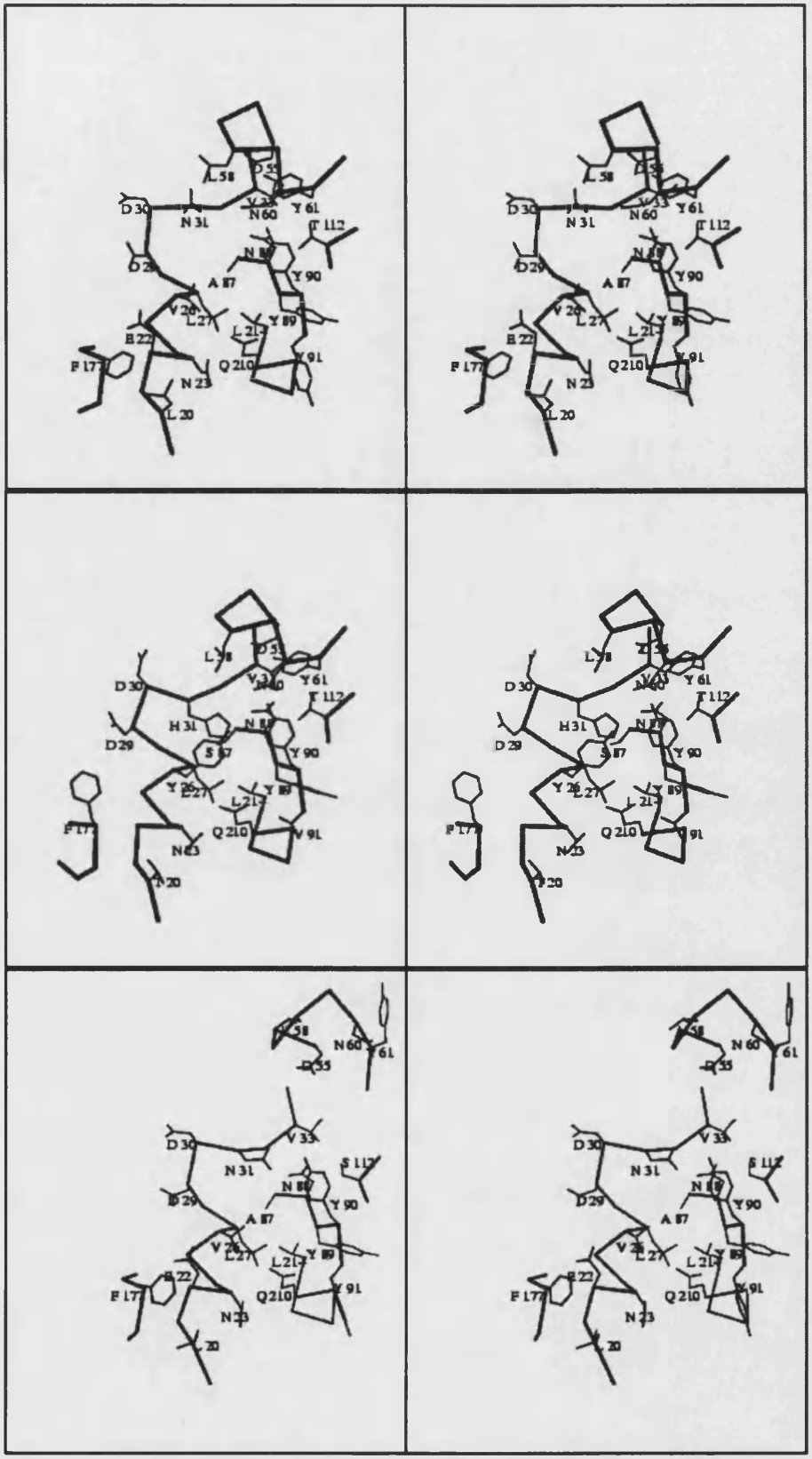

Figure 4.7: Close up stereo view of the TCR site of native SEB (top), SEB in complex with TCR Vβ chain (middle), and SEB Thr 112-Ser variant (bottom). All residues in the putative TCR binding site are shown, note the movement of the β2-β3 loop (residues 55 – 61) in the T112S TCR site.

Table 4.3: Contact between TCR Vβ and SEB for the complex, native and variant forms of SEB.

Hydrogen Bonds

TCR Vβ residue		SEB Residue No.		Bond length Complex	Bond length Native	Bond length Thr 112 Ser variant
G53	O	Q210	N	3.24	3.17	3.71
T55	N	N23	O	3.36	3.28	3.36
	O	N23	N	3.69	3.46	3.72
K57	N[b]	T18	O	3.08	3.02	3.14
P70	O[a]	N60	N	3.27	3.02	14.2

Van der Waals contacts (<4.0A)

TCR Vβ residue	SEB Residue No.	Complex	Native	Thr 112-Ser varaint
H47	L20	✓	✓	✓
	F177	✓	✓	✓
Y50	Y91	✓	✓	✓
A52	Y90	✓	✓	✓
G53	N23	✓	✓	✓
	E22	✓	✓	✓
	F177	✓	✓	✓
E56	L20	✓	✓	✓
	N23	✓	✓	✓
K57	T18	✓	✓	✓
	G19	✓	✓	✓
	L20	✓	✓	✓
Y65	F177	✓	✓	✓
Y66	F177	✓	✓	✓
A67	F177	✓	✓	✓
P70	N60	✓	✓	X (19.55Å)
S71	N60	✓	✓	X (20.01Å)

Comparison of the contacts between the TCR Vβ Chain and SEB, [a] refers to the first complex molecule in the asymmetric unit, and [b] refers to the second. Data for the complex are from Li *et al* (1998), data for the native are from the 1.5A structure Papageorgiou et al (1998). Distances were calculated for both native and variant forms by superimposing each structure on the SEB/TCR complex structure.

The β2-β3 loop (residues 55 –61) is flexible. The positioning of this loop may affect binding to TCR and/or MHC class II and the solvent accessibility of residues such as Asn 88, Tyr 89 and Thr 112 (Figure 4.7A, B, and C). Two residues in this loop, Asn 60 and Tyr 61 are conserved in SEB, SEC and SpeA1 and have been implicated in TCR interactions (Kappler *et al.*, 1992) (Papageorgiou *et al.*, 1999). Tyr 61 in SEB and SEC2 is partially hidden by Tyr 90 and Thr 112 which in turn are implicated in TCR recognition. Thr 112 is buried and as such its affects on TCR recognition are likely to be indirect, for example by perturbation of the local environment such as its hydrogen bond to Tyr 89 which is implicated in TCR and MHC binding (Papageorgiou *et al.*, 1998). The residue Phe 177 is situated within the α4-β9 loop. The loop is a putative TCR interaction region and Phe 177 makes several contacts with the TCR Vβ backbone in the SEB complex (Li *et al.*, 1998). The final region of interest in the site is the α-5 helix and in particular, residue Gln 210. Gln 210 is involved directly in TCR binding in SEB through hydrogen bonding with the Vβ main-chain.

Analysis of the structure of the Thr 112 Ser variant reveals that many of the gross features of the TC binding site are preserved sufficiently to allow interaction with the TCR.

The Mutation site

In the native SEB structure, Thr 112 forms a hydrogen bond with Tyr 89 and has van der Waal contact with Tyr 61. The mutation of Thr 112 to Ser causes the loss of the hydrogen bond with Tyr 89 and more dramatically the van der waals interaction with Tyr 61. As a result the loop region 52 to 64 moves by up to 20 Å causing the distance from Thr 112 to Tyr 61 to be ~12Å (Figure 4.7, Table 4.3). This loop region is already quite flexible and is stabilised by interaction with Thr 112 in the native

structure. The movement of Tyr 61 has implications for T cell recognition (Papageorgiou *et al.*, 1998) (Hayball and Lake, 2000). Asn 60 is also located in this loop and forms part of the TCR binding site. In the variant structure Asn 60 has moved some 14Å from its original position. Leder *et al* (1998) calculated the energetic contribution of the TCR binding site and found that Asn 60 has a modest, yet significant contribution to the overall binding of SEB to TCR . It was also found in binding studies that mutation of Asn 60 resulted in less efficient stimulation of T cells. Superposition of SEB Thr 112-Ser onto the SEB-TCR complex (Li *et al.*, 1998) by least squares superposition reveals that both Asn 60 and Tyr 61 cannot make their usual interactions with the TCR Vβ chain. The remainder of the contacts in the complex are also present in the docked Thr 112 Ser variant – TCR modelled complex. A secondary affect of mutation of Thr 112 to Ser and the subsequent movement of the β2 - β3 loop is the exposure of Thr 112 to the solvent. In this state, Ser 112 forms a hydrogen bond with water molecule 47 (2.88 Å) in a position equivalent to Tyr 61 in the native structure. In turn, this water molecule interacts with a second water molecule (3.04 Å), forms a hydrogen bond with Asn 63 (2.86 Å) and interacts with the sidechain of Val 64. These interactions help to stabilise the local environment of the mutation site in the absence of the β2 - β3 loop. The altered orientation of the β2 - β3 means that it was not possible to carry out energy minimisation of Thr 112-Ser when docked onto TCR. For this reason, no model is shown.

Biological effects

The SEB Tyr 61 deletion mutant (SEBΔ61Y) described by Hayball *et al* (Hayball and Lake, 2000) is able to bind MHC class II molecules as wild type, but behaves as an altered ligand for a T cell clone (AC20) that expresses the Vβ 17 TCR. SEBΔ61Y

possessed the ability to partially activate T celled based on its capacity to induce TCR down-regulation and IL-2 receptor up-regulation, but failed to elicit the secretion of IL-2, IL-3, IL-4, IFNγ or cell proliferation. Similarly, substitution of Tyr61 for alanine also causes a change in its Vβ usage profile (Hayball., 1994).

Work carried out in collaboration with the laboratories of Drs. R. Titball and M.A Kehoe (CBDE, Porton Down, Salisbury, UK) indicates that the Thr 112 Ser variant is, like Tyr 61 mutants, able to bind MHC class II molecules like wild type toxin. In a fashion analogous to the Y61 mutants, the TCR Vβ profile was also changed for the Thr 112 Ser variant compared to wild type response. SEB is known to selectively activate human V_β 3, V_β 12, V_β 14, V_β 15, V_β 17 and V_β 20 T cells. Results from experiments performed by our collaborators indicated that both SEB and Thr 112 Ser variant selectively induced T cells bearing V_β 3.1 and V_β 12. Thr 112 Ser variant and native SEB activated T cells bearing V_β 12 to an equal degree. However, Thr 112 Ser variant activated V_β 3.1 bearing T cells in the range of 24 – 86 % less than native toxin. These data suggest that the specificity of the toxin towards different V_β types has been altered by the introduction of the serine residue at position 112, although the mutation has a more subtle effect on TCR recognition than 60-61 mutants.

MHC class II binding site

The MHC class II binding site as defined by Jardetzky *et al* (1994) and Papageorgiou *et al* (1998) appears to be intact in the Thr 112 Ser varient structure. This site is formed by residues Phe 44 to Phe 47, Glu 67, Tyr 89 to Ser 96, Tyr 115, Asp 209 and Ser 211. The loss of the hydrogen bond between Thr 112

and Tyr 89 seems to have no effect on the architecture of the MHC class II binding site as an overlay of native SEB and Thr 112-Ser reveals all the residues to be in equivalent positions. However, it is unclear if the loss of this interaction would come into play during complex formation yet, MHC binding studies show little or no difference in affinities between SEB and SEB Thr 112-Ser (Baker *et al.*, 2001). Unlike most of the other superantigens, SEB does not possess a zinc binding site as an alternate mode for MHC class II interaction. This highlights the fact that various superantigens have evolved through slightly different mechanisms for their interaction with the immune system.

Conclusions

Clearly, the mutation of Thr 112 to serine has significant effect on T cell response. It would seem that Thr 112 effects TCR binding indirectly through maintaining the local environment of the TCR binding site through its contacts with Tyr 61 and Tyr 89 (Papageorgiou *et al.*, 1998). Unlike Tyr61 deletion mutants, the ability of Thr 112 Ser to stimulate particular subsets of T cells is maintained, but generally at a diminished level. Hayball and Lake (2000) propose that residues Asn 60 and Tyr 61 confer specificity for human TCR Vβ 17 and murine TCR Vβ 7 and 8.1. In the case of Thr 112-Ser, the TCR Vβ repertoire was the same as wild type SEB except that Thr 112-Ser stimulated V_β 3.1 to a lesser extent. In this study human Vβ 17 TCR were not stimulated by either variant or wild type toxin.

Vβ profile does differ between Thr 112 Ser and wild type, but in the Tyr 61 variant, activity is lost not reduced as is the case for the Thr 112 Ser variant, so this suggests a difference between Thr 112 Ser variants and Tyr 61 variants. Structurally these altered specificities could be accounted for by several ways. Firstly, it is important to

note that residues 60 and 61 are located in the middle of a loop region. The flexibility of this loop appears to have increased due to the loss of stabilising interactions with Thr 112. Therefore it is possible that for a proportion of those superantigens binding to TCR; the loop and hence these residues, are in a (near) correct orientation. In turn, this could be dependant on the architecture of particular Vβ chains.

Secondly, contact with the TCR Vβ chain in these positions could be preserved by a network of water molecules replacing Tyr 61 and Asn 60 being replaced by Lys 109. In the model of Thr 112 Ser complexed with TCR Vβ the N atom of Lys109 is in the same region as the N atom of Asn 60, which hydrogen bonds with the TCR Vβ chain. However, it should be noted that Lys 109 is located at the interface between the two molecules in the crystallographic dimer, forming a contact with both residue 17 and 18 of the second molecule. As such it would be impossible to distinguish between any possible role that this residue would have in TCR binding and dimmer formation with the current structure.

The variant produced has a reduced mitogenicity and therefore has the potential for use as a vaccine or therapeutic agent. However, care needs to be taken when assessing a TCR binding site mutants potential as a vaccine as it is possible to create a superantigen with altered TCR specificity or increased affinity.

-5-

Chapter five

Crystal Structures of Toxic Shock Syndrome Toxin –1 (TSST-1) T cell Receptor Binding Site Variants

Introduction

Toxic shock syndrome (TSS) was originally described in 1978 by Todd *et al.*, (1978) in seven children between the ages of 8 – 17, with staphylococcal infection.
More recently, the disease has become almost exclusively associated with tampon use in healthy menstruating women. It is now known that TSS also occurs in non-menstruating women, men, and neonates and has been linked to many bacterial infections including pneumonia, osteomyelitis, sinusitis, and skin and gynaecological infections.
Staphylococcal TSS primarily affects women between the ages of 15 – 35. In the USA, the frequency of the disease ranges from 2.4 – 16 cases per 100, 000 of the population. The highest recorded incidence was in 1980; but, since then, there has been a persistent decline, largely due to the decreased use of super-absorbent tampons. Due to this, a combination of more effective treatments and increased awareness of the disease, mortality is now less than 3%, although recurrences have been reported in 30 – 40% of cases (Salandy, 2001).
The crystal structure of TSST-1 (Prasad *et al.*, 1993), (Acharya *et al.*, 1994), (Papageorgiou *et al.*, 1996) shows the toxin to be composed of a N-terminal domain (residues 1 – 89) and a C-terminal domain (residues 101 – 194). Mutagenesis and structural studies have identified residues of β1, β2 β3, β4, and β5 in the N-terminal domain as being involved in MHC class II binding (Kim *et al.*, 1994). The Crystal structure of TSST-1 in complex with an MHC class II molecule (Kim *et al.*, 1994) shows that TSST-1 extends over almost one-half of the conventional antigen binding site and contacts both the flanking alpha helices of the histocompatibility antigen and the bound peptide (Figure 2.6). Indeed, a series of peptides described Wen *et al,.*(1996)

specifically promote TSST-1 presentation by MHC class II molecules , thus they differentially influence the presentation of bacterial superantigens to T cells.

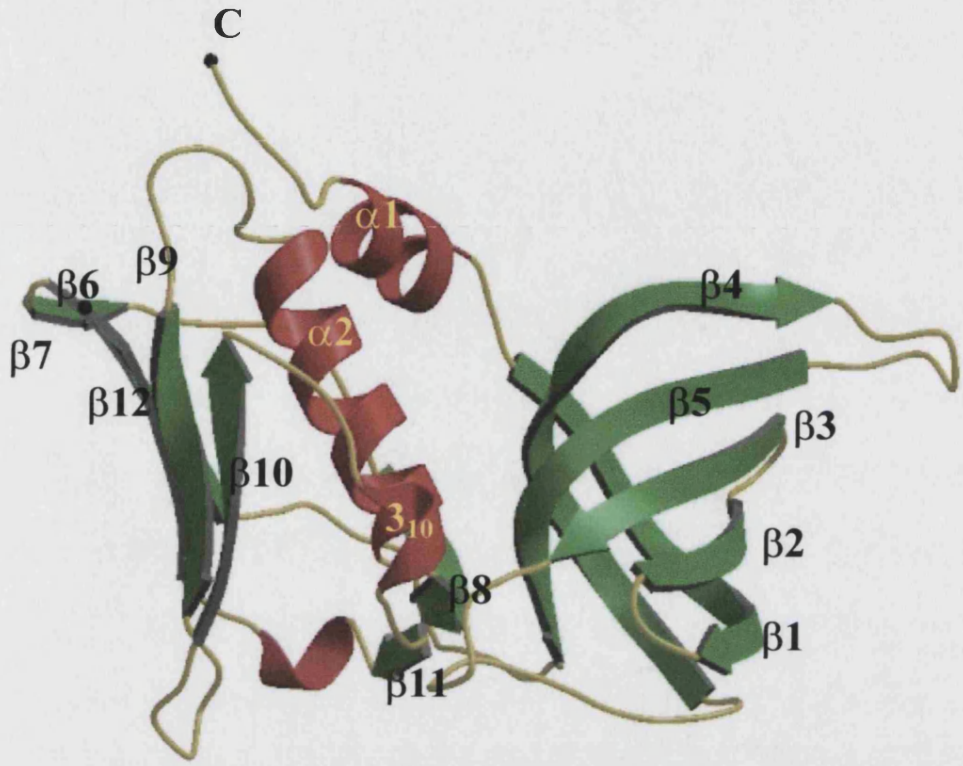

Figure 5.1: The structure of TSST-1 as a representative form of all three variant structures. Secondary structure elements including the 3_{10} helix are labelled.

Unlike many of the other superantigens, TSST-1 does not contain a zinc binding site (Acharya *et al.*, 1994). As such it is limited to its generic site for MHC class II binding. The global location of the TCR site in TSST-1 differs from that of the other superatigens (Figures 5.1 and 5.2). Mutagenesis studies have shown the residues in the region 115 to 144 (particularly Tyr 115, and the α2 helix residues – Glu 132, His 135, Ile 140, and His 141) are involved in TCR recognition by TSST-1 (Murray *et al.*, 1996) (Bonventre *et al.*, 1993). Antibody recognition experiments on these mutants showed that mutant toxin 135 retained recognition with monoclonal antibody 8-5-7 and was conformationally intact, yet was non-mitogenic. Toxin from a double mutant, 141.144, with alanine substitutions at residues 141 (histidine) and 144 (tyrosine), also was

devoid of mitogenic activity. In this case, antibody recognition was lost. Mutant toxins 115 and 141 were found to possess approximately half-maximal mitogenic activity and retained antibody recognition (Bonventre *et al.*, 1993). All of these residues are found in, or very near, a cleft formed by resiues 13 – 19 (α1 helix, β1) 61 – 65 (β4), 115 – 121(β7, β7 - β8 loop, β8), and residues from the α2 helix (Figure 5.1 and 5.10). Together these regions form the TCR binding site.

The native TSST-1 structure is notable for its unusual packing in the unit cell (Acharya *et al.*, 1994). The three molecules in the asymmetric unit are arranged such that two of them are packed next to each other with the third molecule packed on top. It belongs to the orthorombic space group $C222_1$ (cell dimensions a = 108.6, b = 177.6, c = 97.5Å) but due to its unusual packing also possess pseudo-hexagonal symmetry in the space group $P6_322$ (cell dimensions a = b = 104.1, c = 97.5Å) with one molecule per asymmetric unit (Acharya *et al.*, 1994).

Mutant selection criteria and aims

Each mutation site is shown below (Figure 5.2). The residues chosen have previously been shown to be important in TCR recognition by TSST-1 and are located at the rim of the TCR binding site. The crystal structure of the biologically inactive His 135 Ala TSST-1 form of the toxin revealed several important features of the TCR binding site (Papageorgiou *et al.*, 1996). The loss of interaction between the mutated His residue and the α1 helix causes a significant change in the conformation of the helix between residues 14 and 16 making it one residue shorter. This change in conformation could not be predicted from modelling studies alone, thus highlighting the importance of crystallography in examining the effects of individual amino acid

substitutions. This structure also highlighted the intricate nature of the interactions between the α-1 and α2 helices and their contribution to the overall stability of the TCR binding site.

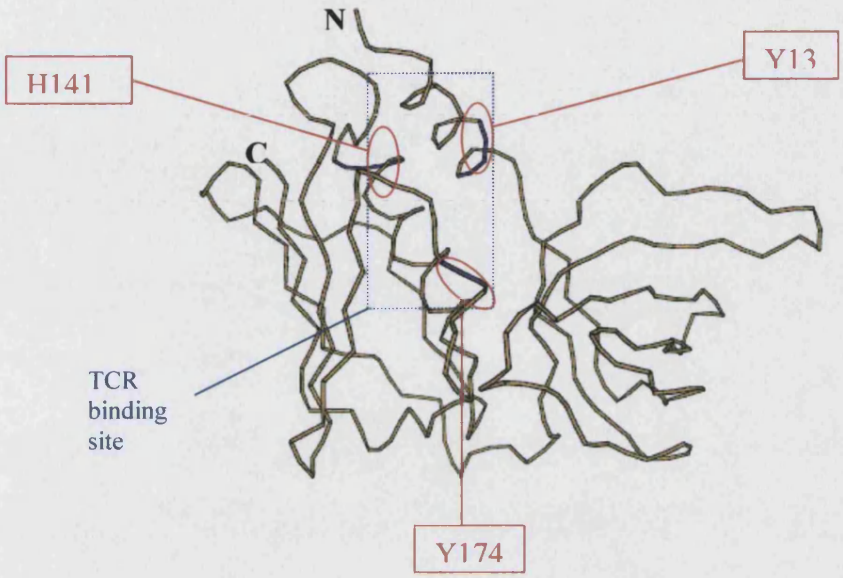

Figure 5.2: The TSST-1 TCR binding site is located in the centre of the toxin and encompasses residues from the α1 and α2 helices.

It remains to be seen whether inactivation of the toxin is caused by local or global conformation changes upon mutating certain amino acids. These mutations may affect the TCR binding by disrupting crucial interactions the global fold of the TSST-1 TCR binding site. It is postulated that mutation of the buried residues Tyr 13 and his 141 would have some effect on TSST-1 structure (Papageorgiou *et al.*, 1996). The effects of a mutation in the 3_{10} helix such as Tyr 174, are unclear at present. In other superantigens such as SEB SEC2 and SEA, the TCR binding site is larger and encompasses a third helix region into the site (α5 SEB and SEA, α6 SEC2) which is analogous to the 3_{10} helix in TSST-1 (Papageorgiou *et al.*, 1996). The aims of these experiments were to purify enough TSST-1 Y13A for crystallisation and subsequent data collection and structure solution, and solve the structures on the previously crystallised Y174A and H141A mutants. Through examining the structures of these

three mutants, it is hoped that their role both in the architecture and function of the TCR site can be better understood.

Materials and methods

Growth and purification of Tyr 13-Ala variant

TSST-1 Tyr 13-Ala was supplied by CAMR in the pEZZXa vector (pharmacia LKB) subcloned into *E.coli* χ1776. This construct produces TSST-1Tyr 13-Ala protein fused with the ZZ domain of protein A for ease of purification with human IgG sepharose matrix.

pEZZXa-TSST-1 Tyr 13-Ala was inoculated into 50 ml of Tryptone Soya Broth (CAMR media) supplemented as follows; 2% 1M Tris-HCL at pH 7.5, 0.5% of a 1% magnesium chloride solution, 1% of 1% diaminopimelic acid, 0.5% of 1% thymidine, 1% of a 50% glucose solution, and 0.1% of 100 mg/ml ampicillin. Cultures were grown overnight at 37° C with constant shaking at 180 rpm, then seeded into two 2.5 L flasks containing 250 ml of supplemented media.

Cells were removed by centrifugation at 6000 rpm (Sorvall RC5 centrifuge, GS3 rotor) for 15 minutes and the supernatant decanted. Ammonium sulphate was added to the supernatant to a final concentration of 60% and the flask left at room temperature for 2 hours. The precipitated protein was then harvested by centrifugation at 12,000 rpm (Sorvall RC5, GSA 3 rotor) for 35 minutes. Protein pellets were resuspended in TE buffer to produce a final volume of 30 ml of crude protein extract, and dialysed overnight at 4° C against pure water. Aliquots of the extract were analysed by SDS PAGE and Western blot.

Purification of TSST-1 Tyr 13-Ala-ZZ fusion protein from crude protein extract

TSST-1 Tyr 13-Ala fusion protein was further purified by affinity chromatography using human IgG sepharose matrix (Sigma) a 1.6 cm diameter column (Pharmacia LKB technology) and a pharmacia LKB P1 pump. Once loaded onto the column the sample was washed with 100ml of 50 mM Tris-HCl pH 7.5 with 100 mM sodium chloride and the fusion protein eluted with 50 ml of 0.1 M glycerine-HCl (pH 3). Fractions were collected in 2 ml aliquots (flow rate of 1ml/min) and analysed at 280 nm. Fractions containing the fusion protein were pooled for further purification.

Factor Xa cleavage of the ZZ domain from TSST-1 Tyr 13-Ala and final purification.

50 μg of factor Xa was added per mg of protein, as assessed by its absorbance at 280 nm, and incubated at room temperature for 48 – 72 hours. The cleaved protein sample was then passed through the column again and eluted in the first wash. Purified protein fractions were then pooled and assessed for purity by SDS PAGE and Western blot (Figure 5.3).

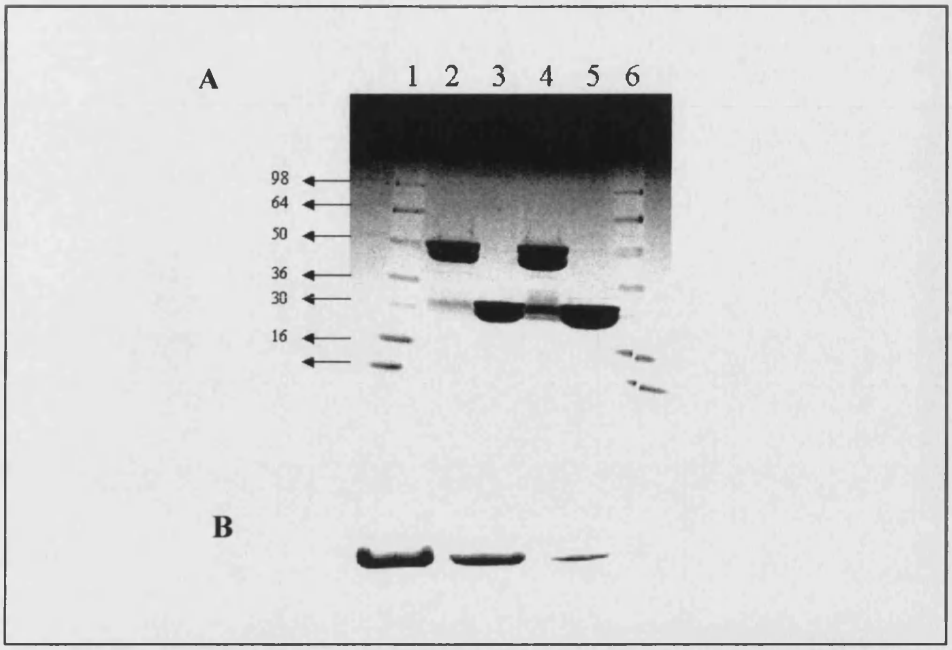

Figure 5.3: Top; the purification and cleavage of TSST-1 Y13A fusion protein. Lane 1. Molecular weight markers, 2) TSST-1 Y13A fusion protein, 3) TSST-1 Y13A fusion protein 72 our digest with factor Xa, 4)As lane two, 5) As lane three, 6) Molecular weight markers. Below; The final purified product as used for crystallisation. Each lane contains pure TSST-1 Y13A in successive 1 in 10 dilution (left to right)

Purified TSST-1 His 141-Ala and Tyr 174-Ala variants were supplied by CAMR, Porton Down, Salisbury, UK as part of a collaboration with Dr Howard Tranter.

Crystallisation of TSST-1 Tyr 13-Ala

Crystal screen conditions were initially set up based on the crystallisation conditions of the His 135-Ala mutant of TSST-1 (Papageorgiou *et al.*, 1996). Using the hanging drop method 24 well plates were set up with varying concentrations of PEG 4000 12-25% and LiCl (0.25- 0.85 M). The conditions that gave the best crystals were 0.1M sodium acetate (pH 4.6), 12% PEG 4000, and 0.55 M LiCl, and 5 mg/ml protein solution.

Crystallisation of His 141-Ala

Crystals were grown using the hanging drop method in 0.2 M sodium acetate, 25% PEG 4000, in Tris/HCl buffer (pH 8).

Crystallisation of Tyr 174-Ala

Crystallisation trials were carried out using the same conditions as TSST-1 H135A mutant (Papageorgiou *et al.*, 1996) as a starting point. Crystals were formed in the space group $C222_1$ under the following conditions 15 – 18 % PEG 4000, 0.65 – 0.85 M lithium chloride, and 100 mM sodium acetate buffer at pH 4.6.

Figure 5.4: Crystals of TSST-1 Y13A

Data collection and refinement

X-ray diffraction data for TSST-1 Tyr 13-Ala to 2.5Å were collected at room temperature at the Synchrotrone Trieste protein crystallography beamline (Italy) equipped with a MAR345 image plate in big Mar mode. Sixty three images were

collected at 180 sec/image, with an oscillation range of 2° per image. A second data set of thirty two images was collected at the SRS, Daresbury, PX 9.5 to 2.6Å resolution using a MAR345 image plate. The exposure time was 180 sec/image and the oscillation range was 1.5°. X-ray diffraction data for TSST-1 His 141-Ala to 2.9Å were collected at room temperature on beamline PX 7.2 (Daresbury, UK) equipped with a MAR345 image plate. Thirty images were collected in dose mode (180 sec/image), with an oscillation range of 1° per image. A second data set was collected at 3.0 Å resolution using a MAR345 image plate. The exposure time was 180 sec/image and the oscillation range was 1.0°. Room temperature data for TSST-1 Tyr 174-Ala to 2.8 Å was collected at the SRS, Daresbury, PX 7.2 (50 images) on a MAR345 image plate with 1.5° oscillation and 180 sec/image. A second dataset was collected to 2.5Å on beamline PX9.6 equipped with a MAR345 image plate. 47 images were collected at 180 sec/image, with an oscillation range of 1° per image. Data processing, scaling and merging was performed using the HKL program suite (Otwinowski and Minor, 1997). The final R_{merge} for TSST-1 Tyr 13-Ala was 12.6 % with an overall completeness of 86.4%, for His 141-Ala the final R_{merge} was 8.7 % with an overall completeness of 85.1%, and for Tyr 174-Ala the final R_{merge} was 11.6 % with an overall completeness of 85% (Table 5.1). In the case of Tyr 13-Ala and Tyr 174-Ala mutants which are isomorphous with native TSST-1, phases were determined using the structure of native TSST-1 (Papageorgiou *et al.*, 1996) as a starting model, which was subjected to an initial round of rigid body refinement. Due to the change in space group and the number of molecules in the asymmetric unit seen in the His 141-Ala mutant, molecular replacement was performed using the crystal structure of native TSST-1 as the search model. AMoRe (Navaza, 1994) gave clear solutions for the two molecules in the asymmetric unit as follows;

SolutionF	46.36	51.29	91.04	0.1918	0.3399	0.0865	40.2	52.0
SolutionF	37.19	109.98	248.28	0.8423	0.2182	0.8388	40.2	52.0

The structures were refined to completion by simulated annealing using tight non-crystallographic symmetry (NCS) restraints and the maximum likelihood target as implemented in the program CNS (Brünger *et al.*, 1998). R_{free} and R_{cryst} were used to follow the progress of refinement (Brünger *et al.*, 1992). At the final stages of refinement B-factor refinement and release of the NCS restraints were performed. For the Y13A and Y174A structures individual B-factor refinement was carried out and for H141A grouped B-factor refinement was used. SigmaA-weighted electron density maps ($|F_o| - |F_c|$, $2|F_o| - |F_c|$) were calculated after each cycle of refinement and visualised using the program 'O' (Jones *et al.*, 1991). Water molecules were added to the Tyr 13-Ala and Tyr 174-Ala models towards the end of refinement with the aid of difference maps and the program water_pick in CNS (Brünger, 1998). The final model of TSST-1 Tyr 13-Ala has a crystallographic R_{factor} (R_{cryst}) of 20.3% for all data from 20 to 2.6Å resolution, and an R_{free} of 22.1% for 5% of the data omitted. The final TSST-1 His 141-Ala model has a crystallographic R_{factor} (R_{cryst}) of 18.7% for all data from 20 to 3.0Å resolution, and an R_{free} of 19.3% for 5% of the data omitted, and the final TSST-1 Tyr 174-Ala structure has a crystallographic R_{factor} (R_{cryst}) of 18.5% for all data from 20 to 2.6Å resolution, and an R_{free} of 19.8% for 5% of the data omitted (Table 5.1).

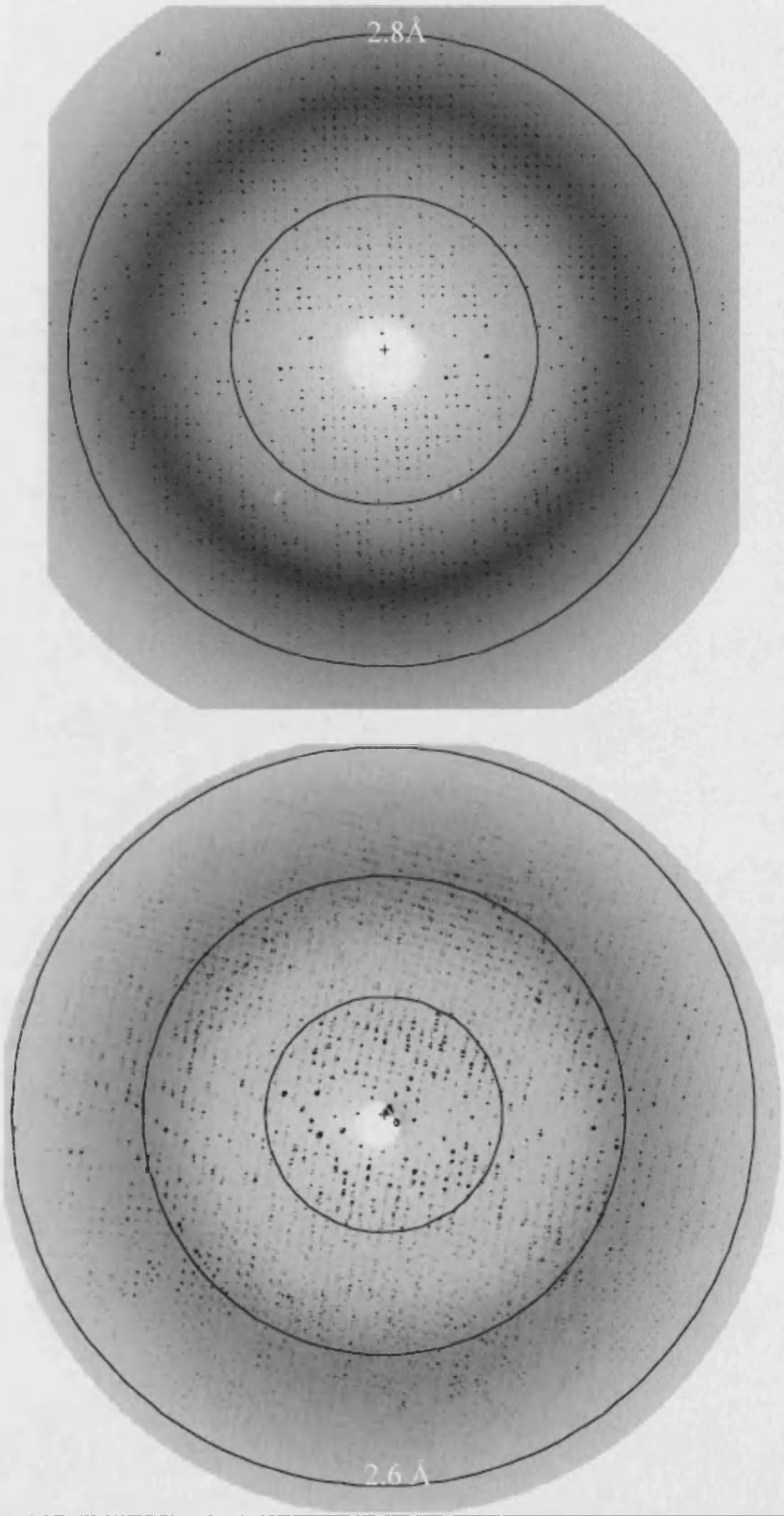

Figure 5.5: Diffraction image from TSST-1 Y13A (top) and TSST-1 Y174A (bottom).

Table 5.1 Crystallographic data collection and refinement statistics

	Tyr 13-Ala	His 141-Ala	Tyr 174-Ala
Cell Dimensions (Å)	a = 107.9, b = 175.1, c = 96.7.0	a = 126.9, b = 101.3, c = 82.0	a = 108.3, b = 176.9, c = 97.3
Space group	$C222_1$;3 mol/a.u.	$P4_12_12$;2 mol/a.u.	$C222_1$;3 mol/a.u.
Resolution (Å)	40.0-2.6	20.0-3.0	40.0-2.6
No. of measurements	90122	94387	83372
No. of unique reflections	38996	18340	32506
Completeness	86.4 (76)[a]	85.1 (87.8)[a]	84.7 (68.8)[a]
I/σ	6.6 (5.0)	6.3 (3.05)	5.1 (4.1)
R_{merge} (%)[b]	12.6 (39.7)	8.7 (54.9)	11.6 (27.8)
Refinement			
R_{cryst} (%)[c]	20.3	18.72	18.5
R_{free}(%)[d]	22.1	19.28	19.8
No. of protein atoms	4656	3082	4656
No. of water molecules	116	-	146
Average temperature factor(Å^2)	27.7	62.5	28.5
RMSD in bond lengths (Å)	0.007	0.007	0.006
RMSD in bond angles (Å)	1.362	1.36	1.342

[a] Outermost shell.
[b] $R_{merge} = \Sigma(|Ij - \langle I \rangle|)/\Sigma\langle I \rangle$, where Ij is the observed intensity of reflection j and <I> is the average intensity of multiple observations.
[c] $R_{cryst} = \Sigma||F_o| - |F_c||/\Sigma|F_o|$, where F_o and F_c are the observed and calculated structure factor amplitudes, respectively.
[d] 5% of the data that were used for the calculation of R_{free} were randomly excluded from the refinement.

Quality of the structures

The details of data collection and refinement for all three structures are shown in Table 5.1. Crystals of TSST-1 Tyr 13-Ala and Tyr 174-Ala contain three molecules in the asymmetric unit and belong to the orthorombic space group $C222_1$. The refined structure contains 194 amino acid residues (4656 protein atoms) with the Tyr 13-Ala

structure containing 116 water molecules and the Tyr 174-Ala structure 146. The overall quality of the final Tyr 13-Ala and Tyr 174-Ala models as assessed by PROCHECK (Laskowski, 1993) are good, with 90.3% of the residues in the most favoured regions and no residues in disallowed regions for both structures.

Superposition of Tyr 13-Ala monomer pair mainchain atoms gave an r.m.s. deviation of 0.21 and 0.23Å for mol1 – mol2, and mol1 – mol3 respectively. The r.m.s deviation for Cα atoms between native and Tyr 13-Ala is 0.36Å. Superposition of monomer pair mainchain atoms of Tyr 174-Ala gave an r.m.s. deviation of 0.25 and 0.25Å for mol1 – mol2, and mol1 – mol3 respectively. The r.m.s deviation for Cα atoms between native and Y174A mol1 is 0.21Å.

Crystals of TSST-1 His 141-Ala contain two molecules in the asymmetric unit and belong to the space group $P4_12_12$. The first three residues were not modelled due to poor density. The refined structure contains 191 amino acid residues (3082 protein atoms). The overall quality of the final model as assessed by PROCHECK (Laskowski, 1993) is good, with 82.5% of the residues in the most favoured regions and no residues in disallowed regions. Superposition of monomer pair mainchain atoms gave an r.m.s. deviation of 0.75 Å for mol1 – mol2. The r.m.s deviation for Cα atoms between native and mutant structures is 1.09 Å, mainly due to differences in the regions involved in crystal packing. Removal of these regions from the calculation give an rms deviation of 0.44 Å.

Crystal packing of TSST-1 Tyr 13-Ala and Tyr 174-Ala

As with native TSST-1, both the Tyr 13-Ala and Tyr 174-Ala variant forms crystallise with three molecules in the asymmetric unit (Papageorgiou *et al.*, 1996). The three molecules are arranged such that two of them (mol 1 and mol 3) are packed next to each other with the third molecule (mol 2) on the top (Figure 5.6). Mol 1 and mol 3 form a non physiological dimer, and mol 1 and mol 2 are related to each other by a two-fold non-crystallographic axis (Acharya *et al.*, 1994). Mol 2 residues 157 – 163 (β9-β10) are close to the concave face of the N-terminal β-barrel of mol 1 and between the β1 strand and the β4 - β5 loop. There is only one hydrogen bond at the interface between mol1 and mol2 (between Asp160 of Mol 2 and Arg 34 from mol 1). There are several van der Waals contacts between mol1 and mol 2 including some water mediated contacts (Papageorgiou *et al.*, 1996).

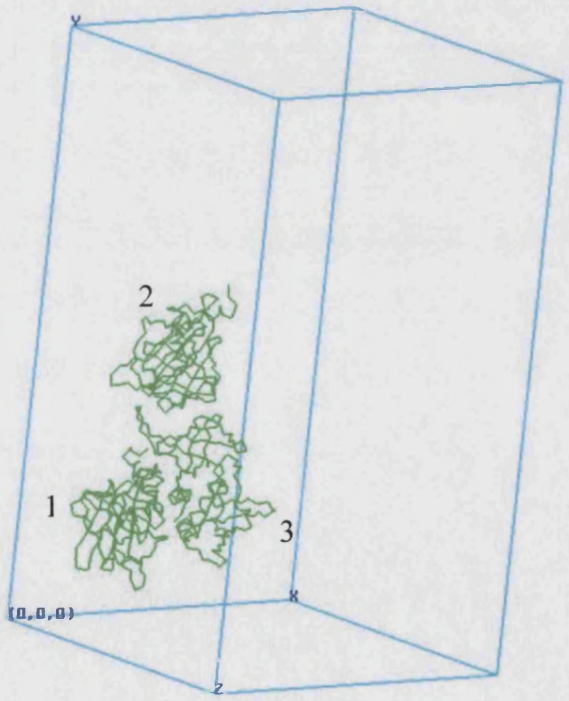

Figure 5.6: The arrangement of the three molecules of TSST-1 in the unit cell of the $C222_1$ form.

Molecules 1 and 3 make extensive contacts, mainly through the N-terminal residues 119 and part of the β4 (60 – 75) and β5 (79 – 89) strands and the loop between them. The formation of the interface corresponds to a loss of approximately 2000Å^2 of accessible surface area. The first 80 N-terminal residues of mol 1 and mol 3 are running almost parallel across the interface but in opposite directions. Part of the β4 and β5 strands from mol 1 runs parallel to the α1 helix of mol3 and several hydrogen bonds are formed (Papageorgiou *et al.*, 1996).

Crystal packing of His 141-Ala alternate crystal form

Interaction between the two molecules in the asymmetric unit is mediated by several residues all in the N-terminal domain. Residues from the β1, β2, β3, β4, β5 strands and the loops in between them from both molecules from van der Waals contact with each other (see Table 5.2).

Table 5.2: Contacts between monomer pairs in the TSST-1 H141A $P4_12_12$ crystal form. Cut-off values (Å); C – C = 4.1, C – N = 3.8, C – O = 3.7, O – O = 3.3, O – N = 3.4, N – N = 4.4.

Mol 1 residues (atom)	Mol2 residues (atom)	Distance (Å)
Ser 29 (OG)	Pro 48 (CB)	3.6
Leu 30 (CD2)	Pro 50 (CB)	3.8
Arg 34 (CZ)	Ile 46 (CD1)	3.5
Leu44 (CD1)	Ser 32 (CB)	4.1
Leu 44 (CD2)	Ile 46 (CG2)	4.1
Ile 46 (CG2)	Leu 30 (CB)	3.7
Lys 70 (CD)	Asp27 (OD2)	2.7
Lys 70 (CD)	Ser 29 (OG)	3.5
Lys 70 (CB)	Arg 34 (NH2)	3.8
Gln 73 (NE2)	Arg 34 (CD)	3.7
Thr 75 (OG1)	Gln 73 (OE1)	3.1
Thr 75 (CG2)	Ile 81 (CG2)	3.7
Ser 76 (CB)	Ser 76 (CB)	4.0
Glu 77 (OE2)	Gln 73 (CB)	2.9
(OE1)	His 74 (ND1)	3.3
Ile 81 (CG1)	Leu 44 (CD1)	4.1
Phe 83 (CE2)	Arg 34 (NH1)	3.2

The total buried surface between monomer pairs is 1481.4 $Å^2$. Due to the low resolution of the structure (3.0Å) it is unclear what part water molecules may play in mediating the contacts between the two monomers. The monomers pack together N – terminal β barrel to N – terminal β barrel (Figure 5.7). The $P4_12_12$ crystal form is unique to TSST-1 His 141-Ala and as a crystallographic dimer represents a new structure.

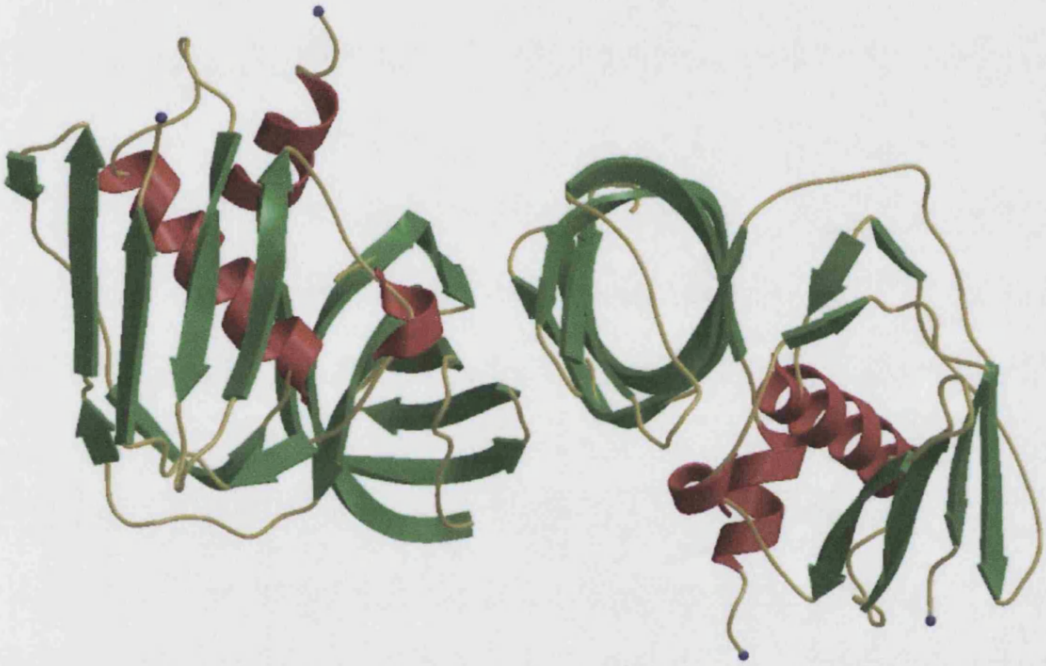

Figure 5.7: The crystal structure of TSST-1 variant H141A as a crystallographic dimmer. Interaction between the two monomers is mediated by several N-terminal domain residues.

Overall structure

The three TSST-1 mutant structures are essentially the same as native TSST-1 in architecture (Papageorgiou *et al.*, 1996). All three comprise of an N- and C-terminal domain packed together to form a compact molecule of approximately 45Å X 45Å X 58Å. Despite the low sequence identity with other superantigens (less than 28%), the

overall structure of TSST-1 and subsequently these three variants is remarkably similar to other superantigens (see Chapter 2). However, TSST-1 exhibits several structural differences. It is 45 residues shorter than SEB and SEC2, and 39 residues shorter than SEA, mainly due to deletions in several loop regions and the absence of a disulphide loop (Papageorgiou *et al.*, 1996).

Effects of mutation

The density for the sidechains at the three mutation sites (Tyr 13, His 141, and Tyr 174) are shown below (Figure 5.8A, B, C). The $2|F_o| - |F_c|$ maps contoured at 1 σ clearly show density for the substitute alanines only.

A

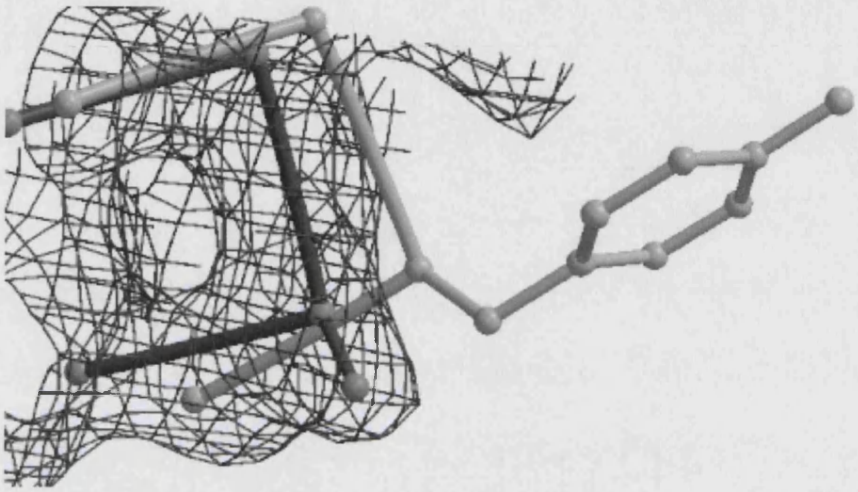

B

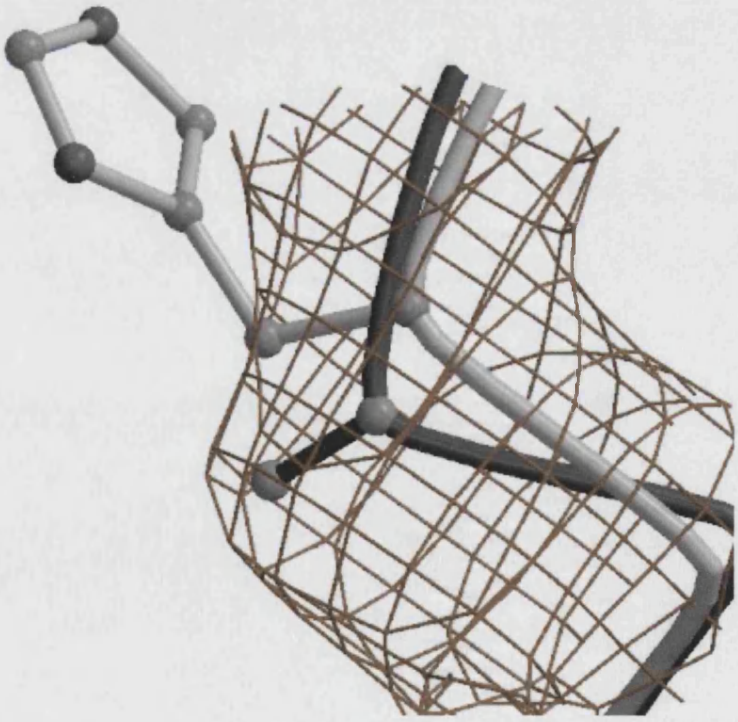

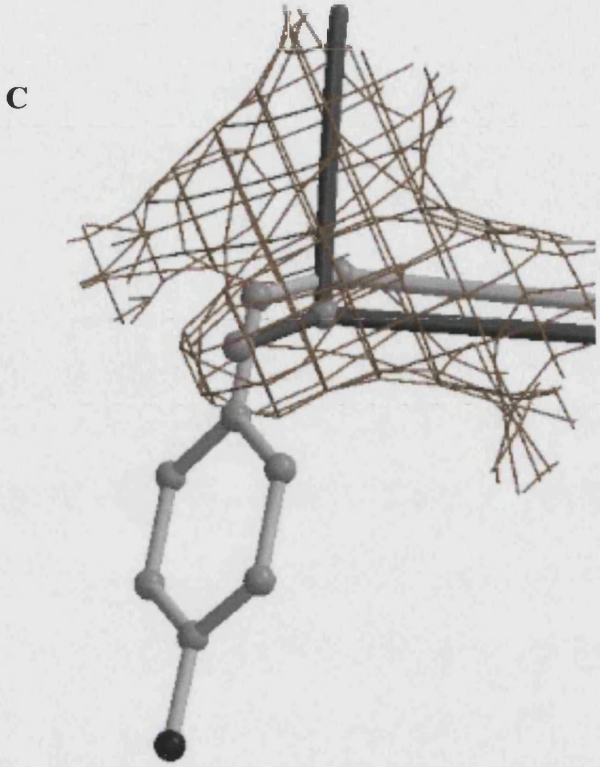

Figure 5.8: Sidechain density at the three mutation sites. **A** Tyr 113, **B** His 141, **C** Tyr 174. Native structure are shown in light grey, mutant structures in light grey. $2|F_o| - |F_c|$ map contoured at 1 σ.

Tyr 13-Ala effects of the mutation

In the native structure, Tyr13 is solvent-inaccessible and participates in hydrogen bond formation with Asp130 and His135 (Papageorgiou *et al.*, 1996) and as such is strongly implicated in the overall architecture of the site (Figure 5.9). In a previous study mutation of Tyr13 to leucine resulted in a toxin with no ability to stimulate human T cell hybridoma cells, but still able to bind MHC class II molecules (Hurley *et al.*, 1995). Of the residues that contact Tyr13, His 135 has been shown to be of great importance for the overall structure and activity of the toxin (Papageorgiou *et al.*, 1996), (Bonventre *et al.*, 1993). Mutation of His 135 to alanine results in the loss of T cell mitogenicity and also loss of toxicity in animal models (Bonventre *et al.*, 1993).

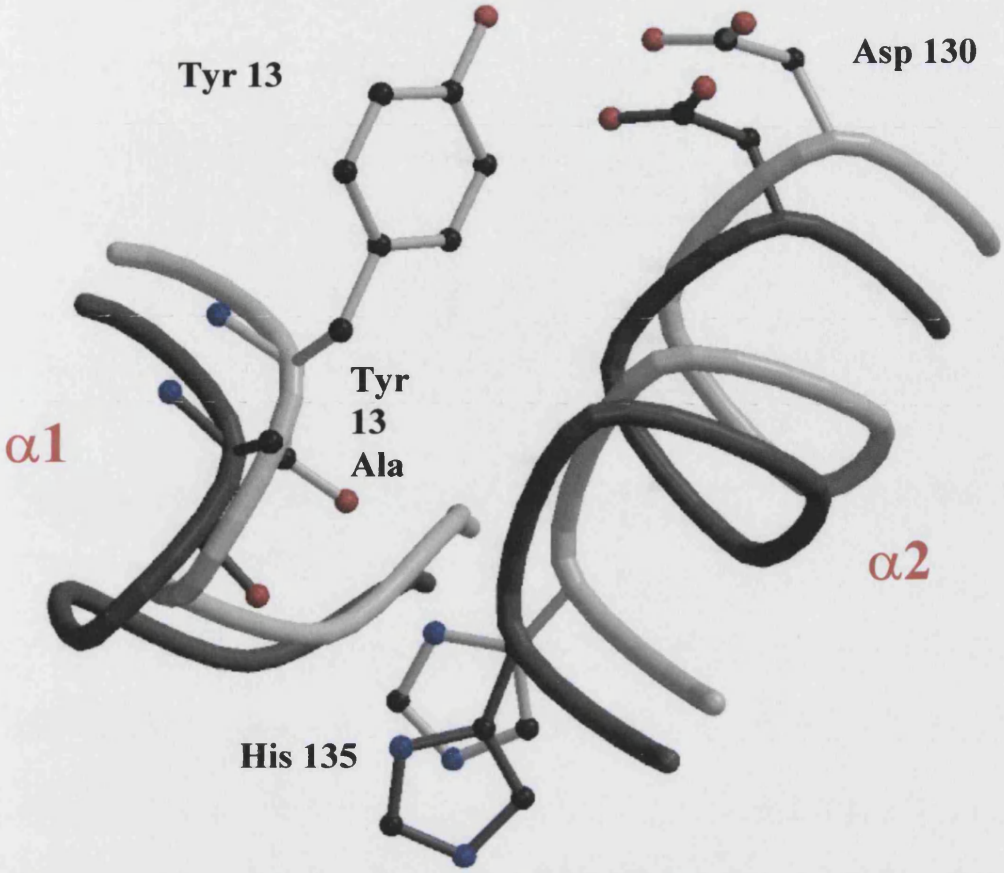

Figure 5.9: The interactions between Tyr 13 and the α 2 helix. Native structure is shown in light grey, mutant in dark grey.

His 135 (α2 helix) is thought to be directly involved in TCR interaction and in the H135A mutant structure its replacement with alanine results in perturbation of the neighbouring α1 helix through loss of helix – helix interaction. However, the conformation of Tyr 13 is preserved in H135A by a stabilising H-bond with Trp12 and aromatic interaction with Asp 130 (Papageorgiou *et al.*, 1996). Clearly, the interaction between α1 and α2 helices is of great importance for TSST-1 with regards to TCR recognition.

In the mutant structure the loss of several interactions between the α1 and α2 helices causes the Cα backbone to move by 1.5 Å (away form the α2 helix) between residues 14 to 18 (the bottom of the α1 helix). The H-bond between residue 13 mainchain O

atom and His 135 sidechain is lost (the distance is 3.46Å compared to 2.7 Å in the native structure) as well as the H-bond between the Tyr 13 sidechain and Asp 130 (5.2 Å compared to 2.89 Å, see Figure 5.9)

Although contacts are preserved between residues in the α1 helix region (Ser 15 and Gly 16) and Lys 67 in the β4 strand. Ala 13 is in contact with two water molecules, also present in the native form which may function to stabilise the mutation site. Figure 5.10 shows a close up view of the TSST-1 TCR binding site including the location of the Tyr 13 and His 135 sidechains. The architecture of the site can be considered in two ways, firstly in terms of those residues thought to make direct contact with the TCR Vβ chain, such as Thr 128, His 135, Gln 139, and Ile 140 (Papageorgiou *et al.*, 1996) and secondly, in terms of those residues that maintain the overall structure of the site allowing optimal contact between TCR and TSST-1, as is the case for Tyr 13.

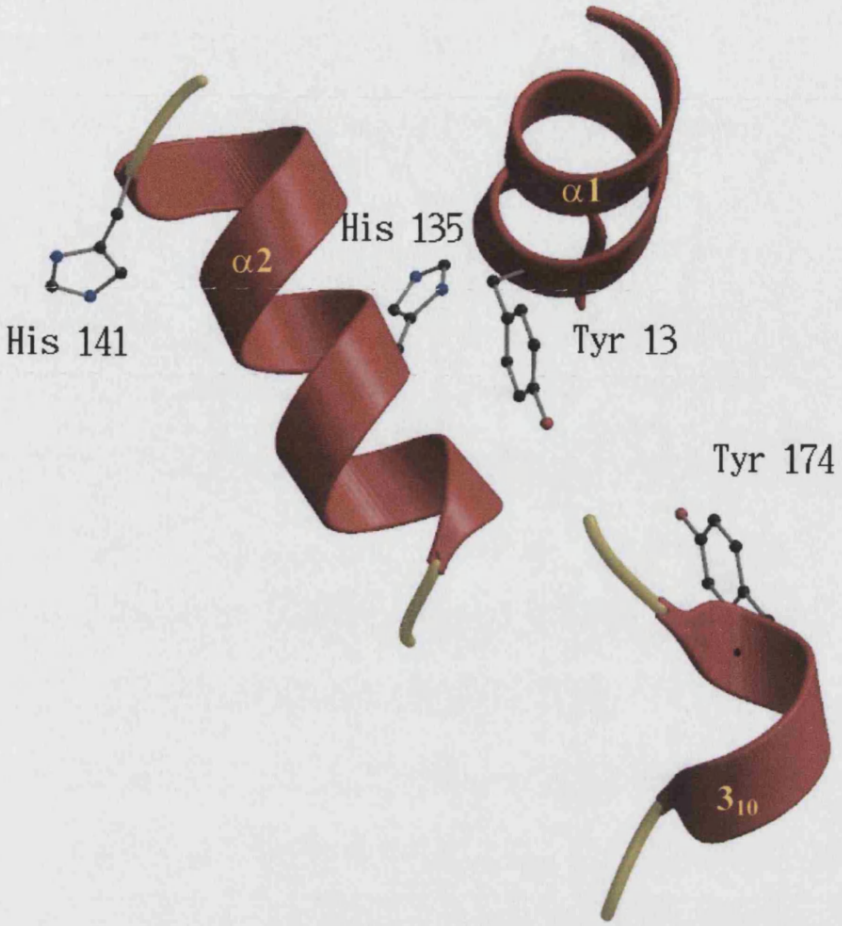

Figure 5.10: A close up view of the TSST-1 TCR binding site. The residues changed in the three variant structures are shown in ball-and-stick representation, along with residue His 135.

H141-Ala effects of the mutation

The most immediate change in the structure of TSST-1 His 141-Ala compared to native TSST-1 is the movement of the β4 strand (residues 74 – 80) by ~7.8Å. The β4 strand is thought to be involved in MHC class II recognition (Papageorgiou *et al.*, 1996). In the His 141-Ala structure this region is located at the interface between the two monomers and is involved in packing. The region encompassing the β6 - β7 loop and part of β7 is also shows some movement (Figure 5.11) probably due to crystal packing.

The region at the end of the α2 helix, residues 139 through to 150, including His 141 also shows some deviation from the native structure (5.11) movement is up to ~1.5 Å away from the α1 helix. Whilst the α1 helix also shows some deviation from that of the native structure.

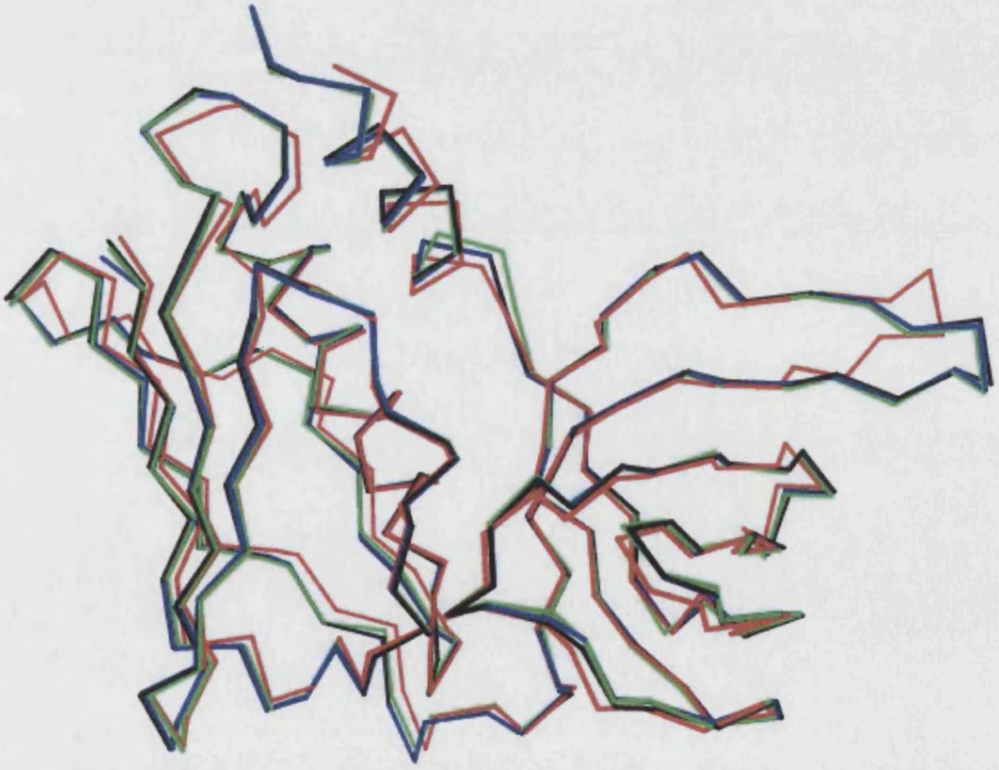

Figure 5.11: The Cα trace of native (dark grey), Y13A (green), Y174A (blue), and H141A (red) forms of TSST-1.

In the native structure, His 141 is located close to the C-terminal end of the α2 helix and is also inaccessible to solvent (Papageorgiou *et al.*, 1996). It is hydrogen bonded to Gln 136 and Ser 111 (Figure 5.12). Several studies have examined the importance of His 141 and its surrounding residues for TCR recognition (Bonventre *et al.*, 1993) (Deresiewicz *et al.*, 1994). His 141-Ala mutants were found to exhibit only half maximal activity, whilst the double mutant H141/Y144A was devoid of mitogenic activity (Bonventre *et al.*, 1993). However His 141-Ala variant toxin still caused lethal shock in rabbits. Mutations in this area seem to interfere in TCR recognition.

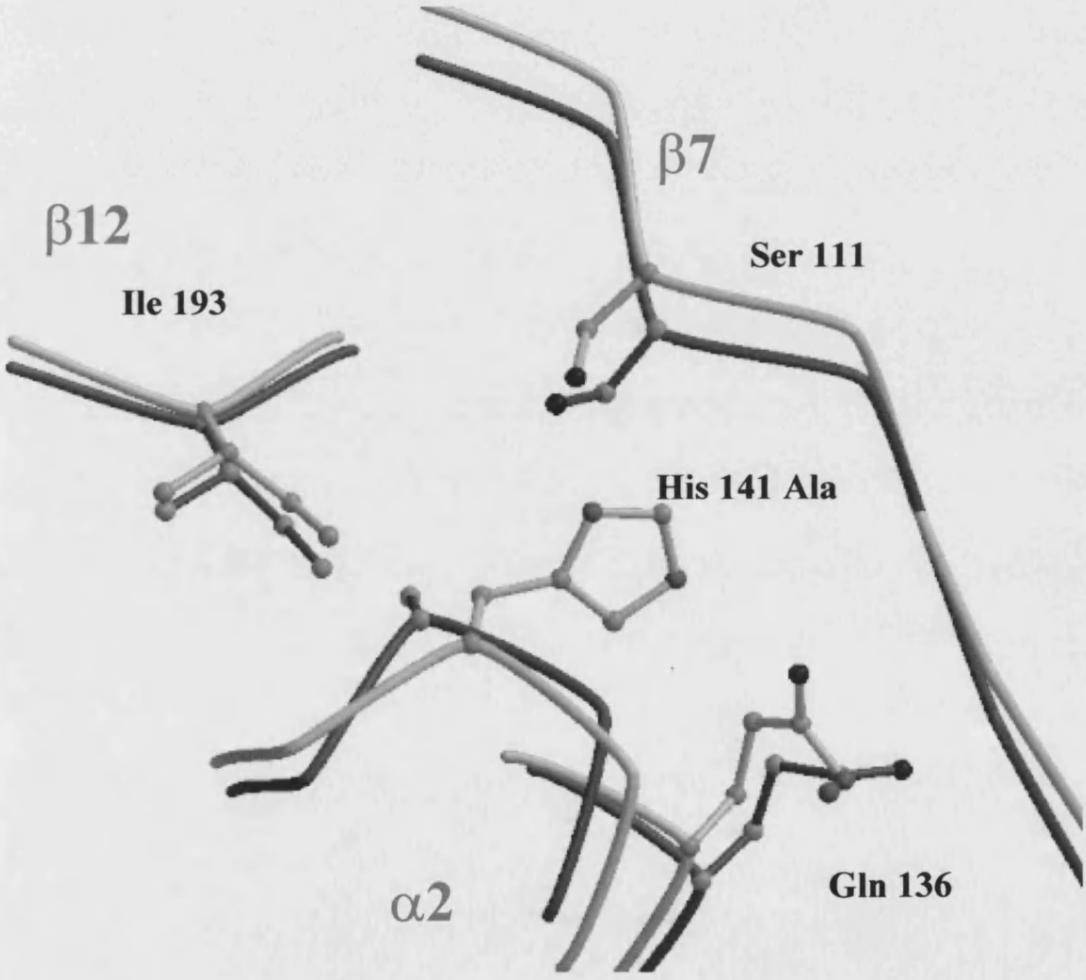

Figure 5.12: Comparison of the interactions of residue 141 in native (light grey) and mutant (dark grey) forms. All residues are labelled.

In the His 141-Ala structure both hydrogen bond contacts to Gln 136 and Ser 111 are lost. The local area is stabilised somewhat by van der Waals interaction between Ala 141 and Ile 193 (Figure 5.12). It is not clear at this resolution what contribution water molecules may make to the stabilisation of the mutation site. Solvent accessibility calculation using the program DSSP (Kabsch and Sander 1983) indicates that the mutation site is inaccessible to solvent.

It is interesting to note that His 141 falls in a region described by Arad *et al* (2000) and Visvanathan *et al* (2001) that defines a peptide protective against superantigen mediated shock both in terms of a vaccine and as a therapy (see Chapter 2 for more details). Although this residue may not be directly involved in TSST-1 TCR binding, it is clearly in an area of significant structural importance and high immunogenicity.

.

Effects of the mutation Tyr 174-Ala

In the native structure Tyr 174 is located at the start of the 3_{10} helix which lies immediately on top of the TCR site. It forms several contacts with other residues including Trp 12 from the α1 helix and Ser 127 from the α2 helix, both of which form part of the TCR binding site. Tyr 174 is orientated into the TCR binding site towards other TCR binding residues (Figure 5.10). It also makes contact with residues Pro 48 and Ile 85, both of which are implicated in MHC class II recognition (Papageorgiou *et al.*, 1996). In the Tyr 174-Ala structure Ala 174 makes almost no contact with any other residues (Figure 5.13). The mutation site is stabilised by the preservation of the contacts in the surrounding residues both with each other and with other parts of the toxin. Lys 171 makes contact with Trp 12, Phe 172 contacts Ser 127, Asp130 and Arg 134. Asn 176 contacts Ala 125 and Ile 126. All of these residues are located in either the α1 or α2 helix.

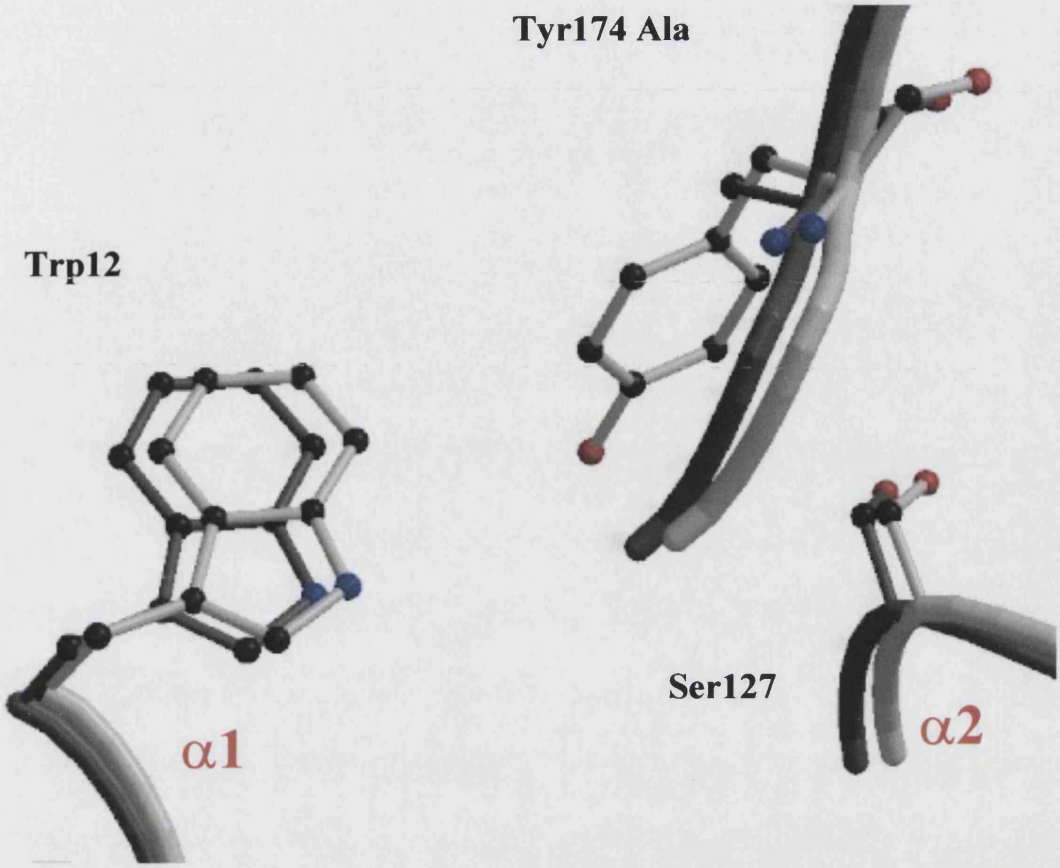

Figure 5.13: Comparison of the interactions of residue 174 and its neighbouring residues. The native structure is shown in light grey, the mutant structure in dark grey.

Two water molecules that are seen in the area of the mutation site in both the mutant and native forms may contribute to the overall stability of this region.

The interactions between this 3_{10} helix and the classically defined TCR binding site may identify a possible role for this region in TCR recognition. Whether this role is structural, in terms of stabilising the TCR site, or functional, in terms of forming direct contact with the TCR remains to be seen. Clearly further work needs to be done in order to further assess the contribution of this residue and the rest of the 3_{10} helix in TCR recognition.

Summary

TCR recognition among bacterial superantigens can be described both in terms of those residues that make direct contact with TCR Vβ and in terms of those residues that preserve the conformation of the binding site. Differences among the Vβ population mean that whilst a core of these residues may be constant for interaction with all Vβ subtypes, other residues will be specific for determining the particular Vβ specificities of each superantigen. As each superantigen binds several Vβ subtypes, these residues may differ for each Vβ type.

Binding studies and T cell proliferation experiments may give us useful information on residues that effect T cell recognition and activation; Similarly, the crystal structures of TCR binding site mutants help us to understand theses effects. But, without crystal structures of each mutant in complex with each TCR Vβ subtype, it is not possible to conclusively determine the contribution of each of these residues to TCR Vβ recognition.

-6-

Chapter six

Purification and Preliminary Crystallisation of Staphylococcal Enterotoxin C2 Zinc Binding Site Mutants

Introduction

The crystal structure of native SEC2 revealed a zinc binding site located between the two domains of the toxin (Figure 6.1). The site is formed by residues Asp 83, His 118, His 122 and Asp 9 from a symmetry related molecule which is most likely replaced with a water molecule under biological conditions (Figure 6.2) (Papageorgiou *et al.*, 1995) (Schad *et al.*, 1997).

The zinc site in SEC2 is superimposable with that of SEA (Schad *et al.*, 1995), SpeA1 (Baker, 2001), and SED (Sundstrom *et al.*, 1996) but differs somewhat in its coordination geometry.

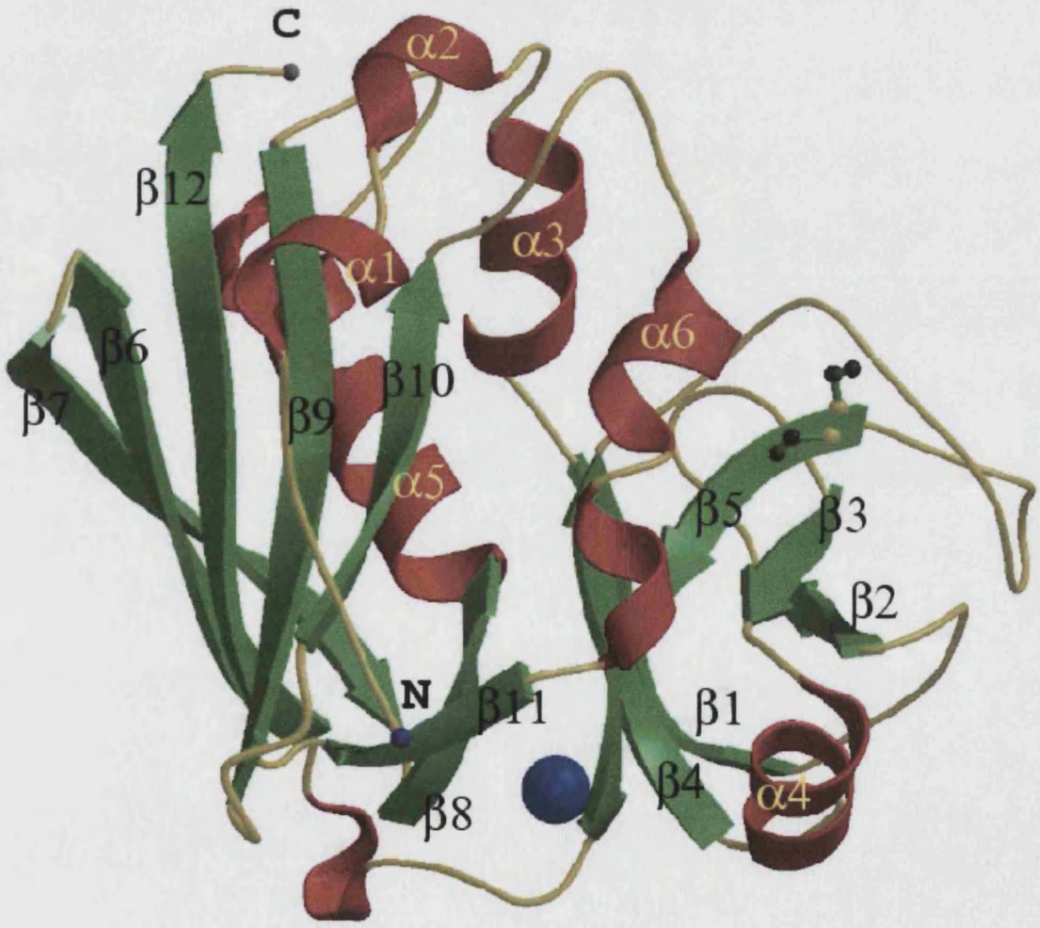

Figure 6.1: The crystal structure of native SEC2. All secondary structure elements are labelled. The zinc ion is represented by a blue sphere.

The residues in the SEC2 zinc correspond to Asp 77, His 106, and His 110 in SpeA1with the fourth ligand being Glu 33, (Baker *et al.*, 2001), and also has analogous residues in SEA (Schad *et al.*, 1997), and SED (Sundstrom *et al.*, 1996).

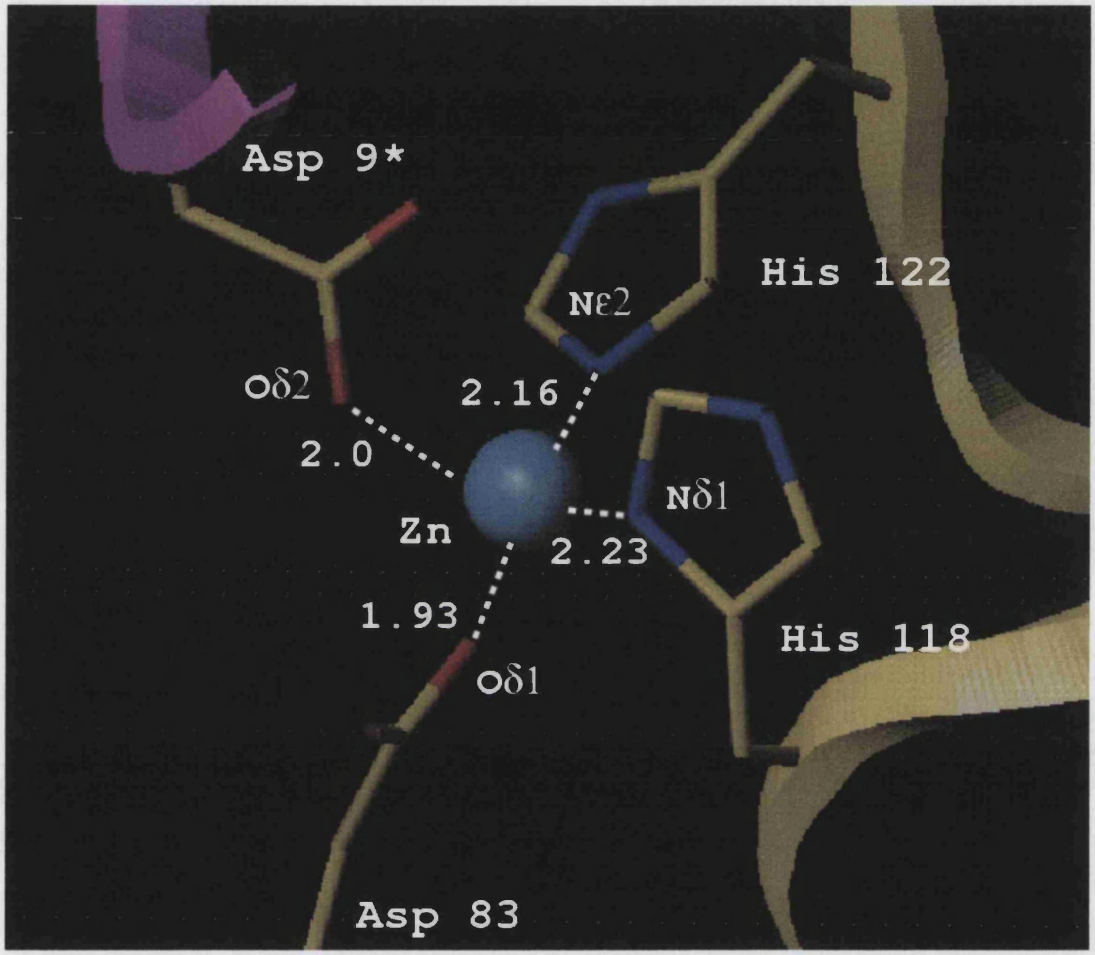

Figure 6.2: A close up view of the zinc binding site of SEC2. All ligands are labelled.

The zinc ion has been shown to be an intrinsic part of SEC2 with a dissociation constant of 1μM (Papageorgiou *et al.*, 1995) and is situated at some distance to the generic binding site on the opposite side of the toxin.

The role of zinc in high affinity MHC class II binding is now well established and in the case of SEC2 represents an alternate mode of MHC class II binding to its generic MHC class II binding site (Papageorgiou *et al.*, 1995; Li *et al.*, 2001; Petersson *et al* , 2001).

Mutant selection criteria and aims

The two SEC2 variants SEC2 H122A and H118:122A contain substition of histidine residues identified as zinc ligands in the native structure of SEC2 (Papageorgiou *et al.*, 1995). Kumaran *et al.*, (2001) attempted to determine the structural contribution of both the zinc binding histidines by determining the structure of SEC2 at various pHs by the molecular-replacement method. Two different crystal forms were found, tetragonal (pH 5.0, 5.5, 6.0 and 6.5) and monoclinic (pH8.0). Below pH 6.0 it was thought that these zinc co-ordinating histidines would be protonated and the zinc leached out. However, in the two lowest pH structures solved (pH 5.0 and 5.5) a zinc ion was still found to be present. Both the B factors and the co-ordination geometry increased at low pH; the bond distance for His 118 – zinc increased by 0.38 Å and for His 122 the bond length increased by 0.28Å.

The aims of these experiments were to express and purify both SEC2 H122A and H118:122A, followed by their crystallisation and structure determination. By studying the effect of mutation of both these histidine residues to alanine it is hoped to further understand the nature of the SEC2 binding site; how it interacts with MHC class II molecules, and the contribution that each of the zinc-binding residues make to the zinc site.

Materials and methods

Over-expression of SEC2 H122A and H118:122A-DE3 clones.

pET30a7SEC2H122A and pET30aSEC2H118:122A cloned in JM109(DE3) were obtained from CAMR. The pET30a vector contains a T7 promoter, a His tag with both

an enterokinase and factor Xa cleavage site and is immobile. Point mutations were introduced into the SEC2 gene by PCR with oligonucleotides containing the desired nucleotide substitution, and the genes inserted into pET30a.

Cultures were grown in as follows;

200ml flasks containing 50ml of LB supplemented with 1% glucose, 100 μg/ml ampicillin were Inoculated with either SEC2H122A or SEC2H118:122A clones and incubated overnight at 37° C with shaking. These 50 ml starter cultures were then transferred into 1l flasks, with 500ml LB, 1 % glucose, 100 μg/ml ampicillin and incubated at 37° C until the optical density reached + 0.7 – 1.0 au (600nm). Expression was induced with IPTG at 100 μm/ml IPTG for H122A (0.2 ml/litre) and 0.5 mM per ml IPTG for H118:122A (1.0 ml/litre) and the flasks incubated for a further 2 – 3 hours at 37°C. Cells were collected by centrifugation at 5000rpm for 25 minutes.

Purification was carried out as described in the pET system manual (Novagen). Briefly, cell pelletes were re-suspended in a total volume of 10 ml of binding buffer and transfered to tubes suitable for sonication. Five rounds of sonication were carried out at 14 microns for 30 seconds followed by 1 minute rest on ice. Samples were then centrifuged at 15,000 rpm for 15-20 minute using RC-5B centrifuge and SS34 rotor. Samples of cleared lysate were then loaded onto an equilibrated Nickel-NTA His-Bind column (Novagen) and the flow through collected for further analysis. The column was then washed with twice with wash buffer and eluted in 5 ml of elution buffer. All fractions were saved for further analysis by SDS gel.

Factor Xa His tag cleavage

The pooled purified toxin fractions were dialysed for 24 hours against two changes of cleavage buffer (20mM Tris-HCl, 100 mM NaCl, 2mM $CaCl_2$ at pH 8.0). Cleavage was carried out at 23°C for 24 – 48 hours using 5 μg of factor Xa per mg of protein as

assessed by absorbance at 280 nm. Purified cleaved protein was obtain by reapplying the sample to the His bind column and collecting the run through.

Immunodiffusion as a way of assessing the presence and concentration of toxin.

0.5g of powdered agar was added to 50 ml of purified distilled water and heated using a microwave oven to produce a 0.1% agar solution. After cooling, 150 µl of 1mg/ml guinea pig anti-SEC2 was added and the agar was then poured into 20 ml plates and left to set at 4°C. Two rows of 5 mm diameter wells were then cut at the top and bottom of the plates. In the top row 25 µl of serial dilutions of native SEC2 were added as a standard, and the samples to be assessed were added to the bottom row. Plates were then left overnight at 4°C. A standard curve was plotted of the square of the diameter of the halo produced by the interaction between SEC2 and antibody against the concentration of SEC2. Sample concentration was calculated using the standard curve.

Mono-S column

Cell pellets were re-suspended in 2ml of 50 mM sodium acetate and sonicated at 14 microns for 5 x 30 seconds interspersed with 1 minute rest on ice. The lysed cells were then spun at 13,000 rpm for 5 minutes and the lysate applied to a Mono-S column equilibrated with 50 mM sodium acetate. The column was washed with 50 mM sodium acetate and the protein eluted on a 0 – 30% 1M NaCl gradient. 1 ml fractions were collected throughout and analysed by spectrophotometer at 280 nm.

Mono-Q column

Cell pellets were re-suspended in 2ml of 20 mM Tris (pH 8.0) and sonicated at 14 microns for 5 x 30 seconds interspersed with 1 minute rest on ice. The lysed cells were then spun at 13,000 rpm for 5 minutes and the lysate applied to a Mono-Q column

equilibrated with 20 mM Tris . The column was washed with 20 mM Tris and the protein eluted on a 0 – 100% 1M NaCl gradient. 1 ml fractions were collected throughout and analysed by spectrophotometer at 280 nm.

Red A column

For a detailed method of purification of staphylococcal enterotoxins using red A see (Brehm *et al.*, 1990). Briefly, 5 ml of Red A was poured into a 5 ml column (pharmacia), washed with 10 mM phosphate buffer (pH 6.5) and left to settle. The column was then cleaned with seven volumes of 8 M urea containing 0.5M NaOH, and equilibrated with 10 mM phosphate buffer (pH 6.5). The sample was then applied to the column which was again washed with 10 mM phosphate buffer at pH 6.5 until the A280 level of flow-through reached a baseline level. The fusion protein was eluted with stepwise increases in KCl concentration (using 10 mM phosphate buffer containing 35 mM KCl at pH 6.5). 1 ml fractions were collected throughout and analysed by spectrophotometer at 280 nm.

Results and Discussion

Figure 6.3A, B, and C show the stages of purification of SEC2 H122A. A majority of the toxin binds to the column (figure 6.3A lanes 3 and 4) although approximately half of it is eluted in the wash fraction (3), perhaps due to overloading of the column.

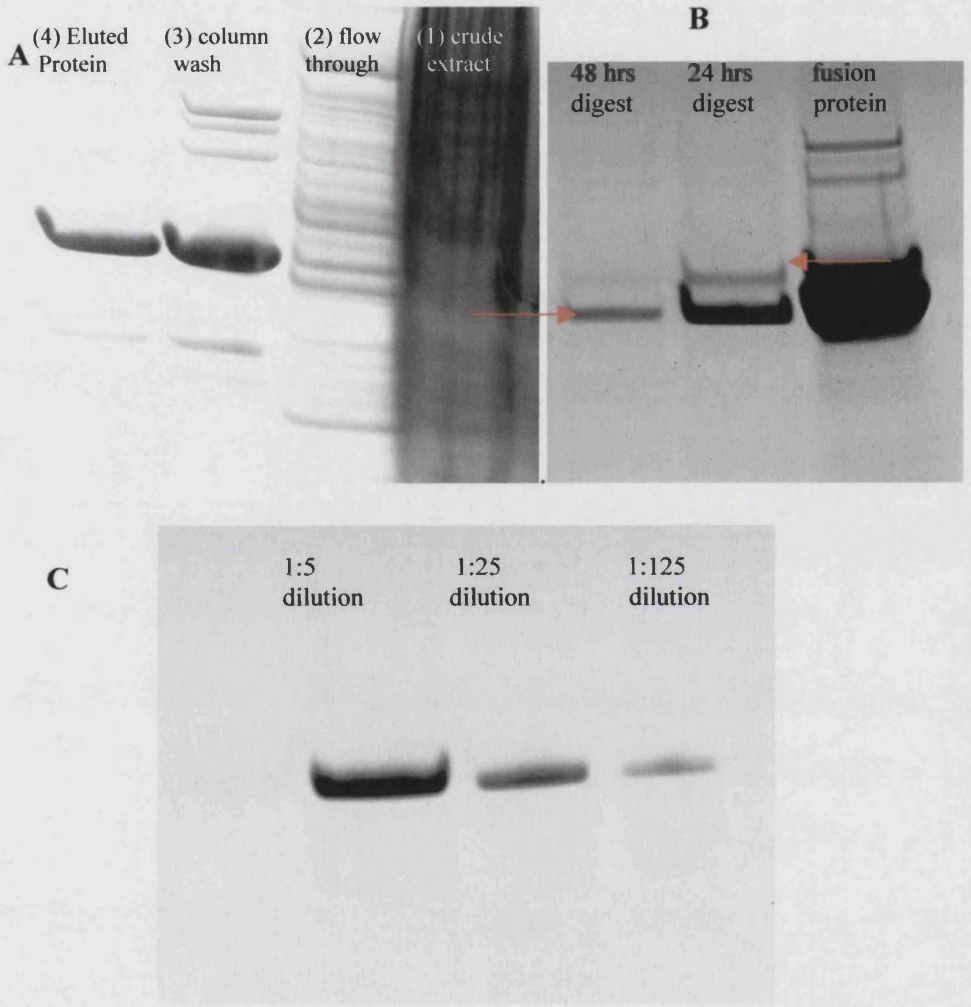

Figure 6.3: The purification of SEC2 H122A. A: purification of fusion protein using His bind resin **A)** Initial purification of fusion protein. **B)** Cleavage of fusion protein using factor Xa. Digest at 24 hours and 48 hours. The upper arrow points to the uncleaved fusion protein whilst the lower on indicates the cleaved toxin **C)** purified cleaved toxin in 1:5 serial dilution (left to right).

This fraction was collected, dialysed against PBS and reapplied to the column in order to maximise the yield. The fourth lane in Figure 6.3A shows that the His bind column allows a relatively pure sample to be obtained. The pooled purified fusion protein samples underwent factor Xa cleavage for 48 hours (Figure 6.3B). After 24 hours the cleavage reaction was not complete so the sample was left a further 24 hours. It is important to note that the cleaved samples in lanes 2 and 3 are diluted by approximately 12 times compared to the fusion protein sample in lane 1. The cleaved His tags were removed by reapplying the sample to the column. Figure 6.3C shows three successive 1:5 serial dilutions of the purified toxin on an SDS gel to illustrate its purity.
Toxin concentration as assessed by absorbance at 280 nm was 26 mg and by immunodiffusion 25 mg.
Figures 6.4A and B show the attempted purification of the SEC2 H118:122A double mutant. From Figure 6.4A it appears that the fusion protein does not bind to the column and is eluted in the two wash steps. Upon rescanning the gel and adjusting the brightness and contrast levels it became apparent that a great amount of the fusion protein was also running straight off the column in the flow through from loading. Also, a second band is shown that corresponds to the cleaved toxin, suggesting that some degradation may be taking place. In order to remedy this, it was decided to lower the concentration of imidazole in the washing buffers from 480mM to 240mM in order to a allow as much toxin to bind as possible.

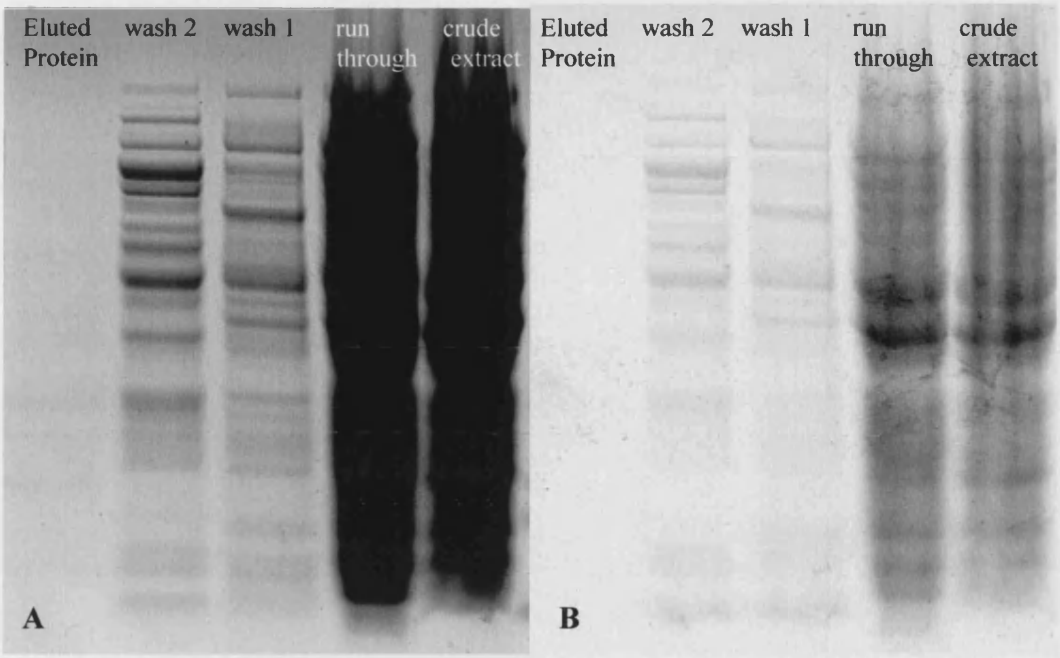

Figure 6.4: His bind purification of SEC2 H118:122A mutant. **A)** Right to left, crude cell extract, column run through, wash 1, wash 2, eluted protein. **B)** Re-scan of A with increased brightness and contrast levels

Decreasing imidazole concentration proved unsuccessful. As a result it was decided to re-sequence the H118:122A fusion protein gene to determine that the His tag was present in its correct form.

AATATGCACCATCATCATCATCATCATTCT

The sequence clearly shows the presence of coding sequence for 6 histidine residues and a band is produced on the gel of the correct size for the fusion protein which suggests that there may be something else effecting its binding to the nickel column. Consequently, it was decided to try other methods to purify the fusion protein: a mono-S column, a mono-Q column and a red A column.

Preliminary trials with a mono-S column failed to bind any protein at all to the column. This method has been used previously to purify native SEC2 in the CAMR laboratories and relies on the sample having a low salt content. The experiment was repeated using

samples dialysed against loading buffer for 24 hours in order to minimise salt content. Again, all of the protein came through in the run through from loading the column. Conversely, the fusion protein bound to the mono-Q column, but could not be eluted; even at 1 M NaCl. Indeed, it was only removed from the column by 8 M urea.
The red A method of toxin purification also failed to produce any further results. The fusion protein yet again failed to bind to the column. Red A has been used very successfully in the past to purify native SEC2 (Brehm *et al.*, 1990) indicating that the nature of the fusion protein differs from that of native SEC2.

Preliminary crystallisation trials with SEC2 His 122-Ala

Initial crystallisation trials were set up using the conditions used for native SEC2 (Papageorgiou *et al.*, 1995); 25 – 28% PEG 8000, 0.15 M ammonium sulphate, 0.02% (w/v) sodium azide and 0.1 M cacodylate buffer. However, these conditioned failed to produce any crystals. Hampton research crystal screen and PEG/ion screen were also tried. Further crystallisation trials are still in progress.

-7-

Chapter seven

Conclusion

The crystal structures of SpeA1 in complex with zinc, SEB variant Thr 112-Ser, and the three TSST-1 mutants Tyr 13-Ala, His 141-Ala, and Tyr 174-Ala presented here, combined with the wealth of structural and biological information available illustrate that although a fundamental set of structural features exist among the superantigen family, subtle differences exist among the functional mechanisms of each toxin.
The zinc site identified in SpeA1 is one such common feature. The zinc ligands are Glu 33, Asp 77, His 106, and His 110; the residues Asp 77, His 106, and His 110 are structurally equivalent to the residues Asp 83, His 110, and His 122 in SEC2, whilst Glu 33 is unique to SpeA1 as a zinc ligand. Further diversity exists as some toxins have multiple zinc sites with differing affinities for MHC class II molecules as well as a generic MHC class II site (SEC2, SED, SEA). In some toxins the zinc ion may be used for dimer formation (SpeC, SEA), whilst other toxins have a single zinc site in combination with a generic MHC site (SpeA1), or simply a zinc site and no generic MHC site (SEH). Questions remain about the use of zinc in dimer formation which will be addressed in chapter VIII. Neither SEB or TSST-1 posses a zinc site, yet are both extremely potent and simply rely on a generic MHC binding site for interaction with MHC class II molecules. Further regulation is provided by the nature of the antigenic peptide in the peptide binding groove of the MHC class II molecule.TSST-1 in complex with MHC class II exhibits extensive contact with the antigenic peptide. Indeed, TSST-1 presentation by MHC class II molecules has been shown to be enhanced or diminished depending on the composition of the antigenic peptide. The SEH – SpeC - MHC II complex structures indicate that extensive contact with the peptide is also made during zinc mediated SAg/MHC II interactions, which could allow some aspect of peptide control to SAg presentation.

The multiplicity that exists within the toxin family with regard to TCR binding can be described both in terms of those residues that support the architecture of the TCR binding site and in terms of those residues that bind directly to the TCR. This can be further subdivided into those residues that form a common core of TCR binding residues and those that govern specificity of binding to TCR Vβ elements. The structure of SEB Thr 112-Ser highlights the role that structural residues play in maintaining the integrity of the TCR binding site and how such residues can affect the strength and type of response. The three TSST-1 mutants Tyr 13-Ala, His 141-Ala, and Tyr 174-Ala illustrate that further diversity exists among the family as the TCR binding site is located in a different position in the toxin. Again, these structures have highlighted the contribution that certain residues can make to maintaining the integrity the TCR binding site. Additional differences are also found between TSST-1 and the other members of the superantigen family. It does not possess a disulphide loop which is thought to cause emesis. This is consistent with its role in TSS.

Various combinations of generic and zinc mediated MHC class II binding sites and the slight differences between the toxins in other functional regions such as the TCR site would allow each toxin to modulate the immune system in an appropriate manner. For example, the 3-dimensional structure of SpeA1 illustrates that it has the potential to act as a monomer or dimer, and can use a generic or zinc MHC class II binding site or perhaps both. The use of these elements may vary within the context of the disease. Subtleties within the finer points of their mechanism such as those illustrated by the SEB Thr 112-Ser variant could propagate different strengths, quality, and quantity of response by different T cells bearing different TCR Vβ elements. In turn this may facilitate TCR clustering giving rise to a more apposite response.

-8-

Chapter eight

Future Directions

Within the scope of this project further work is imperative. In order to fully characterise the three TSST-1 mutants additional biological work needs to be performed. The crystallisation and structure solution of the SEC2 mutants, along with biological studies would help us further understand the nature of zinc mediated MHC class II binding. Beyond this, several additional crystallographic and biological experiments would greatly enhance our understanding of the mechanics of superantigenicty. By studying the nature of the toxin in the context of the MHC class II – SAg – TCR complex: the crystal structure of the tri-molecular complex of toxin TCR and MHC may show some features that are not apparent from either SAg – MHC or SAg – TCR complex alone. Such features are not likely to be deduced from modelling. Further to this, investigations into multiple complexes of toxin(s) and MHC and TCR would illustrate the mechanics of receptor clustering for TCR and dimer formation for superantigens. By examining the conditions under which dimerisation and/or zinc ions are used by each toxin further light would be shed onto the strategies used by each toxin to produce an optimal affect under differing conditions. These multiple mechanisms may well act as a kind of self-regulatory element within each toxin so as to elucidate a distinct response from the immune system to allow the causation of disease. Superantigens are implicated in many different diseases and a comprehensive study of how their role changes within the context of different diseases may further increase our understanding of the disease as well as identify any additional intricacies within the mechanisms of these toxins.

-9-

Chapter nine

Publications

1) Baker M, Gutman DM, Papageorgiou AC, Collins CM and Acharya KR (2001) Structural features of a zinc-binding site in the superantigen Streptococcal pyrogenic exotoxin A (SpeA1): Implications for MHC class II recognition. *Protein Sci.* **10**, 1268-1273.

2) Baker, M., Papageorgiou A.C., Titball, R., Cavanagh, D., Kehoe, M.A., and Acharya K.R. (2002) Structural and Functional Role of Threonine 112 in a Superantigen Staphylococcus aureus Enterotoxin B. *J Biol Chem.* **277**(4), 2756-2762.

3) Baker, M., and Acharya, K.R.(2002) Superanitigens: structure Function and Diversity. *Methods in Mol Biol,* Humana press

4) Baker, M., Papageorgiou, A.C., Acharya, K.R. The Crystal Structures of Three Toxic Shock Syndrome T cell Receptor Binding Site mutants. *In preparation.*

-10-

Chapter ten

References

Abrahmsen, L., Dohlsten, M., Segren, S., Bjork, P., Jonsson, E., and Kalland, T. (1995) Characterization of two distinct MHC class II binding sites in the superantigen staphylococcal enterotoxin A. *Embo J* **14**, 2978-2986.

Acharya, K. R., Passalacqua, E. F., Jones, E. Y., Harlos, K., Stuart, D. I., Brehm, R. D., and Tranter, H. S. (1994) Structural basis of superantigen action inferred from crystal structure of toxic-shock syndrome toxin-1. *Nature* **367**, 94-97.

Adams, P. D., Pannu, N.S., Read, R.J. and Brunger, A.T. (1997) Cross-validated maximum likelihood enhances crystallographic simulated annealing refinement. *Proc Nat Acad Sci (USA)* **94**, 5018-5023.

Alber, G., Hammer, D.K., and Fleischer, B. (1990) Relationship between enterotoxic- and T lymphocyte-stimulating activity of staphylococcal enterotoxin B. *J. Immunol* **144**, 4501-4506.

Alberts, I. L., Nadassy, K., and Wodak, S.J. (1998) Analysis of zinc binding sites in protein crystal structures. *Protein Sci* **7**, 1700-1716.

Arad, G., Levy, R., Hillman, D., and Kaempfer, R. (2000) Superantigen antagonist protects against lethal shock and defines a new domain for T-cell activation. *Nat Med* **6**, 414-421.

Avena, R. M., and Bergdoll, M. S. (1967) Purification and some physicochemical properties of enterotoxin C, Staphylococcus aureus strain 361. *Biochemistry* **6**, 1474-1480.

Baker, M., Gutman D.M., Papageorgiou A.C., Collins C.M., and Acharya K.R. (2001) Structural features of a zinc binding site in the superantigen streptococcal pyrogenic exotoxin A1 (SpeA1): implications for MHC class II recognition. *Protein Sci* **10**, 1268-1273.

Baker, M., Papageorgiou A.C., Titball, R., Cavanagh, D., Kehoe, M.A., and Acharya K.R. (2001) Structural Basis for the altered T cell receptor specificity in a microbial superantigen Staphylococcus aureus enterotoxin B varient. *In preparation*

Bavari, S., Dyas, B., and Ulrich, R. G. (1996) Superantigen vaccines: a comparative study of genetically attenuated receptor-binding mutants of staphylococcal enterotoxin A. *J Infect Dis* **174**, 338-345.

Bavari, S., and Ulrich, R. G. (1995) Staphylococcal enterotoxin A and toxic shock syndrome toxin compete with CD4 for human major histocompatibility complex class II binding. *Infect Immun* **63**, 423-429.

Bergdoll, M. S. (1966) Immunization of Rhesus monkeys with enterotoxoid B. *J Infect Dis* **116**, 191-196.

Bergdoll, M. S. (1988) Monkey feeding test for staphylococcal enterotoxin. *Methods Enzymol* **165**, 324-333.

Bernal, A., Proft, T., Fraser, J. D., and Posnett, D. N. (1999) Superantigens in human disease. *J Clin Immunol* **19**, 149-157.

Bernstein F. C., Koetzle T. F., Williams G. J. B., Meyer E. F. Jr, Brice M. D., Rogers J. R., Kennard O., Shimanouchi T., and Tasumi M . (1977) The Protein Data Bank: a computer-based archival file for macromolecular structures. *J. Mol. Biol* **112**, 535-542.

Blundell, T. L., Johnson, L.N. (1976) *Protein Crystallography.*, Academic Press. (2001).

Bohach, G. A., and Schlievert, P. M. (1988) Detection of endotoxin by enhancement with toxic shock syndrome toxin-1 (TSST-1). *Methods Enzymol* **165**, 302-306.

Bonventre, P. F., Heeg, H., Cullen, C., and Lian, C. J. (1993) Toxicity of recombinant toxic shock syndrome toxin 1 and mutant toxins produced by Staphylococcus aureus in a rabbit infection model of toxic shock syndrome. *Infect Immun* **61**, 793-799.

Braun, M. A., Gerlach, D., Hartwig, U. F., Ozegowski, J. H., Romagne, F., Carrel, S., Kohler, W., and Fleischer, B. (1993) Stimulation of human T cells by streptococcal "superantigen" erythrogenic toxins (scarlet fever toxins). *J Immunol* **150**, 2457-2466.

Brehm, R. D., Tranter, H. S., Hambleton, P., and Melling, J. (1990) Large-scale purification of staphylococcal enterotoxins A, B, and C2 by dye ligand affinity chromatography. *Appl Environ Microbiol* **56**, 1067-1072.

Bremell, T., Lange, S., Holmdahl, R., Ryden, C., Hansson, G. K., and Tarkowski, A. (1994) Immunopathological features of rat Staphylococcus aureus arthritis. *Infect Immun* **62**, 2334-2344.

Bremell, T., and Tarkowski, A. (1995) Preferential induction of septic arthritis and mortality by superantigen-producing staphylococci. *Infect Immun* **63**, 4185-4187.

Brocke, S., Gaur, A., Piercy, C., Gautam, A., Gijbels, K., Fathman, C. G., and Steinman, L. (1993) Induction of relapsing paralysis in experimental autoimmune encephalomyelitis by bacterial superantigen. *Nature* **365**, 642-644.

Brocke, S., Hausmann, S., Steinman, L., and Wucherpfennig, K. W. (1998) Microbial peptides and superantigens in the pathogenesis of autoimmune diseases of the central nervous system. *Semin Immunol* **10**, 57-67.

Brünger, A. T. (1992) Free R value: a novel statistical quantity for assessing the accuracy of crystal structures. *Nature* **355**, 472-475.

Brünger, A. T. and Rice, L.M. (1997) Crystallographic refinement by simulated annealing: Methods and applications. *Methods Enzymol* **277**, 243-269.

Brünger, A. T., Adams, P.D., Clore, G.M., DeLano, W.L., Gros, P., GrosseKunstleve, R.W., Jiang, J.S., Kuszewski, J., Nilges, M., Pannu, N.S., Read, R.J., Rice, L.M., Simonson, T. and Warren, G.L. (1998) Crystallography & NMR system: A new software suite for macromolecular structure determination. *Acta Crystallogr D* **54**, 905-921.

CCP4. (1994) The CCP4 suite : Programs for Protein Crystallography. *Acta Crystallogr, D* **50**, 760-763.

Chu, F. S., Thadhani, K., Schantz, E. J., and Bergdoll, M. S. (1966) Purification and characterization of staphylococcal enterotoxin A. *Biochemistry* **5**, 3281-3289.

Cole, B. C., Knudtson, K. L., Oliphant, A., Sawitzke, A. D., Pole, A., Manohar, M., Benson, L. S., Ahmed, E., and Atkin, C. L. (1996) The sequence of the Mycoplasma arthritidis superantigen, MAM: identification of functional domains and comparison with microbial superantigens and plant lectin mitogens. *J Exp Med* **183**, 1105-1110.

Conrad, B., Weissmahr, R. N., Boni, J., Arcari, R., Schupbach, J., and Mach, B. (1997) A human endogenous retroviral superantigen as candidate autoimmune gene in type I diabetes. *Cell* **90**, 303-313.

Couper, J. J., Kallincos, N., Pollard, A., Honeyman, M., Prager, P., Harrison, L. C., and Rischmueller, M. (2000) Toxic shock syndrome associated with newly diagnosed type I diabetes. *J Paediatr Child Health* **36**, 279-282.

Crossley,K.B., and Archer, G.L. (1997) in *The Staphylococci in human disease*, Churchill Livingstone Inc.

Dauter, Z. (1997) Data collection strategy. *Methods Enzymol* **276**, 326-344.

Deresiewicz, R. L., Woo, J., Chan, M., Finberg, R. W., and Kasper, D. L. (1994) Mutations affecting the activity of toxic shock syndrome toxin-1. *Biochemistry* **33**, 12844-12851.

Deringer, J. R., Ely, R. J., Stauffacher, C. V., and Bohach, G. A. (1996) Subtype-specific interactions of type C staphylococcal enterotoxins with the T-cell receptor. *Mol Microbiol* **22**, 523-534.

Dohlsten, M., Lando, P. A., Bjork, P., Abrahmsen, L., Ohlsson, L., Lind, P., and Kalland, T. (1995) Immunotherapy of human colon cancer by antibody-targeted superantigens. *Cancer Immunol Immunother* **41**, 162-168.

Dohlsten, M., Hansson, J., Ohlsson, L., Litton, M., and Kalland, T. (1995) Antibody-targeted superantigens are potent inducers of tumor- infiltrating T lymphocytes in vivo. *Proc Natl Acad Sci (U S A)* **92**, 9791-9795.

Dohlsten, M., Kalland, T., Gunnarsson, P., Antonsson, P., Molander, A., Olsson, J., d'Argy, R., Ohlsson, L., Soegaard, M., Persson, R., and Brodin, T. N. (1998) Man-made superantigens: Tumor-selective agents for T-cell-based therapy. *Adv Drug Deliv Rev* **31**, 131-142.

Earhart, C. A., Vath, G. M., Roggiani, M., Schlievert, P. M., and Ohlendorf, D. H. (2000) Structure of streptococcal pyrogenic exotoxin A reveals a novel metal cluster. *Protein Sci* **9**, 1847-1851.

Ende, I. A., Terplan, G., Kickhofen, B., and Hammer, D. K. (1983) Chromatofocusing: a new method for purification of staphylococcal enterotoxins B and C1. *Appl Environ Microbiol* **46**, 1323-1330.

Fagin, U., Hahn, U., Grotzinger, J., Fleischer, B., Gerlach, D., Buck, F., Wollmer, A., Kirchner, H., and Rink, L. (1997) Exclusion of bioactive contaminations in Streptococcus pyogenes erythrogenic toxin A preparations by recombinant expression in Escherichia coli. *Infect Immun* **65**, 4725-4733.

Fields, B. A., Malchiodi, E. L., Li, H., Ysern, X., Stauffacher, C. V., Schlievert, P. M., Karjalainen, K., and Mariuzza, R. A. (1996) Crystal structure of a T-cell receptor β-chain complexed with a superantigen. *Nature* **384**, 188-192.

Fraser, J. D., Urban, R. G., Strominger, J. L., and Robinson, H. (1992) Zinc regulates the function of two superantigens. *Proc Natl Acad Sci (U S A)* **89**, 5507-5511.

Freedman, J. D., and Beer, D.J. (1991) Expanding perspectives on the toxic shock syndrome. *Adv. intern. Med* **36**, 363-397.

Friedman, S. M., Tumang, J. R., and Crow, M. K. (1993) Microbial superantigens as etiopathogenic agents in autoimmunity. *Rheum Dis Clin North Am* **19**, 207-222.

Garman, E. F. and Schnieder, T.R. (1997) Macromolecular cryocrystallography. *Journal of Applied Crystallography* **30**, 211-237.

Gaur, A., Fathman, C. G., Steinman, L., and Brocke, S. (1993) SEB induced anergy: modulation of immune response to T cell determinants of myoglobin and myelin basic protein. *J Immunol* **150**, 3062-3069.

Gerlach, D., Fleischer, B., Wagner, M., Schmidt, K., Vettermann, S., and Reichardt, W. (2000) Purification and biochemical characterization of a basic superantigen (SPEX/SMEZ3) from Streptococcus pyogenes. *FEMS Microbiol Lett* **188**, 153-163.

Germain, R. N. (1997) T-cell signaling: the importance of receptor clustering. *Curr Biol* **7**, R640-644.

Hansson, J., Ohlsson, L., Persson, R., Andersson, G., Ilback, N. G., Litton, M. J., Kalland, T., and Dohlsten, M. (1997) Genetically engineered superantigens as tolerable antitumor agents. *Proc Natl Acad Sci (U S A)* **94**, 2489-2494.

Hakansson, M., Petersson, K., Nilsson, H., Forsberg, G., Bjork, P., Antonsson, P., and Svensson, L. A. (2000) The crystal structure of staphylococcal enterotoxin H: implications for binding properties to MHC class II and TcR molecules. *J Mol Biol* **302**, 527-537.

Helliwell, J. R. (1992) Macromolecular crystallography with synchrotron radiation, first ed., Cambridge University press.

Hartwig, U. F., and Fleisher, B. (1993) Mutations affecting MHC class II binding of the superantigen streptococcal erythrogenic toxin A. *Eur. J. Immunol* **5**, 869-875.

Harris, T. O., and Betley, M. J. (1995) Biological activities of staphylococcal enterotoxin type A mutants with N-terminal substitutions. *Infect Immun* **63**, 2133-2140.

Hauser, A. R., Vath, G.M., Ohlendorf, D.H.,and Schlievert, P.M. (1995) in Bacterial Superantigens : Structure, function and therapeutic potential. (Thibodeau, J.,and Sekaly, R.P., Ed.)

Hauser, A. R., Stevens, D.L., and Schlievert, P.M. (1991) Molecular analysis of pyrogenic exotoxins from *Streptococcuc pyogenes* islates associated with toxic shock-like syndrome. *J. Clin. Microbiol* **29**, 1562-1567.

Hayball, J. D., and Lake, R. A. (2000) Partial T cell activation with an altered superantigenic ligand. *Immunol Cell Biol* **78**, 13-19.

Hayball, J. D., Robinson, J.H., O'Hehir, R.E., Verhoef, A., Lamb, J.R., Lake, R.A. (1994) Identification of two binding sites n staphylococcal entertoxin B that confer specificity for TCR V β gene products. *int. immunol* **6**, 199-211.

Herman, A., Kappler, J. W., Marrack, P., and Pullen, A. M. (1991) Superantigens: mechanism of T-cell stimulation and role in immune responses. *Annu Rev Immunol* **9**, 745-772.

Hendrickson, W. A. (1991) Determination of macromolecular structures from anomalous diffraction of synchrotron radiation. *Science* **254**, 51-58.

Hoffman, M., Tremaine, M., Mansfield, J., and Betley, M. (1996) Biochemical and mutational analysis of the histidine residues of staphylococcal enterotoxin A. *Infect Immun* **64**, 885-890.

Hohlfeld, R., Toyka, K. V., Heininger, K., Grosse-Wilde, H., and Kalies, I. (1984) Autoimmune human T lymphocytes specific for acetylcholine receptor. *Nature* **310**, 244-246.

Hovde, C. J., Marr, J. C., Hoffmann, M. L., Hackett, S. P., Chi, Y. I., Crum, K. K., Stevens, D. L., Stauffacher, C. V., and Bohach, G. A. (1994) Investigation of the role of the disulphide bond in the activity and structure of staphylococcal enterotoxin C1. *Mol Microbiol* **13**, 897-909.

Huber, B. T., Hsu, P. N., and Sutkowski, N. (1996) Virus-encoded superantigens. *Microbiol Rev* **60**, 473-482.

Huber, B. T. (1995) The role of superantigens in virus infection. *J Clin Immunol* **15**, 22S-25S.

Hudson, K. R., Robinson, H., and Fraser, J. D. (1993) Two adjacent residues in staphylococcal enterotoxins A and E determine T cell receptor V β specificity. *J Exp Med* **177**, 175-184.

Hurley, J. M., Shimonkevitz, R., Hanagan, A., Enney, K., Boen, E., Malmstrom, S., Kotzin, B. L., and Matsumura, M. (1995) Identification of class II major histocompatibility complex and T cell receptor binding sites in the superantigen toxic shock syndrome toxin 1. *J Exp Med* **181**, 2229-2235.-48, R.G. Landes Company, Austin.

Jardetzky, T. S., Brown, J. H., Gorga, J. C., Stern, L. J., Urban, R. G., Chi, Y. I., Stauffacher, C., Strominger, J. L., and Wiley, D. C. (1994) Three-dimensional structure of a human class II histocompatibility molecule complexed with superantigen. *Nature* **368**, 711-718.

Jones, T. A., Zou, J.Y., Cowan, S.W. and Kjeldgaard, M. (1991) Improved methods for building models in electron density maps & the location of errors in these models. *Acta CrystallogrA* **47**, 110-119.

Kabsch, D. and Sander, L. (1983) Dictionary of protein secondary structure: pattern recognition of hydrogen bonded and geometrical features. *Biopolymers* **22**, 2577 - 2637.

Kappler, J. W., Herman, A., Clements, J., and Marrack, P. (1992) Mutations defining functional regions of the superantigen staphylococcal enterotoxin B. *J Exp Med* **175**, 387-396.

Ke, H. M. (1997) Overview of isomorphous replacement phasing. *Methods Enzymol* **276**, 448-461.

Keane, W. F., Gekker, G., Schlievert, P. M., and Peterson, P. K. (1986) Enhancement of endotoxin-induced isolated renal tubular cell injury by toxic shock syndrome toxin 1. *Am J Pathol* **122**, 169-176.

Kim, J., Urban, R. G., Strominger, J. L., and Wiley, D. C. (1994) Toxic shock syndrome toxin-1 complexed with a class II major histocompatibility molecule HLA-DR1. *Science* **266**, 1870-1874.

Kline, J. B., and Collins, C. M. (1997) Analysis of the interaction between the bacterial superantigen streptococcal pyrogenic exotoxin A (SpeA) and the human T-cell receptor. *Mol Microbiol* **24**, 191-202.

Kline, J. B., and Collins, C. M. (1996) Analysis of the superantigenic activity of mutant and allelic forms of streptococcal pyrogenic exotoxin A. *Infect Immun* **64**, 861-869.

Kotzin, B. L., Leung, D. Y., Kappler, J., and Marrack, P. (1993) Superantigens and their potential role in human disease. *Adv Immunol* **54**, 99-166.

Krakauer, T. (1995) Differential inhibitory effects of interleukin-10, interleukin-4, and dexamethasone on staphylococcal enterotoxin-induced cytokine production and T cell activation. *J Leukoc Biol* **57**, 450-454.

Kumaran, D., Eswaramoorthy, S., Furey, W., Sax, M., Swaminathan, S (2000) Structure of staphylococcal enterotoxin C2 at various pH levels. *Acta Crystallogr D* **57**, 1270-5.

Laskowski, R. A., Macarthur, M.W., Moss, D.S. and Thornton, J.M. (1993) Procheck - a Program to Check the Stereochemical Quality of Protein Structures. *Journal of App Crystallog* **26**, 283-291.

Lavoie, P. M., Thibodeau, J., Erard, F., and Sekaly, R. P. (1999) Understanding the mechanism of action of bacterial superantigens from a decade of research. *Immunol Rev* **168**, 257-269.

Leder, L., Llera, A., Lavoie, P. M., Lebedeva, M. I., Li, H., Sekaly, R. P., Bohach, G. A., Gahr, P. J., Schlievert, P. M., Karjalainen, K., and Mariuzza, R. A. (1998) A mutational analysis of the binding of staphylococcal enterotoxins B and C3 to the T cell receptor β chain and major histocompatibility complex class II. *J Exp Med* **187**, 823-833.

Lehnert, N. M., Allen, D.L., Allen, B.L., Catasti, P., Shiflett, P.R., Chen, M., Lehnert, B.E., and Gupta, G. (2001) Structure-based design of a bispecific receptor mimic that inhibits T cell responses to a superantigen. *Biochemistry* **40**, 4222-4228.

Leslie, A. G. W. (1992) Recent changes to the MOSFLM package for processing film and image plate data. *Joint CCP4 ESF-EAMCB newsletter on Protein crystallogaphy.*

Li, Y., Li, H., Dimasi, N., McCormick, J. K., Martin, R., Schuck, P., Schlievert, P. M., and Mariuzza, R. A. (2001) Crystal Structure of a Superantigen Bound to the High-Affinity, Zinc- Dependent Site on MHC Class II. *Immunity* **14**, 93-104.

Li, H., Llera, A., Tsuchiya, D., Leder, L., Ysern, X., Schlievert, P. M., Karjalainen, K., and Mariuzza, R. A. (1998) Three-dimensional structure of the complex between a T cell receptor β chain and the superantigen staphylococcal enterotoxin B. *Immunity* **9**, 807-816.

Li, H., Llera, A., and Mariuzza, R. A. (1998) Structure-function studies of T-cell receptor-superantigen interactions. *Immunol Rev* **163**, 177-186.

Litton, M. J., Dohlsten, M., Lando, P. A., Kalland, T., Ohlsson, L., Andersson, J., and Andersson, U. (1996) Antibody-targeted superantigen therapy induces tumor-infiltrating lymphocytes, excessive cytokine production, and apoptosis in human colon carcinoma. *Eur J Immunol* **26**, 1-9.

Lowell, G. H., Colleton ,C., and t ,D. (1996) Immunogenicity and efficacy against lethal Aerosol Staphylococcal enterotoxin B challenge in Monkeys by intramuscular and Respiratory delivery of Proteosome-toxoid Vaccines. *Infect and immun* **64**, 4686-4693.

MacDonald, H. R. (1996) Superantigens in disease. *Springer Semin Immunopathol* **17**, 283-284.

Malchiodi, E. L., Eisenstein, E., Fields, B. A., Ohlendorf, D. H., Schlievert, P. M., Karjalainen, K., and Mariuzza, R. A. (1995) Superantigen binding to a T cell receptor β chain of known three- dimensional structure. *J Exp Med* **182**, 1833-1845.

Marrack, P., and Kappler, J. (1990) The staphylococcal enterotoxins and their relatives. *Science* **248**, 705-711.

Mehta, B. A., and Maino, V. C. (1997) Simultaneous detection of DNA synthesis and cytokine production in staphylococcal enterotoxin B activated CD4+ T lymphocytes by flow cytometry. *J Immunol Methods* **208**, 49-59.

Miethke, T., Wahl, C., Holzmann, B., Heeg, K., and Wagner, H. (1993) Bacterial superantigens induce rapid and T cell receptor V β- selective down-regulation of L-selectin (gp90Mel-14) in vivo. *J Immunol* **151**, 6777-6782.

Miethke, T., Wahl, C., Regele, D., Gaus, H., Heeg, K., and Wagner, H. (1993) Superantigen mediated shock: a cytokine release syndrome. *Immunobiology* , 270-284.

Munson, S. H., Tremaine, M. T., Betley, M. J., and Welch, R. A. (1998) Identification and characterization of staphylococcal enterotoxin types G and I from Staphylococcus aureus. *Infect Immun* **66**, 3337-3348.

Murray, D. L., Earhart, C. A., Mitchell, D. T., Ohlendorf, D. H., Novick, R. P., and Schlievert, P. M. (1996) Localization of biologically important regions on toxic shock syndrome toxin 1. *Infect Immun* **64**, 371-374.

Murzin, A. G., Brenner, S.E., Hubbard, T., Chothia, C. (1995) SCOP-A structural classification of protein database for the investigationn of sequence and structure. *J. Mol. Biol* **247**, 536-540.

Musser, J. M., Hauser, A.R., Kim, M.H., Schlievert, P.M., Nelson, K., and Selander, R.K. (1991) *Streptococcus pyogenes* causing toxic shock-like syndrome and their invasive diseases: Clonal diversity and pyrogenic exotoxin expression. *Proc Natl Acad Sci (U S A)* **88**, 2668-2672.

Navaza, J. (1994) AMoRe : an automated package for molecular replacement. *Acta Crystallogr A* **50**, 157-163.

Navaza, J. and Saludjian, P. (1987) AMoRe: An automated molecular replacement program package. *Methods Enzymol* **276**, 581-594

Ostrand-Rosenberg, S., Pulaski, B. A., Clements, V. K., Qi, L., Pipeling, M. R., and Hanyok, L. A. (1999) Cell-based vaccines for the stimulation of immunity to metastatic cancers. *Immunol Rev* **170**, 101-114.

Otwinowski, Z. and. Minor., W. (1997) Processing of X-ray diffraction data collected in oscillation mode. *Methods Enzymol* **276**, 307-326

Parsonnet, J., Gillis, Z. A., Richter, A. G., and Pier, G. B. (1987) A rabbit model of toxic shock syndrome that uses a constant, subcutaneous infusion of toxic shock syndrome toxin 1. *Infect Immun* **55**, 1070-1076.

Papageorgiou, A. C., and Acharya, K. R. (2000) Microbial superantigens: from structure to function. *Trends Microbiol* **8**, 369-375.

Papageorgiou, A. C., Collins, C. M., Gutman, D. M., Kline, J. B., O'Brien, S. M., Tranter, H. S., and Acharya, K. R. (1999) Structural basis for the recognition of superantigen streptococcal pyrogenic exotoxin A (SpeA1) by MHC class II molecules and T-cell receptors. *Embo J* **18**, 9-21.

Papageorgiou, A. C., Tranter, H. S., and Acharya, K. R. (1998) Crystal structure of microbial superantigen staphylococcal enterotoxin B at 1.5 Å resolution: implications for superantigen recognition by MHC class II molecules and T-cell receptors. *J Mol Biol* **277**, 61-79.

Papageorgiou, A. C., and Acharya, K. R. (1997) Superantigens as immunomodulators: recent structural insights. *Structure* **5**, 991-996.

Papageorgiou, A. C., Acharya, K. R., Shapiro, R., Passalacqua, E. F., Brehm, R. D., and Tranter, H. S. (1995) Crystal structure of the superantigen enterotoxin C2 from Staphylococcus aureus reveals a zinc-binding site. *Structure* **3**, 769-779.

Papageorgiou, A. C., Quinn, C. P., Beer, D., Brehm, R. D., Tranter, H. S., Bonventre, P. F., and Acharya, K. R. (1996) Crystal structure of a biologically inactive mutant of toxic shock syndrome toxin-1 at 2.5 Å resolution. *Protein Sci* **5**, 1737-1741.

Papageorgiou, A. C., Brehm, R. D., Leonidas, D. D., Tranter, H. S., and Acharya, K. R. (1996) The refined crystal structure of toxic shock syndrome toxin-1 at 2.07 Å resolution. *J Mol Biol* **260**, 553-569.9) .

Parsonnet, J., Hickman, R. K., Eardley, D. D., and Pier, G. B. (1985) Induction of human interleukin-1 by toxic-shock-syndrome toxin-1. *J Infect Dis* **151**, 514-522.

Petersson, K., Hakansson, M., Nilsson, H., Forsberg, G., Svensson, L.A., Liljas, A., and Walse, B. (2001) Crystal structure of a superantigen bound to MHC class II displays zinc and peptide dependence. *Embo J* **20**, 3306-3312.

Picker, L. J., Singh, M. K., Zdraveski, Z., Treer, J. R., Waldrop, S. L., Bergstresser, P. R., and Maino, V. C. (1995) Direct demonstration of cytokine synthesis heterogeneity among human memory/effector T cells by flow cytometry. *Blood* **86**, 1408-1419.

Prasad, G. S., Earhart, C. A., Murray, D. L., Novick, R. P., Schlievert, P. M., and Ohlendorf, D. H. (1993) Structure of toxic shock syndrome toxin 1. *Biochemistry* **32**, 13761-13766.

Proft, T., Moffatt, S. L., Berkahn, C. J., and Fraser, J. D. (1999) Identification and characterization of novel superantigens from Streptococcus pyogenes. *J Exp Med* **189**, 89-102.

Proft, T., Moffatt, S. L., Weller, K. D., Paterson, A., Martin, D., and Fraser, J. D. (2000) The streptococcal superantigen SMEZ exhibits wide allelic variation, mosaic structure, and significant antigenic variation. *J Exp Med* **191**, 1765-1776.

Redpath, S., Alam, S. M., Lin, C. M., O'Rourke, A. M., and Gascoigne, N. R. (1999) Cutting edge: trimolecular interaction of TCR with MHC class II and bacterial superantigen shows a similar affinity to MHC:peptide ligands. *J Immunol* **163**, 6-10.

Renno, T., and Acha-Orbea, H. (1996) Superantigens in autoimmune diseases: still more shades of gray. *Immunol Rev* **154**, 175-191.

Reynolds, D., Tranter, H. S., Sage, R., and Hambleton, P. (1988) Novel method for purification of staphylococcal enterotoxin A. *Appl Environ Microbiol* **54**, 1761-1765.

Rhodes, G. (1993) Crystallography Made Crystal Clear. Academic Press, London.

Robern, H., Stavric, S., and Dickie, N. (1975) The application of QAE-Sephadex for the purification of two staphylococcal enterotoxins. I. Purification of enterotoxin C2. *Biochim Biophys Acta* **393**, 148-158.

Rodgers, D. W. (1994) Cryocrystallography. *Structure* **2**, 1135-1140.

Roggiani, M., Stoehr, J. A., Leonard, B. A., and Schlievert, P. M. (1997) Analysis of toxicity of streptococcal pyrogenic exotoxin A mutants. *Infect Immun* **65**, 2868-2875.

Rossman, M. G. (ed). (1972) *The Molecular Replacement Method.*, Gordon and Breach, New York

Roussel, A., Anderson, B. F., Baker, H. M., Fraser, J. D., and Baker, E. N. (1997) Crystal structure of the streptococcal superantigen SPE-C: dimerization and zinc binding suggest a novel mode of interaction with MHC class II molecules. *Nat Struct Biol* **4**, 635-6430.

Salandy, D., and Brenner, B. (2001) Toxic shock syndrome. *eMedicine journal* **2**, 1 - 10.

Schad, E. M., Papageorgiou, A. C., Svensson, L. A., and Acharya, K. R. (1997) A structural and functional comparison of staphylococcal enterotoxins A and C2 reveals remarkable similarity and dissimilarity. *J Mol Biol* **269**, 270-280.

Schad, E. M., Zaitseva, I., Zaitsev, V. N., Dohlsten, M., Kalland, T., Schlievert, P. M., Ohlendorf, D. H., and Svensson, L. A. (1995) Crystal structure of the superantigen staphylococcal enterotoxin type A. *Embo J* **14**, 3292-3301.

Schiffenbauer, J., Didier, D.K., Klearman, M., Rice, K., Shuman, S.,Tieber, V.L., Kittleson, D.J., Schwartz, B.D. (1987) Complete sequence of the HLA-DQ α and β cDNA from DRS/DQW3 cell line. *J. Immunol* **139**, 228-233.

Schlievert, P. M. (1993) Role of superantigens in human disease. *J. infect. Dis* **167**, 997-1002.

Schlievert, P. M., Jablonski, L. M., Roggiani, M., Sadler, I., Callantine, S., Mitchell, D. T., Ohlendorf, D. H., and Bohach, G. A. (2000) Pyrogenic toxin superantigen site specificity in toxic shock syndrome and food poisoning in animals. *Infect Immun* **68**, 3630-3634.

Schlievert, P. M. (1988) Immunochemical assays for toxic shock syndrome toxin-1. *Methods Enzymol* **165**, 339-344.

Schlievert, P. M. (1982) Enhancement of host susceptibility to lethal endotoxin shock by staphylococcal pyrogenic exotoxin type C. *Infect Immun* **36**, 123-128.

Soos, J. M., Schiffenbauer, J., Torres, B. A., and Johnson, H. M. (1997) Superantigens as virulence factors in autoimmunity and immunodeficiency diseases. *Med Hypotheses* **48**, 253-259.

Spero, L., and Morlock, B.A. (1978) Biological activities of the peptides of Staphylococcal enterotoxin C formed by limited tryptic hydrolysis. *J. Biol. Chem* **253**, 8787-8791.

Sriskandan, S., Moyes, D., Buttery, L. K., Krausz, T., Evans, T. J., Polak, J., and Cohen, J. (1996) Streptococcal pyrogenic exotoxin A release, distribution, and role in a murine model of fasciitis and multi-organ failure due to Streptococcus pyogenes. *J Infect Dis* **173**, 1399-1407.

Sriskandan, S., Moyes, D., and Cohen, J. (1996b) Detection of circulating bacterial superantigen and lymphotoxin-α in patients with streptococcal toxic-shock syndrome . *Lancet* **348**, 1315-1316.

Sundberg, E., and Jardetzky, T. S. (1999) Structural basis for HLA-DQ binding by the streptococcal superantigen SSA. *Nat Struct Biol* **6**, 123-129.

Sundstrom, M., Hallen, D., Svensson, A., Schad, E., Dohlsten, M., and Abrahmsen, L. (1996) The Co-crystal structure of staphylococcal enterotoxin type A with Zn^{2+} at 2.7 Å resolution. Implications for major histocompatibility complex class II binding. *J Biol Chem* **271**, 32212-32216.

Sundstrom, M., Abrahmsen, L., Antonsson, P., Mehindate, K., Mourad, W., and Dohlsten, M. (1996) The crystal structure of staphylococcal enterotoxin type D reveals Zn^{2+}- mediated homodimerization. *Embo J* **15**, 6832-6840.

Swaminathan, S., Furey, W., Pletcher, J., and Sax, M. (1992) Crystal structure of staphylococcal enterotoxin B, a superantigen. *Nature* **359**, 801-806.

Tiedemann, R. E., Urban, R. J., Strominger, J. L., and Fraser, J. D. (1995) Isolation of HLA-DR1.(staphylococcal enterotoxin A)2 trimers in solution. *Proc Natl Acad Sci (U S A)* **92**, 12156-12159

Todd, J., Fishaut, M., Kapral, F., and Welch, T. (1978) Toxic-shock syndrome associated with phage-group-I Staphylococci. *Lancet* **2**, 1116-1118.

Ulrich, R. G., Olson, M. A., and Bavari, S. (1998) Development of engineered vaccines effective against structurally related bacterial superantigens. *Vaccine* **16**, 1857-1864.

Visvanathan, K., Charles, A., Bannan, J., Pugach, P., Kashfi, K., and Zabriskie, J. B. (2001) Inhibition of bacterial superantigens by peptides and antibodies. *Infect Immun* **69**, 875-884.

Wen, R., Cole, G. A., Surman, S., Blackman, M. A., and Woodland, D. L. (1996) Major histocompatibility complex class II-associated peptides control the presentation of bacterial superantigens to T cells. *J Exp Med* **183**, 1083-1092.

Wen, R., Broussard, D. R., Surman, S., Hogg, T. L., Blackman, M. A., and Woodland, D. L. (1997) Carboxy-terminal residues of major histocompatibility complex class II-associated peptides control the presentation of the bacterial superantigen toxic shock syndrome toxin-1 to T cells. *Eur J Immunol* **27**, 772-781.

White, J., Herman, A., Pullen, A. M., Kubo, R., Kappler, J. W., and Marrack, P. (1989) The V β-specific superantigen staphylococcal enterotoxin B: stimulation of mature T cells and clonal deletion in neonatal mice. *Cell* **56**, 27-35.

Woodland, D. L., Wen, R., and Blackman, M. A. (1997) Why do superantigens care about peptides? *Immunol Today* **18**, 18-22.

Wucherpfennig, K. W., Weiner, H. L., and Hafler, D. A. (1991) T-cell recognition of myelin basic protein. *Immunol Today* **12**, 277-282.